STRUCTURAL OPTIMIZATION OF A COMPOSITE WING

A THESIS SUBMITTED TO
THE GRADUATE SCHOOL OF NATURAL AND APPLIED SCIENCES
OF
MIDDLE EAST TECHNICAL UNIVERSITY

BY

ÖZLEM SÖKMEN

IN PARTIAL FULFILLMENT OF THE REQUIREMENTS
FOR
THE DEGREE OF MASTER OF SCIENCE
IN
AEROSPACE ENGINEERING

SEPTEMBER 2006

Approval of the Graduate School of Natural and Applied Sciences

Prof. Dr. Canan ÖZGEN
Director

I certify that this thesis satisfies all the requirements as a thesis for the degree of Master of Science.

Prof. Dr. Nafiz ALEMDAROĞLU
Head of Department

This is to certify that we have read this thesis and that in our opinion it is fully adequate, in scope and quality, as a thesis for the degree of Master of Science.

Prof. Dr. Mehmet A. AKGÜN
Supervisor

Examining Committee Members

Assoc. Prof.Dr. Altan KAYRAN	(METU, AEE)	_____
Prof. Dr. Mehmet A. AKGÜN	(Yeditepe Uni.)	_____
Prof. Dr. Yusuf ÖZYÖRÜK	(METU, AEE)	_____
Asst. Prof.Dr. Melin ŞAHİN	(METU, AEE)	_____
Dr. Özge ŞEN	(TÜBİTAK-SAGE)	_____

I hereby declare that all information in this document has been obtained and presented in accordance with academic rules and ethical conduct. I also declare that, as required by these rules and conduct, I have fully cited and referenced all material and results that are not original to this work.

Name, Last name: Özlem SÖKMEN

Signature :

ABSTRACT

STRUCTURAL OPTIMIZATION OF A COMPOSITE WING

Sökmen, Özlem

M.Sc., Department of Aerospace Engineering

Supervisor: Prof. Dr. Mehmet A. AKGÜN

September 2006, 125 pages

In this study, the structural optimization of a cruise missile wing is accomplished for the aerodynamic loads for four different flight conditions. The flight conditions correspond to the corner points of the V-n diagram. The structural analysis and optimization is performed using the ANSYS finite element program. In order to construct the flight envelope and to find the pressure distribution in each flight condition, FASTRAN Computational Fluid Dynamics program is used.

The structural optimization is performed for two different wing configurations. In the first wing configuration all the structural members are made up of aluminum material. In the second wing configuration, the skin panels are all composite material and the other members are made up of aluminum material. The minimum weight design which satisfies the strength and buckling constraints are found for both wings after the optimization analyses.

Keywords: Structural Optimization, Composite Wing, Finite Element Analysis, Buckling, V-n diagram

ÖZ

KOMPOZİT BİR KANADIN YAPISAL ENİYİLEMESİ

Sökmen, Özlem

Yüksek Lisans, Havacılık ve Uzay Mühendisliği Bölümü

Tez Yöneticisi: Prof. Dr. Mehmet A. AKGÜN

Eylül 2006, 125 sayfa

Bu çalışmada, bir seyir füzesi kanadının, dört farklı manevra durumundaki aerodinamik yükler altında yapısal eniyilemesi gerçekleştirilmiştir. Sözkonusu manevra durumları V-n grafiğinin köşe noktalarına karşılık gelmektedir. Yapısal analiz ve eniyileme için ANSYS sonlu elemanlar programı, manevra zarfının oluşturulması ve her bir uçuş durumundaki basınç dağılımlarının elde edilebilmesi için FASTRAN hesaplamalı akışkanlar dinamiği programı kullanılmıştır.

Yapısal eniyileme, iki farklı kanat konfigürasyonu için gerçekleştirilmiştir. İlk kanat konfigürasyonunda bütün yapısal elemanlar alüminyum malzemeden oluşmaktadır. İkinci kanat konfigürasyonunda ise kanat kaplamaları kompozit malzemeden, diğer yapısal elemanlar alüminyum malzemeden meydana gelmektedir. Her iki kanat için de, eniyileme analizleri sonucunda dayanım ve burkulma kısıtlarını sağlayan en düşük ağırlıklı kanat tasarımları elde edilmiştir.

Anahtar Kelimeler: Yapısal Eniyileme, Kompozit Kanat, Sonlu Elemanlar Analizi, Burkulma, V-n grafiği

To My Family

ACKNOWLEDGMENTS

I would like to express my gratitude to Prof. Dr. Mehmet A. AKGÜN for his unique guidance, supervision, understanding and encouragement in every phase of the study. I am deeply grateful to him for additional workload that he spared to me after he retired from METU. I would also like to thank Prof. Dr. Yusuf ÖZYÖRÜK for his interest and support.

I would like to express my deepest appreciation to Mr. Erdinç Nuri YILDIZ for his invaluable discussions, useful remarks, and support. I cannot thank to him enough.

I would like to thank my coordinator Dr. Mutlu Devrim CÖMERT and my chiefs Dr. Serkan GÖZÜBÜYÜK and Dr. Özge ŞEN for their support and understanding.

I would like to thank Mr. H. Özgür DEMİR, Mr. Bora YAZICI, Mr. Osman BAŞOĞLU and Dr. Lütfi Oktay GÖNÇ for their help and discussions on the aerodynamic solutions.

Analyses carried out on ANSYS and FASTRAN were performed using the facilities at TÜBİTAK-SAGE, which is greatly acknowledged.

Special thanks go to my parents Nurhan and Seyit Ahmet SÖKMEN for their endless support, patience and encouragement throughout my all education. I would also like to thank my sister Özgül and my brother Özkan for their love, support and patience.

Finally, I would like to express my special thanks to Bülent SÜMER for his love, understanding, patience and support. Without him, none of this would have been possible.

TABLE OF CONTENTS

LIST OF TABLES

LIST OF FIGURES

NOMENCLATURE

A	Extensional Stiffness Matrix
B	Coupling Matrix
c	Chord Length
C_L	Wing Lift Coefficient
$C_{L,,max}$	Maximum Lift Coefficient
$C_{L,,min}$	Minimum Lift Coefficient
C_p	Pressure Coefficient
C_{xy}	Coupling Coefficient for Tsai-Wu Failure Criterion
D	Flexural Stiffness Matrix
E_1	Elasticity Modulus in Longitudinal Direction
E_2	Elasticity Modulus in Transverse Direction
G_{12}	In-plane Shear Modulus
L	Lift
M	Mach Number
n	Load Factor
n_{max}	Maximum Load Factor
N	In-plane Stress Resultants
P_∞	Atmospheric Pressure
q	Dynamic Pressure
S	Wing Surface Area
S_{1t}	Tensile Strength in Longitudinal Direction
S_{1c}	Compressive Strength in Longitudinal Direction
S_{2t}	Tensile Strength in Transverse Direction
S_{2c}	Compressive Strength in Transverse Direction
S_{12}	In-plane Shear Strength
u	Velocity Component in the Chordwise Direction
u_x	Displacement in x-direction
u_y	Displacement in y-direction
u_z	Displacement in z-direction
V_D	Design Dive Speed

W	Weight
α	Angle of Attack
ε^o	Mid-plane Strain
ε_{1t}	Failure Tensile Strain in Longitudinal Direction
ε_{1c}	Failure Compressive Strain in Longitudinal Direction
ε_{2t}	Failure Tensile Strain in Transverse Direction
ε_{2c}	Failure Compressive Strain in Transverse Direction
ε_{12}	In-plane Failure Strain
κ	Curvature of the Layer
λ_c	Buckling Load Factor due to a Combination of Normal and Shear Loads
λ_n	Buckling Load Factor due to Normal Loads
λ_s	Buckling Load Factor due to Shear Loads
ρ	Density
ν_{12}	In-plane Poisson's Ratio

ABBREVIATIONS

APDL	ANSYS Parametric Design Language
C	Chordwise Forces
CFD	Computational Fluid Dynamics
DV	Design Variable
FEM	Finite Element Method
GUI	Graphical User Interface
GA	Genetic Algorithm
N	Normal Forces
NACA	National Advisory Committee for Aeronautics
NHAA	Negative High Angle of Attack
NLAA	Negative Low Angle of Attack
NS	Navier-Stokes
PHAA	Positive High Angle of Attack
PLAA	Positive Low Angle of Attack
SUMT	Sequential Unconstrained Maximization/Minimization Technique
SV	State Variable
W.S.	Wing Station

CHAPTER 1

INTRODUCTION

The main objective of this thesis is to design and optimize the wing structure of a cruise missile. The aerodynamic and geometrical properties of the wing are taken from the Tomahawk Cruise Missile. The aerodynamic loads acting on the wing are found by the use of a commercial Computational Fluid Dynamics (CFD) program for different flight conditions. With the aid of predicted aerodynamic properties of the wing, a V-n diagram is constructed and the design and optimization of the wing is carried out for four different loading conditions. Deformation of the wing under the applied aerodynamic loading and the relevant boundary conditions are solved using the ANSYS finite element program. In addition, weight minimization of the wing structure subjected to strength and buckling constraints is achieved by use of the optimization routines embedded into the ANSYS Finite Element program.

The traditional way of designing a wing structure is based on a trial and error procedure, and in most of the time this procedure involves the participation of different groups in a company. As soon as the wing shape is determined, the structural sizing of wing structural components is performed by the stress group of the company based upon multiple criteria (stress, buckling, aeroelastic considerations, etc.).

Structural design is usually limited to an adequate design that meets the major requirements of the problem. For a number of load cases, the wing structure is analyzed until multiple design criteria are satisfied. The design process ends up with a design that meets the major structural constraints. However, in this design process the final design may not be the optimum design.

Minimum weight design is an important issue in airframe design process since reduction in weight results in a high performance and cost effective flight vehicle. More formal ways of structural design is needed in order to ensure that the resulting design satisfies

the minimum weight criterion; in addition to that, all the other structural criteria should also be satisfied.

Structural optimization has been efficiently applied to airframe structural design, in particular to wing structural design by many researchers. The structural optimization is a highly automated process which starts with an initial prediction to the optimum design. The initial design is first analyzed for the design requirements and results are evaluated and necessary design changes are made. The resulting design is analyzed again, and process loops until the optimum design is reached.

1.1 CRUISE MISSILES

Cruise Missiles are tactical missile systems that are used for critical, long range and precision strike missions against high value targets. After they are launched from a platform, these missiles are accelerated up to their cruise flight conditions with the aid of their solid propellant boosters. The thrust needed for the cruise phase is supplied from a turbojet or turbofan motor depending on the required range. Typical high technology long range cruise missile design consists of a turbofan engine which gives higher values of specific impulse when compared to a turbojet system and a wing which increases the lift-to-drag ratio of the vehicle. The wing of the cruise missile must have sufficient strength to withstand several loading scenarios. The minimum weight design of both cruise missile fuselage and wing is important since reduction in the structural weight of the missile leads to an increase in the useful payload that can be carried. A photograph of the Tomahawk Cruise Missile is shown in Figure 1.1.

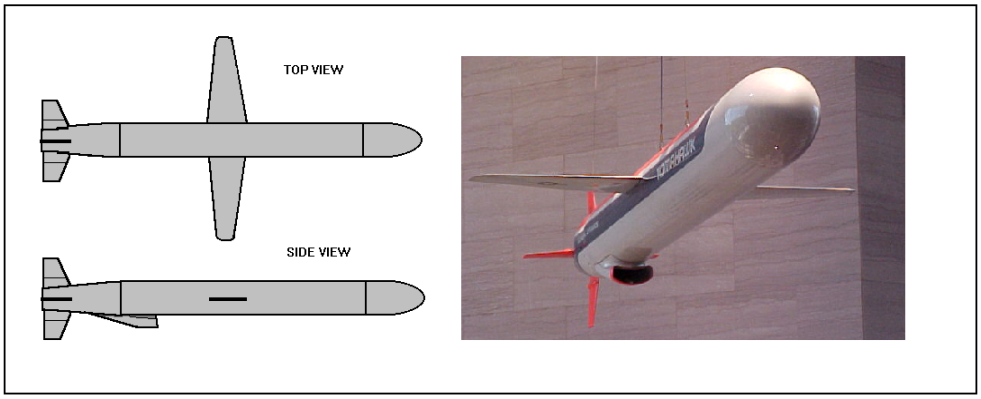

Figure 1.1 Tomahawk cruise missile.

1.2 WING DESIGN

A wing is essentially a beam, which gathers and transmits all of the applied airload to the central attachment to the fuselage. As soon as the basic wing shape has been decided, a preliminary layout of the wing structure must be indicated to a sufficient strength, stiffness and lightweight structure with a minimum of manufacturing problems [1].

A wing is composed of many structural elements, as shown in Figure 1.2. Wing structure needs longitudinal members to withstand bending loads which occur during flight. It is a decision made by the designer whether a large percentage of the bending load is carried by the spars or by the skin. In situations where the decision making does not depend on more critical issues, it is more advantageous to use the skin as the primary bending material since it has to be there being a torsion material as well. In addition to the wing skin, spars also resist torsional loading on the wing [1].

During flight, aerodynamic loads on a wing bend it upwards; as a result, the upper side of the wing is loaded in compression and buckling becomes a problem at these regions. Stiffeners attached to the skin increase the wing skin resistance to buckling.

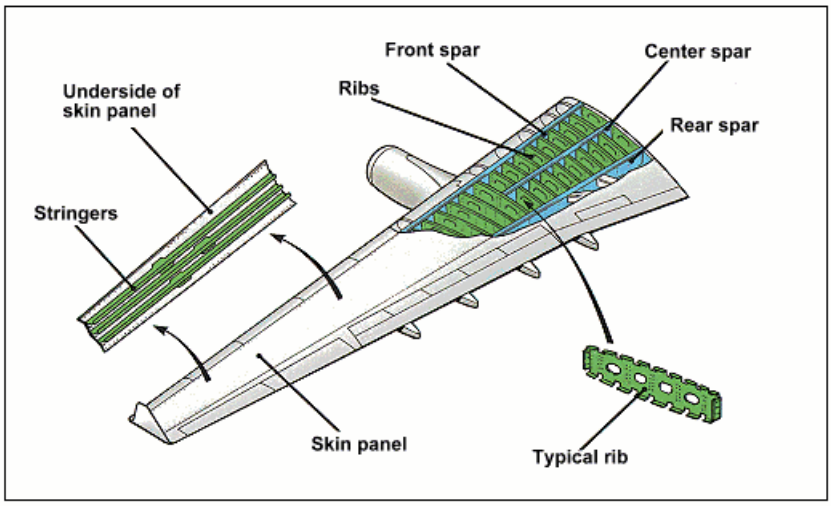

Figure 1.2 Wing structural components.

Aerodynamic contour of a wing has to be maintained without appreciable distortion. Wing ribs are used to contour the wing skin to the desired aerodynamic shape and maintain it. In addition, wing ribs are responsible for transferring surface air loads to the cellular beam structure. To transfer large concentrated loads into cellular beam structure, heavy ribs (bulkheads) are used [2].

1.3 FINITE ELEMENT METHOD FOR STRUCTURAL ANALYSIS AND DESIGN

In the absence of powerful computing resources and strong numerical methods like the finite element method (FEM), most of the wing stress analysis depended on the flexural beam theory which uses simplifying assumptions (see [2] for detailed wing stress analysis methods).

Today, wing structures consisting of spars, ribs, skin panel and stiffeners with arbitrary loading conditions, can be easily modeled and solved using the finite element method. In the finite element method, a wing structure is divided into finite elements and the problem is solved for each and every one of them. By this way the governing partial differential equation turn into a set of algebraic equations. The solution of these equations gives the entire displacement field under the action of applied loads and boundary conditions.

1.4 OPTIMIZATION OF COMPOSITE STRUCTURES

Structural designers seek the best possible design. In the case of aerospace structures the best possible design would be the one that satisfies the strength and stiffness requirements with minimum weight. Traditionally structural engineer first looks for a sufficient design that meets the major requirements of the problem, and makes necessary changes in the design to make it structurally efficient and light. In the case of a designer with limited experience such a way to design a structure may require large amount of iterations that makes the design procedure cumbersome.

Over the past two decades, mathematical optimization, which deals with either the maximization or minimization of an objective function subject to constraint functions, has emerged as a powerful tool for structural design [3]. On the other hand the use of composite materials such as Glass/Epoxy and Carbon/Epoxy has become widespread in the aerospace industry due to their high strength to weight ratios.

Optimization of composite structures is expensive to perform, with computational costs depending on three indices of complexity namely, modeling complexity, analysis complexity, and optimization complexity, as shown in Figure 1.3.

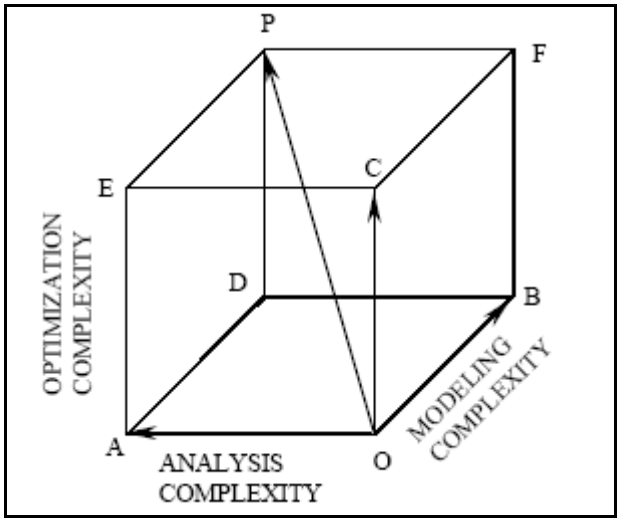

Figure 1.3 Schematic showing types of complexity encountered in composite structure optimization [4].

Since designers have finite resources, it has been impossible to solve problems with the most complex models, analysis and optimization simultaneously. Hence much of the literature can be found on one of the coordinate planes in Figure 1.3. For example complex optimization is often applied to problem of laminate design with displacement or stress constraints where the model and analysis are simple. Conversely, simple local optimization has often been used for complex models, requiring a detailed finite element analysis [4].

Modeling complexity is related with the choice of modeling the structural problem. For unstiffened and uniformly stiffened composite panels one can apply simplifying assumptions like orthotropic material properties and solve the governing equations for simple loading conditions. For example, [5] gives practices for predicting buckling of uniform stiffened and unstiffened isotropic/orthotropic shells under various loading conditions. In the case of a wing structure with composite skin panels and stiffeners subject to arbitrary loading conditions, the structure has to be modeled with finite elements.

In terms of analysis complexity, linear elastic analysis is the simplest, and it is convenient to measure other types of analysis by their cost relative to the linear analysis. This is particularly meaningful since often more complex analysis, such as nonlinear elastic analysis and, linear buckling analysis, or dynamic response analysis use linear analysis as a repeating step [6].

In terms of optimization complexity the most complex and expensive problems are reliability based optimization problems, and the easiest problems are the optimization of a laminate stacking sequence using lamination parameter graphs [4].

The optimization of wing box structures made up of composite laminates has been an interesting problem. As early as 1973, Khot and Venkayya [7] developed an optimization method, which is based on constraint gradients, to optimize cantilever composite wing structure. The spars and panels were idealized by bars and shear panels and the top and bottom skin were idealized by membrane elements. The two design variables were the thicknesses of shear panels/membrane elements and the area of the rod elements. Later they also present a method based on optimality criterion for

designing minimum weight fiber reinforced composite structures with stress and displacements constraints. They solved the structural problem with finite elements and used 80 composite elements consisting in three layers with fiber orientations 0^o, 45^o,-45^o directions [8].

Haftka and Starnes [9] used Sequential Unconstrained Maximization/Minimization Technique (SUMT) with a quadratic extended exterior penalty function to obtain minimum mass design of structures subjected to stress, strain and displacement constraints. By introducing the design constraints as penalty functions, the SUMT method transformed a constrained optimization problem into an unconstrained optimization problem. They applied the optimization procedure to a high aspect ratio graphite/epoxy composite wing consisting of ribs, spars and cover panels. The wing was subjected to a uniform pressure loading and a concentrated engine load. The cover panels of the structural box consisted of composite material with 0^o, 90^o, 45^o and -45^o ply orientations and are represented by 192 finite elements. The ribs and spars consisted of $\pm 45^o$ material and were represented by 98 shear web elements. The high aspect ratio wing was studied using 13, 25, 32, 50, 74 and 146 design variables. Later on they used the same technique and introduced wing twist and panel buckling constraints to the problem [10].

Liu and Lin [11] combined the finite element method with a refined optimality criterion method and optimized an aluminum triple spar wing structure under two independent loading conditions. Displacement constraints were imposed on the tip in the transverse direction while size and stress constraints were imposed on all elements. The minimum weight was found to be 42.28 kg with a 25.4 cm tip displacement constraint and reduced to a minimum weight of 35.2 kg when the tip constraint was released to a value of 35.2 cm. Buckling constraints were also added as a third case which leaded to a minimum weight of 34.88 kg.

The composite version of the three spar wing configuration was optimized by the same method [12]. The wing structure was idealized by membrane quadrilaterals, shear panels and bars. The top and the bottom skin were graphite/epoxy layered elements with 0^o, 90^o and $\pm 45^o$ fibers. The spars and ribs were idealized by aluminum shear panels. Three

different constraint conditions were investigated in which stress, local buckling and twist constraints were imposed on the wing design.

Nagendra and Fleury [13] presented the capabilities of MSC/NASTRAN in optimizing the composite structures. The optimization algorithm was based on a dual approach in which the constrained problem was replaced by maximizing an unconstrained dual function and used the convex linearization scheme. They demonstrated the capabilities of the program by optimizing a delta wing structure with graphite epoxy skins and titanium webs subjected to pressure and temperature loading.

Yurkovich [14] applied Taguchi technique coupled with ASTROS code in order to optimize wing structures and determined wing external and internal geometry for minimum wing weight. He used seven design parameters but eventually realized that the number of spars and ribs were not significant parameters in determining the weight of the wing. In this study buckling was not taken into account.

Röhl, Mavris and Schrage [15] also used ASTROS for structural optimization of a High Speed Civil Transport (HSCT) wing in a multilevel decomposition approach. With the help of ASTROS structural optimization tool, the wing structure was sized subject to strength, buckling and aeroelastic constraints.

Liu, Haftka and Akgün [16, 17] proposed a two-level wing design optimization subjected to strength and buckling constraints. They considered an unswept, untapered wing box with four spars and three ribs made of graphite-epoxy. The wing box was clamped at the root and subjected to a distributed tip load. In the wing-level optimization, the objective function was the structure weight and the continuous design variables were the ply thicknesses with orientations of 0^o, 90^o and $\pm 45^o$ for each panel. In the panel-level, symmetric and balanced stacking sequence optimization of the wing panels was accomplished to maximize the buckling load by the use of a permutation genetic algorithm (GA). A response surface was then fitted to the optimum buckling load as a function of number of 0^o, 90^o and $\pm 45^o$ stacks and In-plane loads. The resulting response surface was used for the wing-level optimization. Later, Liu and Haftka [18] imposed continuity constraints and demonstrated the tradeoffs between weight and continuity using the same composite wing example.

In the case of composite materials a designer can change either the ply thicknesses or the ply orientation angles to achieve the desired material strength. The optimization ply angles, which are usually restricted to a small set of discrete angles (0^o, 90^o and $\pm 45^o$), can be achieved by the use of GA's. Liu, Haftka, Akgün and Todoroki [19] developed a gene-ranked GA and used this method in the panel level optimization of a composite wing box [16, 17].

Kapania and Chun [20] used a simple beam-type structural model and a conjugate gradient/steepest descent type optimization method to determine the structural weight of a wing box, subjected to a twist constraint, to carry aerodynamics loads for a wing in transonic flow field.

Engelstad *et al.* [21] compared three different optimization strategies used in the minimum weight design of an F/A 22 horizontal stabilizer structure. The horizontal stabilizer was a rib stiffened all composite design with honeycomb edges.

CHAPTER 2

LOADS ACTING ON THE CRUISE MISSILE WING

2.1 INTRODUCTION

Before the structural design of a wing can be made, the external forces acting on the wing must be known. The main design flight conditions for the cruise missile can be prescribed by stating the limiting values of acceleration and speed. In graphical form, design requirements can be represented by plotting load factor (n) versus flight velocity to obtain a diagram as shown in Figure 2.1. This diagram is generally referred to as V-n diagram.

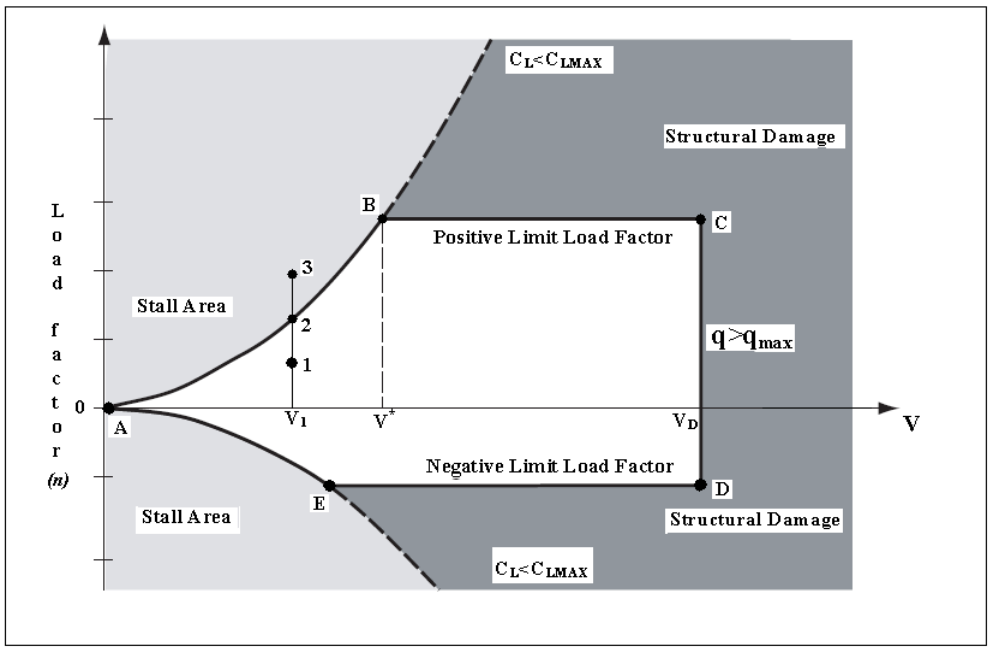

Figure 2.1 V-n diagram.

In level unaccelerated flight, the wing produces sufficient lift to balance the weight of a cruise missile. When a cruise missile has to make a maneuver, additional loads are created. The amount of additional load depends on the severity of the maneuvers and is measured in terms of load factor [1]. Load factor is defined as follows where $q=\rho V^2/2$ is the dynamic pressure:

$$n = \frac{L}{W} = \frac{qSC_L}{W} \tag{2.1}$$

The V-n diagram, once constructed for a particular flight vehicle, involves valuable information about aerodynamic and structural limits of the flight vehicle.

At low speeds maximum load factor (n_{max}) is a function of the maximum lift coefficient ($C_{L,max}$). The equation of the curve AB in Figure 2.1 can be found by plugging $C_{L,max}$ in Equation (2.1).

At speed V_1, flight vehicle can have three possible angle of attack values. At point 1, the flight vehicle has a low angle of attack value and the resulting load factor is smaller than the maximum load factor at this speed. At point 2, the flight vehicle has an angle of attack value sufficient to obtain $C_{L,max}$ and the load factor is maximum. It is not possible for the flight vehicle to fly at a higher angle of attack at this speed (point 3) since a further increase in angle of attack results in stalling of the wing.

Maximum load factor increases with velocity up to a certain speed (V^*) and beyond that speed structural damage may occur in the structure. At velocities higher than V^* the flight vehicle has to fly at a C_L value less than $C_{L,max}$ which is dictated by the limit load factor of the flight vehicle. Again the velocity can increase up to a certain limit beyond which structural damage occurs due to very large dynamic pressures. This limiting speed is called the design dive speed (V_D) and it is the maximum speed for the structural design. It is a statistically determined speed sufficiently greater than the cruising speed to provide for safe recovery from inadvertent upsets [1]. The design dive speed is generally taken as 1.2-1.5 times the cruise speed of the flight vehicle [1, 2, 22, 23, and 24].

In Figure 2.1, the points B and C correspond to Positive High Angle of Attack (PHAA) and Positive Low Angle of Attack (PLAA) flight conditions respectively, and points E and D correspond to Negative High Angle of Attack (NHAA) and Negative Low Angle of Attack (NLAA) flight conditions respectively. These conditions represent symmetrical flight maneuvers; i.e., there is no motion normal to the plane of symmetry of the flight vehicle [22].

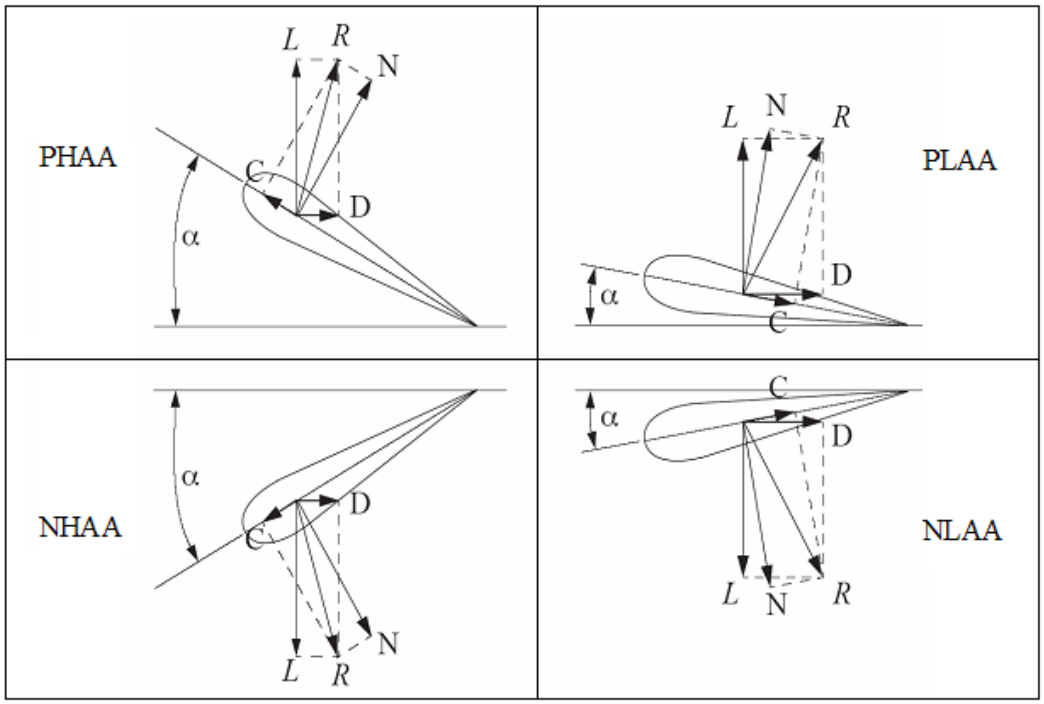

Figure 2.2 Forces acting on the wing for each flight condition.

Bending moments created by the normal forces (N) shown in Figure 2.2 produce compressive stresses on the upper side of the wing in the PHAA and PLAA conditions, on the bottom side of the wing in the NHAA and NLAA conditions. On the other hand, bending moments created by the chordwise forces (C) produce compressive stresses on the leading edge of the wing in the PHAA and NHAA conditions, on the trailing edge of the wing in the PLAA and NLAA conditions. Each of these four flight conditions produces the highest load somewhere on the wing as shown in Figure 2.3 [22].

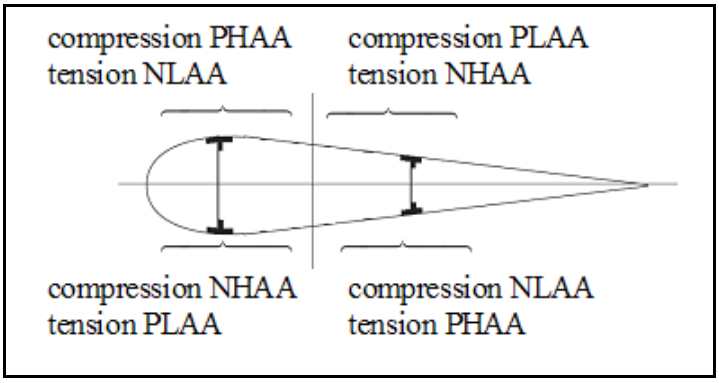

Figure 2.3 Critical locations on the wing for each flight condition.

Generally speaking, if the flight vehicle is designed for the air loads produced by the velocity and acceleration conditions at points, B, C, D and E, it should be safe from a structural strength viewpoint if flown within the specified limits regarding velocity and acceleration [2].

2.2 CONSTRUCTING THE V-N DIAGRAM

The cruise missile wing has a basic trapezoid shape, an aspect ratio of 6.0, a taper ratio of 0.5, leading edge sweep angle of 6.34^{o} and NACA 64A208.2 airfoil profile [25]. The wing planform considered in this study is shown in Figure 2.4.

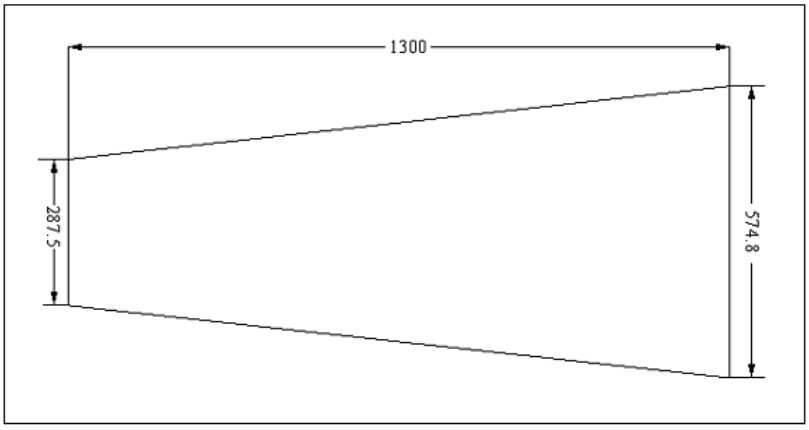

Figure 2.4 Cruise missile wing planform (All dimensions are in mm's).

As a starting point for constructing the V-n diagram for the cruise missile wing, the velocity is chosen as 238.5 m/s which corresponds to Mach 0.7 at sea level conditions for the PHAA and NHAA flight conditions. At this Mach number and sea level conditions, Computational Fluid Dynamic (CFD) analyses of the wing are performed for different angles of attack using the CFD-FASTRAN program. Then, the negative and positive stall angle of attack values are predicted by solving the Reynolds Averaged Navier Stokes Equations with Spalart-Allmaras turbulence model.

The CFD solution domain is a rectangular prism with dimensions 30x30x16 m. The solution domain consists of 1,276,697 hexahedral cells and 5,000 surface elements. The mesh spacing in the normal direction to the surface is $2x10^{-6}$ m for turbulent flow calculations. The CFD solution domain and the surface mesh are given in Figure 2.5.

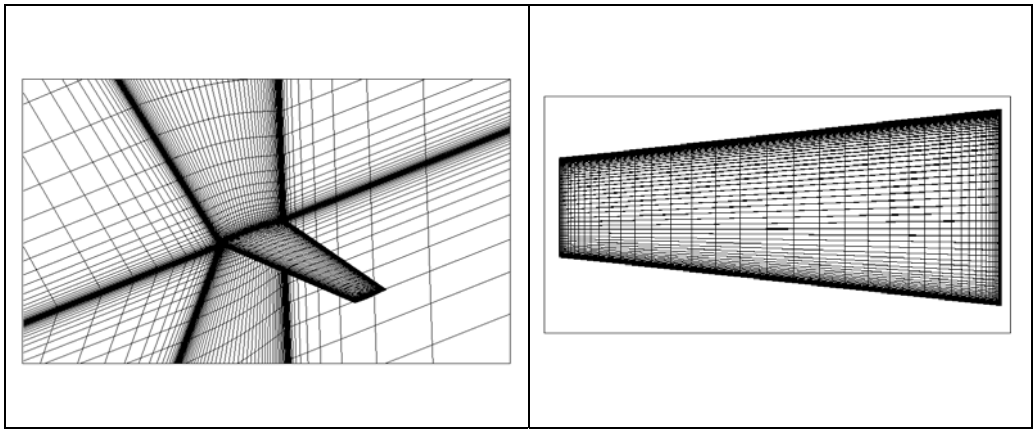

Figure 2.5 CFD solution domain and wing surface mesh.

After performing several analyses for different angles of attack, the lift coefficient (C_L) versus angle of attack (α) curve is constructed. C_L-α curve is given in Figure 2.6, where lift coefficient is calculated using the following formula:

$$C_L = \frac{L}{q.S} \tag{2.2}$$

The C_L-α graph obtained from Euler solutions is also given in Figure 2.6 for comparison. As expected, the stall phenomenon can not be predicted by solving Euler equations. But it can be seen that at small angles of attack, the C_L-α graph is nearly same for the viscous and inviscid solutions.

Comparison of u velocity contours at 25%, 50% and 75% spanwise locations for $\alpha=7^o$ and $\alpha=8^o$ is given in Figure 2.7 and for $\alpha=-4^o$ and $\alpha=-5^o$ is given in Figure 2.8. u velocities are the velocity components in chordwise direction and the regions with negative velocities ($u\leq 0$) in these figures are the regions of separated flow.

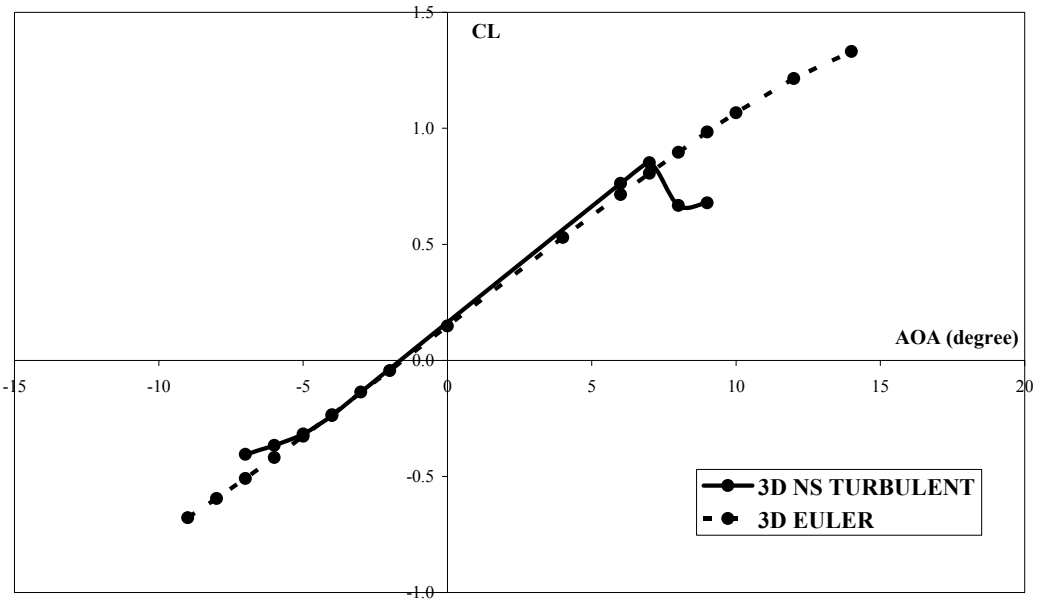

Figure 2.6 Lift coefficient versus angle of attack graph for M=0.7.

The stall angle of attack is predicted when one of the two conditions is provided: the decrease of C_L and flow separation. At M=0.7, the positive stall angle of attack is found as 8^o and the negative stall angle of attack is found as -5^o. After $\alpha=7^o$ C_L decreases, but after $\alpha=-4^o$ C_L continues to increase (Figure 2.6). However, flow separation occurs beyond both of these angles of attack and it is more severe in board of 75% spanwise location (Figure 2.7 and 2.8). Downwash effects caused by the vorticies occurring at the tip of the wing prevents the flow separation at these regions.

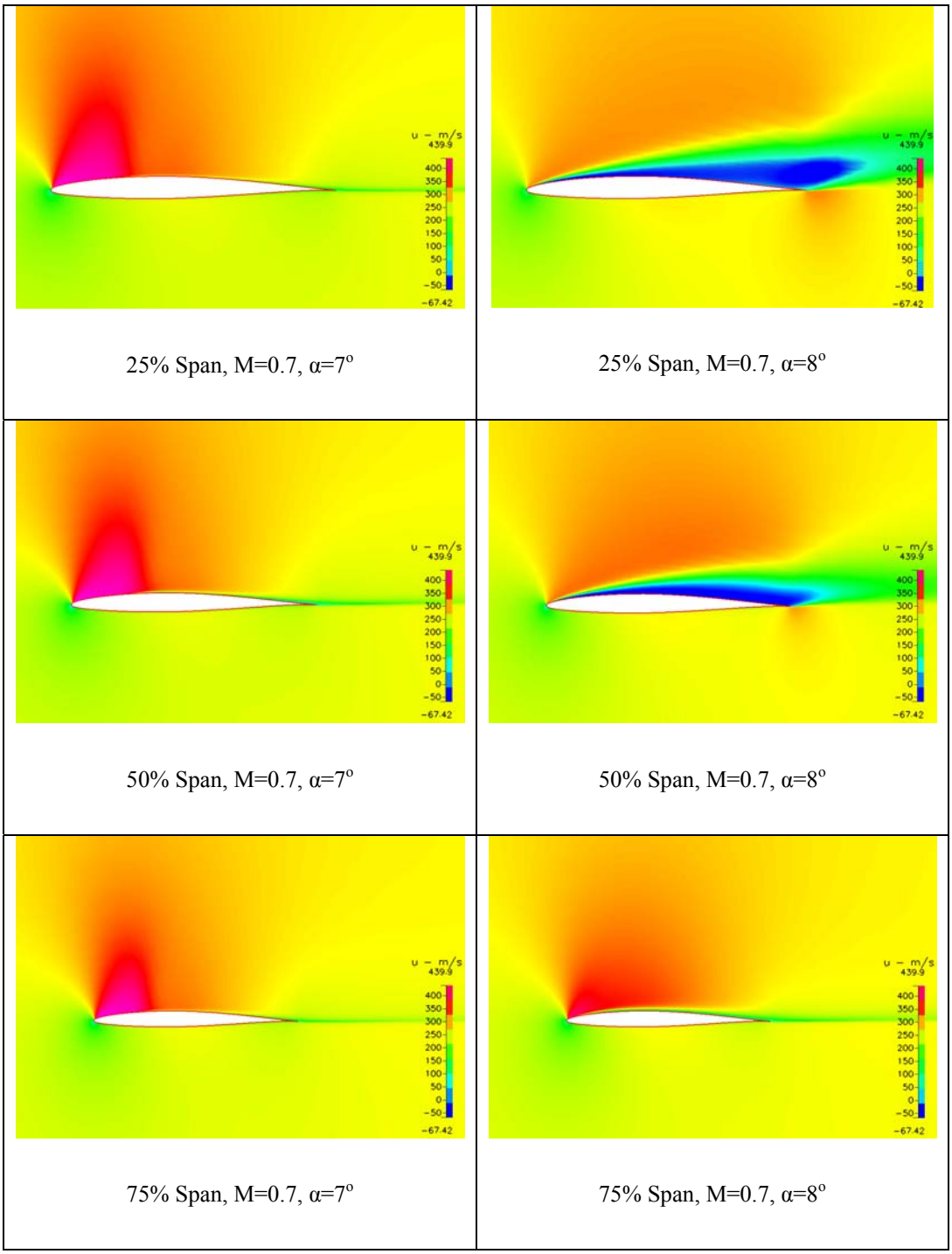

25% Span, M=0.7, α=7^o | 25% Span, M=0.7, α=8^o

50% Span, M=0.7, α=7^o | 50% Span, M=0.7, α=8^o

75% Span, M=0.7, α=7^o | 75% Span, M=0.7, α=8^o

Figure 2.7. Comparison of u velocity contours at different spanwise locations for M=0.7 α=7^o and M=0.7 α=8^o.

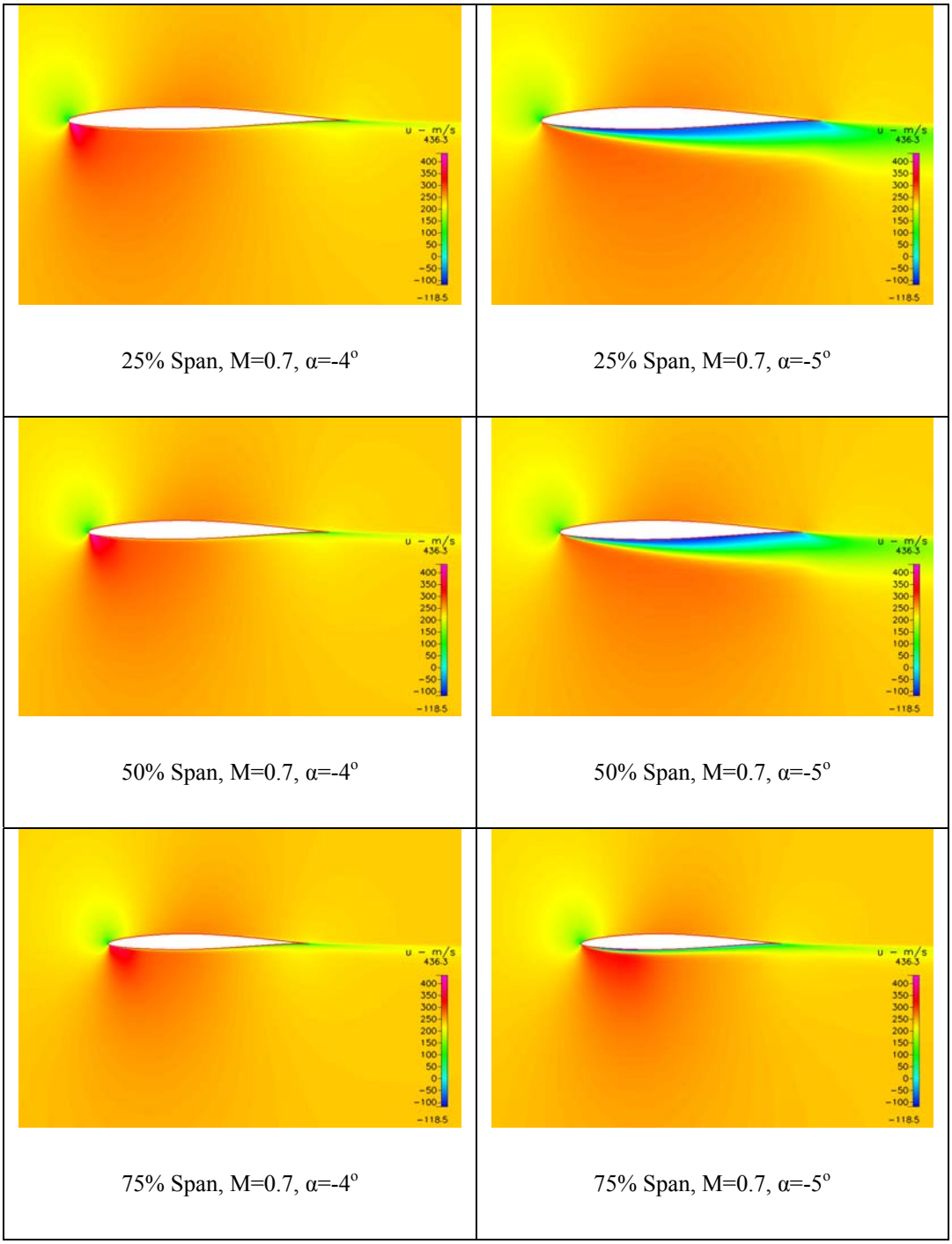

25% Span, M=0.7, α=-4^{o} | 25% Span, M=0.7, α=-5^{o}

50% Span, M=0.7, α=-4^{o} | 50% Span, M=0.7, α=-5^{o}

75% Span, M=0.7, α=-4^{o} | 75% Span, M=0.7, α=-5^{o}

Figure 2.8 Comparison of u velocity contours at different spanwise locations for M=0.7 α=-4^{o} and M=0.7 α=-5^{o}.

From Figure 2.9 and 2.10, it is seen that the pressure coefficient distribution differs for α=7° and α=8° especially for upper surface and for α=-4° and α=-5° especially for bottom surface where the flow separates. Furthermore occurrence of shock, which is a sudden reduction of Mach number and increase of pressure, vanishes for the regions where flow separates. Pressure coefficient is calculated using the following formula where P_∞ is the atmospheric pressure:

$$C_P = \frac{P - P_\infty}{q} \tag{2.3}$$

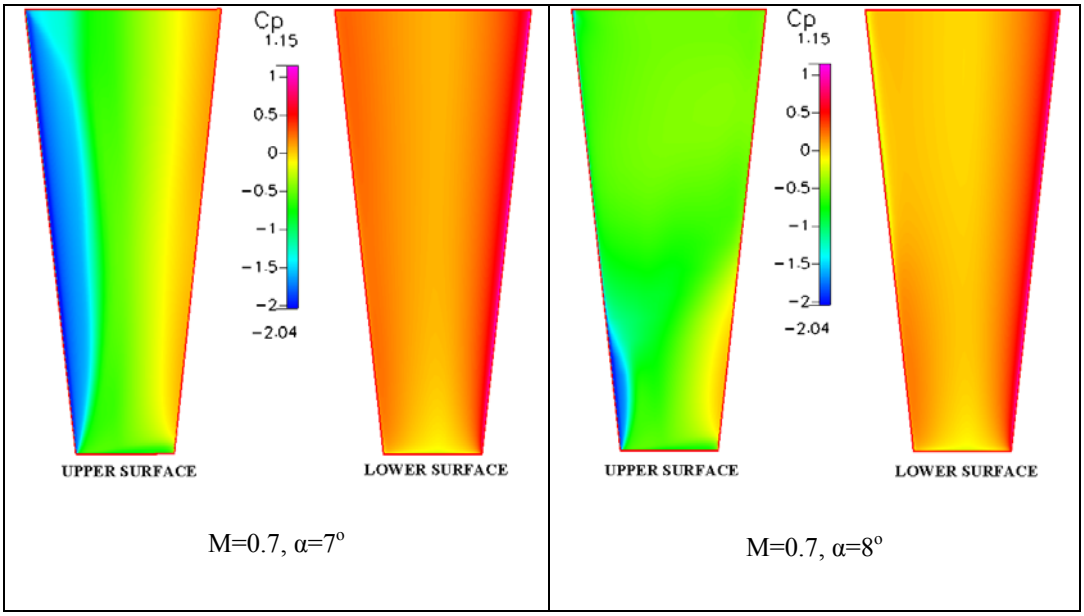

Figure 2.9 Comparison of pressure coefficient distribution for M=0.7 α=7° and M=0.7 α=8°.

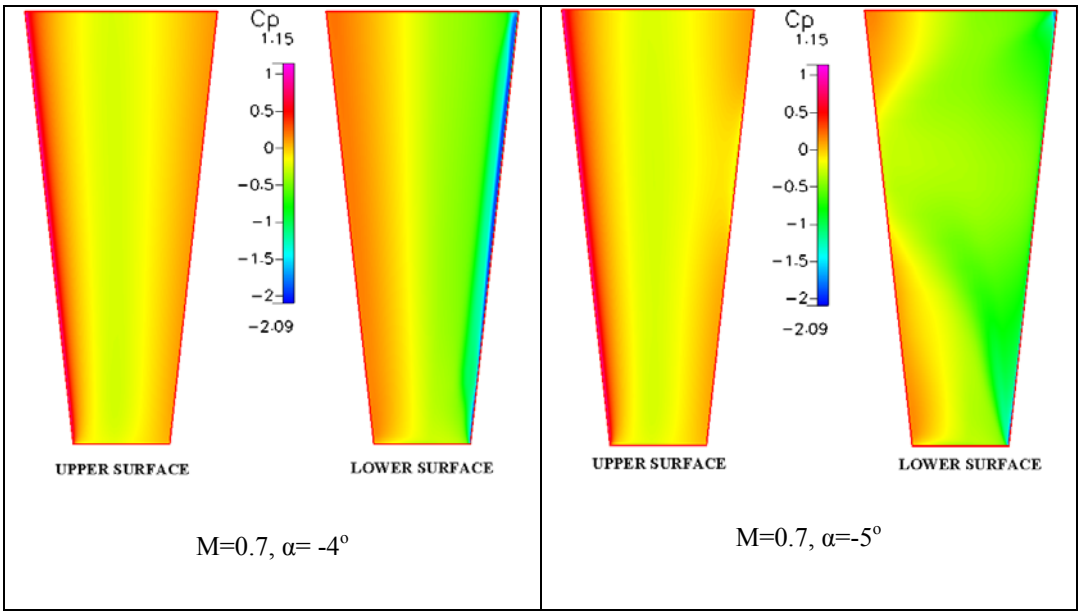

Figure 2.10 Comparison of pressure coefficient distribution for M=0.7 α=-4° and M=0.7 α=-5°.

Angles of attack just before stall are taken as the PHAA and NHAA which are 7° and -4°, respectively. Lift coefficients at M=0.7 corresponding to -4° and 7° angles of attack are found as -0.24 and 0.85 for the cruise missile wing. The load factors, using these lift coefficients and a weight (W) of 1200 kg in Equation (2.1), are calculated as -0.8 and 2.8.

Rooney and Craig [25] found the aerodynamic coefficients by analytical predictions, sub-scale and full scale wind tunnel tests and flight tests over the Mach number range 0.45 to 0.83 for the same cruise missile geometry considered in this study. Lift coefficients at M=0.7 corresponding to -4° and 7° angles of attack were found as -0.4 and 0.85 from the flight test results.

The lift coefficient for α=7° at M=0.7 found in this study is the same as the lift coefficient for α=8° found in [25]. The lift coefficient for α=8° is found as 0.67 in this study. The lift coefficient for α=-4° at M=0.7 is smaller in magnitude than the lift coefficient for the same condition found from the flight test results in [25]. But it is satisfactory to see that the results are comparable since only the wing is modeled and some geometrical properties given in [25] are disregarded in this study. The disregarded

geometrical properties for the wing are the 1.716^{o} incidence at wing station (W.S.) 10 (10 inch from the root), -4^{o} twist about trailing edge from W.S. 10 to W.S. 50.91 and 2.747^{o} dihedral at the trailing edge.

Besides M=0.7, CFD analyses are performed for M=0.6 also to compare the maximum positive load factors. It is found that after $\alpha=6^{o}$, lift starts to decrease and flow separates for M=0.6. At this speed the lift coefficient for $\alpha=6^{o}$ is calculated as 0.68 which corresponds to a load factor of 1.7. This result is also consistent with [25], in which $C_{L,max}$ versus M graph is given (without exact numerical values). From [25], it is known that the cruise missile can experience a load of 2.8g, hence it is verified that taking M=0.7 for the PHAA and NHAA condition is an appropriate decision.

After determining the positive and negative load factors to determine the PLAA and NLAA points (point C and D in Figure 2.1), dive speed is chosen as Mach 0.95 which is 1.3 times the cruise speed of the cruise missile (M=0.72). At this Mach number and sea level conditions, CFD analyses of the wing are performed for different angles of attack until the load factors obtained are the same as the load factors for PHAA and NHAA conditions. The angles of attack, which create -0.8 and 2.8 load factors at M=0.95 are found as -1.3^{o} and 4.2^{o}, respectively.

In Figure 2.11, Mach number distribution is given for PLAA and NLAA flight conditions. At these flight conditions, shock occurs both at the top and bottom of the wing. Furthermore, there is a small region of flow separation at the trailing edge. But this region is not so widespread to affect the flight performance of the cruise missile. Pressure coefficient distributions for these flight conditions are given in Figure 2.12.

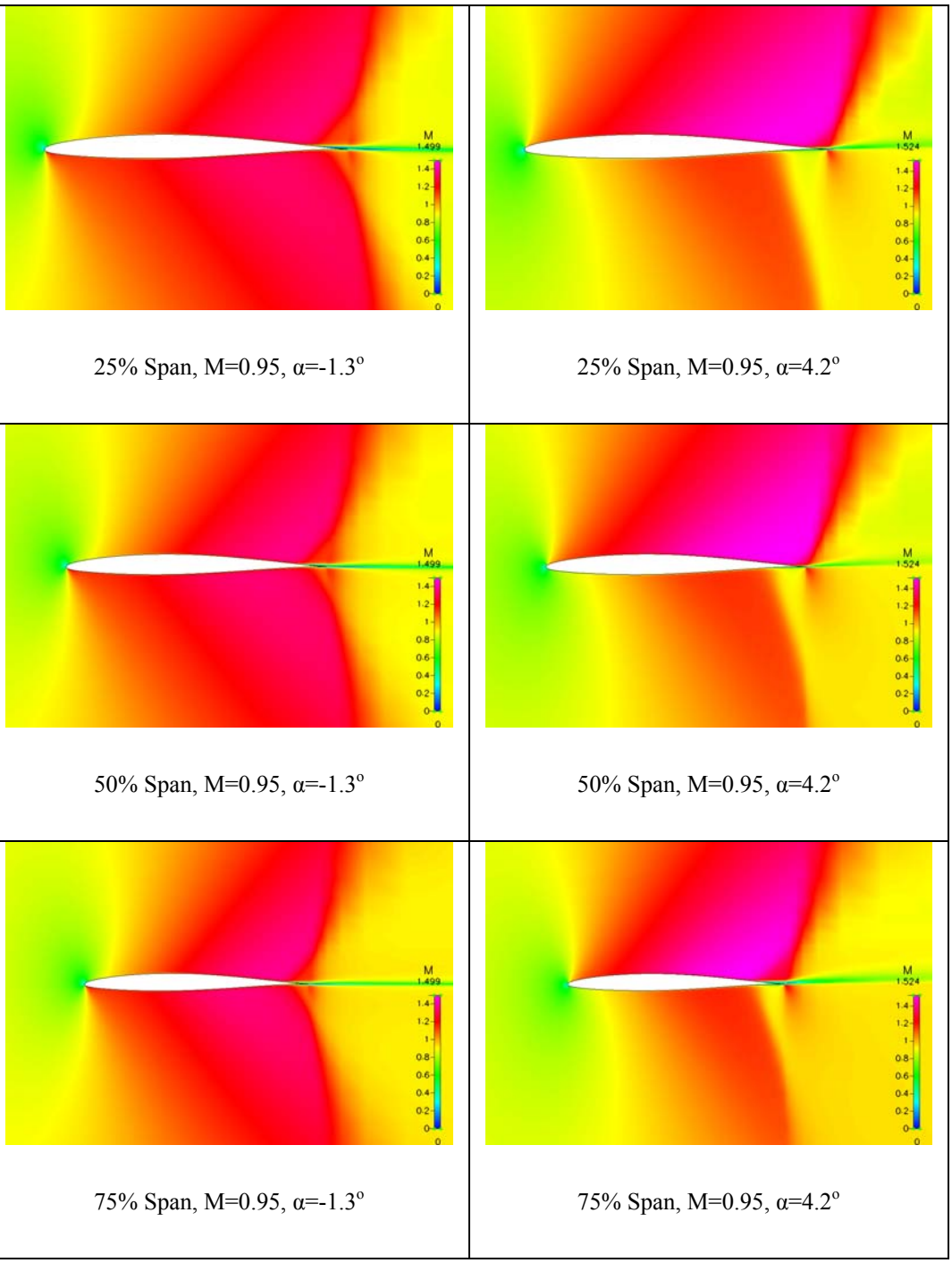

Figure 2.11 Mach Contours at different spanwise locations for M=0.95 α=-1.3° and M=0.95 α=4.2°.

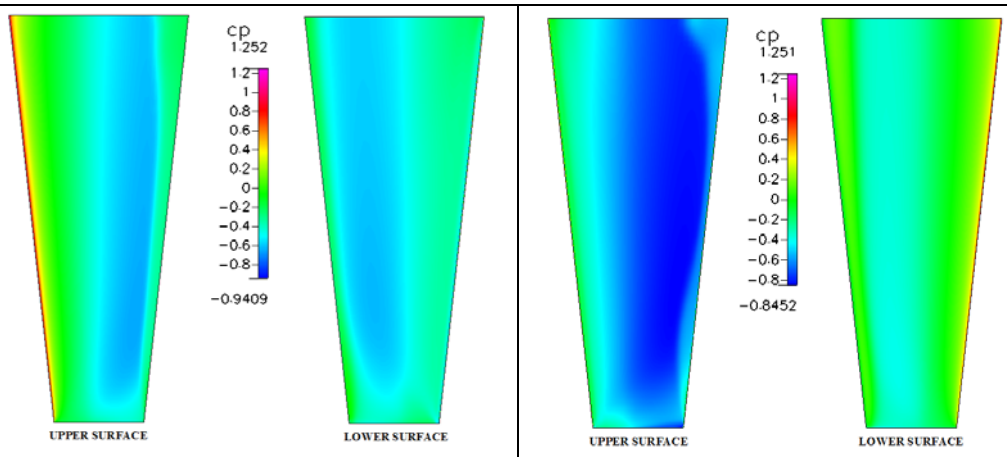

M=0.95, α= -1.3^{o} | M=0.95, α=4.2^{o}

Figure 2.12 Pressure coefficient distribution for M=0.95 α=-1.3^{o} and M=0.95 α=4.2^{o}.

After determining the four critical flight conditions, V-n diagram is constructed as shown in Figure 2.13. The parabolic lines are constructed for illustration purposes only by using the value of $C_{L,max}$ and $C_{L,min}$ for M=0.7 in Equation (2.1). In reality, values of $C_{L,max}$ and $C_{L,min}$ change with velocity.

In general, some modifications to V-n diagram are made to account for gust loads which can increase angles of attack. But since cruise missiles are one-shot flight vehicles and large gust speeds occur rarely, gust effect is ignored in this study.

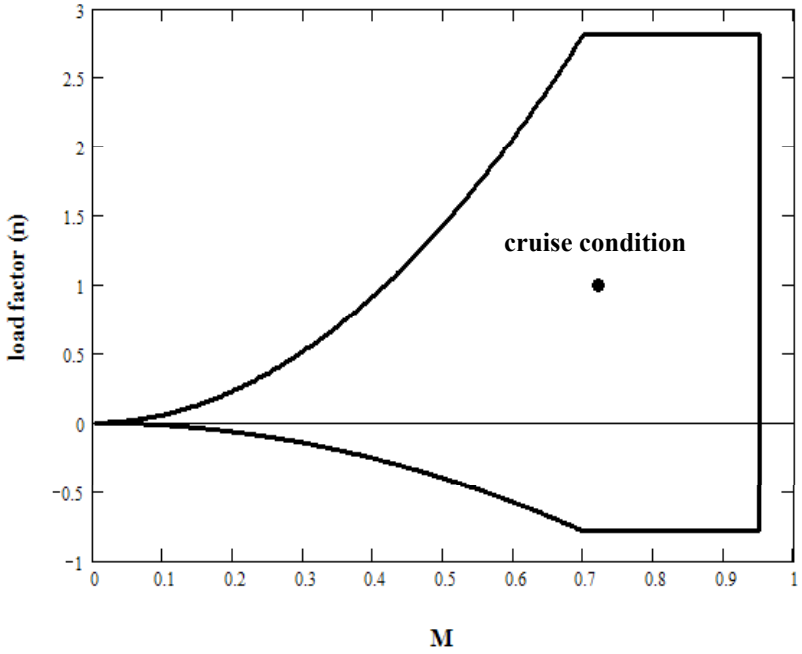

Figure 2.13 V-n diagram for the cruise missile.

2.3 LOAD TRANSFER METHOD

In order to perform structural analyses for different flight conditions, aerodynamic pressure data obtained from FASTRAN should be transferred to the finite element model. Since the fluid and the structural meshes do not match at the wing surface, pressure data must be expressed as a function or in a tabular fashion to be able to transfer the pressures from CFD nodes to the finite element nodes.

A code written in MATLAB is used to arrange the pressure data in a tabular fashion. This code creates a rectangle which covers the wing surface, creates nodes by dividing the rectangle into equal cells and evaluates the pressure values with linear interpolation at the new nodes. If a node is outside the boundary of the surface, the pressure value of the nearest node at the wing surface is given. This procedure is repeated for upper skin, bottom skin and tip of the wing for each of the four flight conditions. Then, the location and pressure data created by MATLAB is read into ANSYS and a pressure table is created for each surface of the wing.

To verify the sufficiency of the load transfer method, the total force perpendicular to chordwise direction (F_y) obtained from FASTRAN is compared with the total force obtained from ANSYS. The mesh in MATLAB is chosen to minimize the percent error in F_y. For the upper and bottom skins, a 65x65 mesh for the PHAA, NHAA and NLAA flight conditions, and a 66x66 mesh for the PLAA condition are created in MATLAB. For the tip rib, 49x49 mesh is created for all of flight conditions. The reason for choosing F_y for comparison is the dominance of it over the forces in other directions.

For the four critical flight conditions, the percent error in F_y for different element sizes in ANSYS is given in Table 2.1. The computational times for stress and buckling analyses for different element sizes are also given in Table 2.1. These analyses are performed for the aluminum wing for one flight condition using a personal computer with 3 GHz Intel-Pentium processor and 2 GB of RAM.

As the element size decreases, percent error in F_y decreases, but the increase in computational time for the analyses are much higher especially when the element size is smaller than 20 mm. Since too many analyses have to be performed for optimization and small element size will increase optimization time, element size is chosen as 40 mm for the skin panels and 30 mm for the spar and rib webs.

Table 2.1 The percent error in the total force perpendicular to chordwise direction.

Element size	**% Error in F_y**				**Time (seconds)**	
	PHAA	**NHAA**	**PLAA**	**NLAA**	**Stress Analysis**	**Buckling Analysis**
10 mm	1.42	3.98	0.85	2.48	225	395
20 mm	2.07	6.82	1.33	4.72	28	77
30 mm	3.42	10.76	2.34	6.63	12	21
40 mm	4.56	12.55	3.54	7.22	6	13

Wing surface mesh used in ANSYS with element size of 40 mm is given in Figure 2.14. It must be noted that the sizes of the elements are not actually 40 mm in the structural model. When an element size is defined in ANSYS, the number of divisions is

automatically calculated from the line length. Quotients of the division of line length to element size is rounded upward to next integer and taken as the number of divisions for that line. For example, if 40 mm element size is defined for an 81x120 mm rectangle, a 3x3 mesh is created on that area.

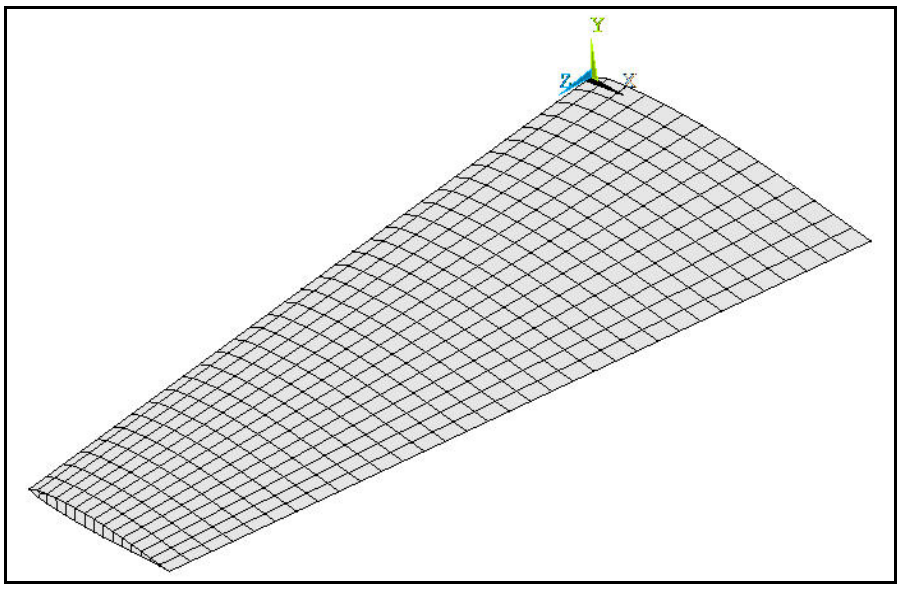

Figure 2.14 Wing surface mesh used in ANSYS with element size of 40 mm.

The occurrence of shock has a negative effect on the percent error in F_y, since it causes high gradients in pressure distribution. When the element size in ANSYS is increased, the possibility of catching the maximum pressure values decreases.

In Table 2.2, comparison of total forces and moments in all directions obtained from FASTRAN with the values obtained from ANSYS for the critical flight conditions is given. The coordinate system is the same for both models in FASTRAN and ANSYS as given in Figure 2.14. The structural model used has an element size of 40 mm. It can be seen that other forces and moments are also close to each other. The reason for higher percent errors in F_y in NHAA and NLAA conditions is because of relatively small values of F_y. Although the percent error in NHAA condition is the highest, the total force difference can be ignored.

Table 2.2 Comparison of total forces and moments in FASTRAN and ANSYS (Element size in ANSYS=40 mm)

	F_x (N)	F_y (N)	F_z (N)	M_x (N.mm)	M_y (N.mm)	M_z (N.mm)
			PHAA			
FASTRAN	-874	16618	-1418	-9421800	-133970	3204500
ANSYS	-874	15860	-1420	-8918555	-147549	3123262
			NHAA			
FASTRAN	-36	-4641	-1603	2615700	368300	-306700
ANSYS	-45	-4059	-1609	2275154	350635	-277611
			PLAA			
FASTRAN	1905	16675	-1377	-9351600	1381700	5090300
ANSYS	1915	16085	-1389	-8991225	1375126	4867998
			NLAA			
FASTRAN	1965	-4718	-1438	2468400	1439400	-569210
ANSYS	1939	-4377	-1450	2261601	1406833	-580058

The upper surface pressure distribution in FASTRAN, the distribution after transferring pressure data into MATLAB, and then to ANSYS for the NLAA flight condition can be seen in Figure 2.15. Although the contour settings are not exactly the same, the pressure distributions in the three programs seem quite agreeable. But the main justification for the sufficiency of the load transfer method comes from the comparison of the total forces and moments obtained from ANSYS and FASTRAN given in Table 2.1 and Table 2.2.

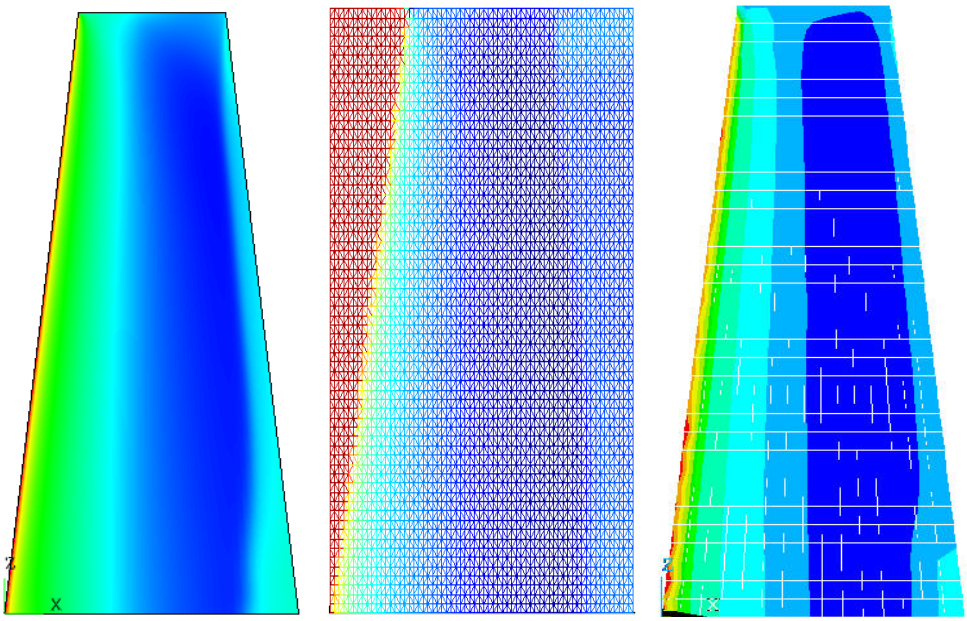

Figure 2.15 Comparison of upper surface pressure distributions in FASTRAN, MATLAB and ANSYS for NLAA flight condition.

CHAPTER 3

PARAMETRIC MODELING OF THE WING

3.1 INTRODUCTION

The finite element method is a numerical procedure that can be used to obtain solutions to a large class of engineering problems. ANSYS has many finite element analysis capabilities, ranging from a simple, linear, static analysis to a complex, nonlinear, transient dynamic analysis. The growing popularity of structural optimization as a tool for industrial applications is generating demand for the introduction of optimization capabilities into general-purpose analysis packages like ANSYS, NASTRAN and I-DEAS.

There are many advantages of using ANSYS as a basic Finite Element Analysis package for structural optimization. It integrates preprocessing, solution, postprocessing and optimization processors in one package and is a multi-physics analysis package for which coupled analysis is possible. It provides a very powerful macro language (APDL: ANSYS Parametric Design Language) and also provides interface to call external programs in macro language, which makes the interaction between the optimizer and the analysis easier.

In this study, weight minimization of a cruise missile wing is accomplished for both metal and composite wing configurations using the ANSYS finite element solver and optimization algorithms. In the first wing configuration all the structural members are made up of aluminum. In the second wing configuration the skin panels are all composite and other members (spars, ribs, spar caps and rib caps) are made up of aluminum.

In order to perform optimization analyses in ANSYS, a parametric model for the cruise missile wing must be built. In the parametric model, the quantities to be used as optimization variables (design variables, state variables and objective function) must be available as parameters. By the use of APDL, ANSYS command input files for the two wing configurations are written using a text editor.

In this chapter, after brief information about finite element method and optimization procedures in ANSYS, modeling details, boundary conditions, loading types and optimization variables for wing configurations are presented.

In ANSYS, as the number of design variables increases it gets more difficult to obtain a global optimum. For this reason, it is important to keep the number of design variables as low as possible. So techniques used for decreasing the number of design variables are also presented.

3.2 FINITE ELEMENT ANALYSIS

3.2.1 ANSYS Parametric Design Language

The finite element method is a numerical procedure for analyzing structures and continua. Usually the problem is too complicated to be solved satisfactorily by classical analytical methods. The finite element procedure produces many simultaneous algebraic equations, which are generated and solved on a digital computer [27].

ANSYS is one of the commercial packages which is used to solve structural mechanics problems. The easiest way to communicate with ANSYS is by using the ANSYS menu system, called the Graphical User Interface (GUI). The GUI consists of windows, menus, dialog boxes, and other components that let you enter input data and execute ANSYS functions simply by picking buttons with a mouse or typing in responses to prompts. Another way to communicate with ANSYS is to use the ANSYS Parametric Design Language (APDL) which is a scripting language that one can use to automate common task or build the finite element model. APDL also provides features like

repeating a command, macros, if-then-else branching, do loops, scalar, vector and matrix operations. APDL is also the foundation for design optimization using ANSYS.

Parameters

Parameters are APDL variables, which are similar to FORTRAN variables. The parameter does not to be declared as integer or real, and all numeric values are stored as double-precision values. Scalar and array parameters can be defined in ANSYS.

A parameter can be used directly as an argument to any ANSYS command; the parameter is evaluated and its current value is used for that argument. For example, if you assign the value 10 to a parameter named “rad” and then issue the command

CYL4, 0, 0, rad

ANSYS will interpret the command as

CYL4, 0, 0, 10

which creates a solid circle with radius 10 and center at the origin.

Array parameters can also be defined in ANSYS. This option is useful when distributed pressure or temperature data is read into ANSYS; ANSYS reads the distributed pressure data and stores it as an array inside the program with the array parameter name.

By the use of APDL one can input model dimensions, material properties, etc. in terms of parameters rather than numbers and retrieve information from the ANSYS database, such as maximum stress and displacement on a node.

3.2.2 ANSYS Finite Elements Used in Structural Analysis

SHELL93 Element

SHELL93 is an eight node shell element which is particularly well suited to model curved shells. The element has six degrees of freedom at each node; translations in the nodal x, y, and z directions and rotations about the nodal x, y, and z-axes. The deformation shapes are quadratic in both in-plane directions. The geometry, node locations, and coordinate systems for this element are shown in Figure 3.1. The element is defined by eight nodes, four thicknesses, and material properties.

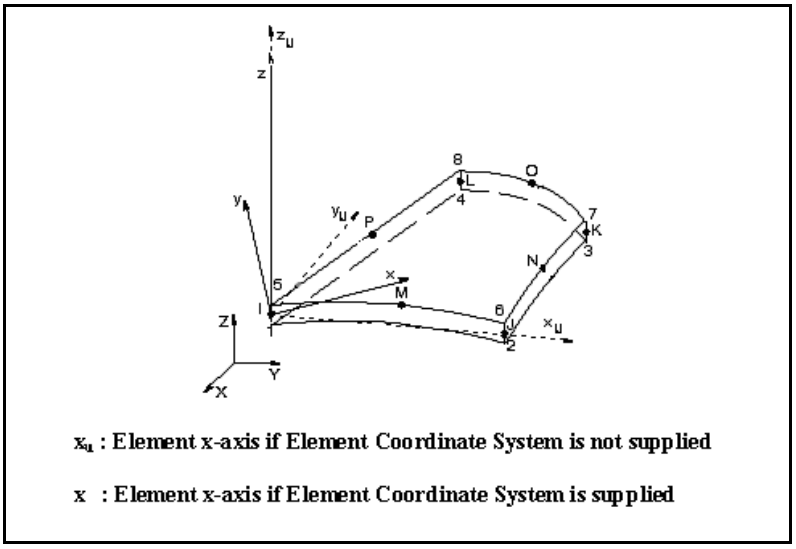

Figure 3.1 ANSYS SHELL93 element [28].

SHELL99 Element

SHELL99 can be used for layered applications of a structural shell model. The element is defined by eight nodes, average or corner layer thicknesses, layer material direction angles, and orthotropic material properties. Shell 99 can allow up to 250 layers. The element has six degrees of freedom at each node; translations in the nodal x, y, and z directions and rotations about the nodal x, y, and z-axes. The geometry, node locations, and coordinate systems for this element are shown in Figure 3.2.

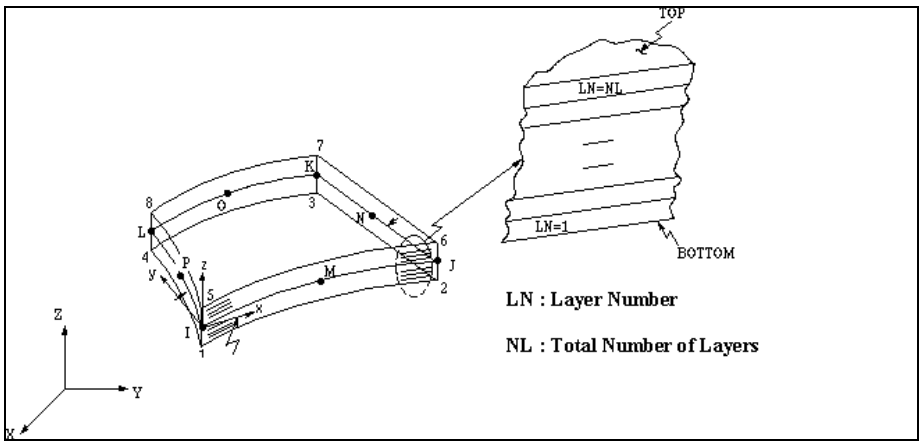

Figure 3.2 ANSYS SHELL99 element [28].

BEAM189 Element

BEAM189 is an element suitable for analyzing slender to moderately stubby/thick beam structures. This element is based on Timoshenko beam theory. Shear deformation effects are included. BEAM189 is a quadratic beam element (3-node) in 3-D with six degrees of freedom at each node. The degrees of freedom at each node includes translations in x,y, and z directions, and rotations about the x,y, and z directions. Warping of cross sections is assumed to be unrestrained. The geometry, node locations, and the coordinate system for this element are shown in Figure 3.3. BEAM 189 is defined by nodes I, J, and K in the global coordinate system. Node L is required to define the orientation of the element.

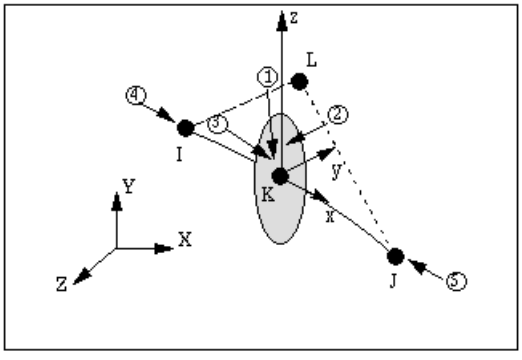

Figure 3.3 ANSYS BEAM189 element [28].

3.3 STRUCTURAL OPTIMIZATION WITH ANSYS

Optimization of an aircraft structure seeks most of the time for a minimum weight design. The weight of the structural element is the objective function. In general the choice of the structural design has some limits on it, such as displacement constraints, allowable stress and natural frequency constraints. In addition, the optimization problem has some design variables so that by changing the design variables the optimum design is found. Design variables can be either continuous or discrete.

The standard form of the optimization problem can be written as [3]

Minimize $f(\vec{x}) \quad \vec{x} \in X^n$

Subjected to $h_i(\vec{x}) = 0, \quad i = 1,.....,n_e$

$g_j(\vec{x}) \le 0, \quad j = 1,.....,n_g$

$\vec{x}^L < \vec{x} < \vec{x}^U$

In this mathematical formulation $\vec{x}$ is a vector of n components to describe design variables and X^n is the domain of design variables. The objective function is designated with $f(\vec{x})$ and the equality and inequality constraints are designated with $h(\vec{x})$ and $g(\vec{x})$, respectively. The elements of the vectors $\vec{x}^L$ and $\vec{x}^U$ are the lower and upper bounds on the values of design variables.

3.3.1 Basic Definitions and Preparation of the Analysis File

A typical design optimization problem in ANSYS consists of three parts [28, 29]:

- Objective Function: Item that is minimized (e.g. weight of the wing) or maximized.

- Design Variables: Design characteristics that are varied to achieve the objective (e.g, thickness of the wing skin panel, etc).

- State Variables: Conditions that the design must meet. (e.g. allowable stress on the wing, allowable tip deflection of the wing, etc).

A feasible design is within all the Design Variable (DV) and State Variable ranges. Generally, the DVs are always inside their permitted range. An infeasible design is one that violates at least one constraint. ANSYS can achieve an optimum design even if the initial design is infeasible.

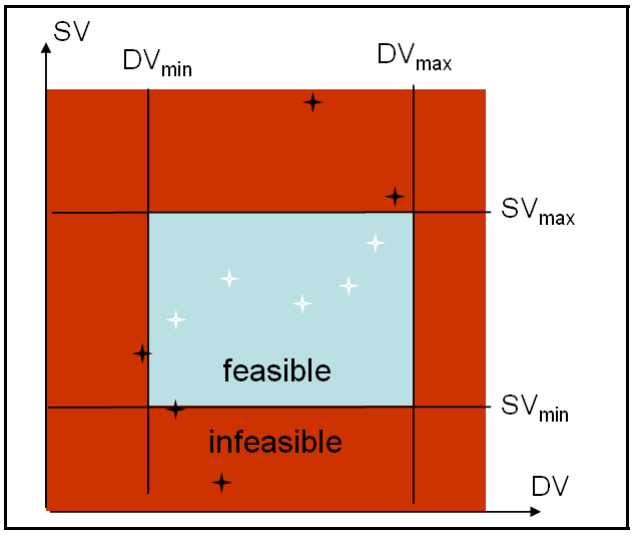

Figure 3.4 Feasible and infeasible designs [29].

The best design is one that has the lowest objective function value and most closely meets all the constraints. If no feasible designs are available, the best design is one that most closely meets all the constraints, not the one with the lowest objective function value. The design domain (or design space) is the region defined by all possible feasible designs.

The ANSYS optimization procedure is shown in Figure 3.5.

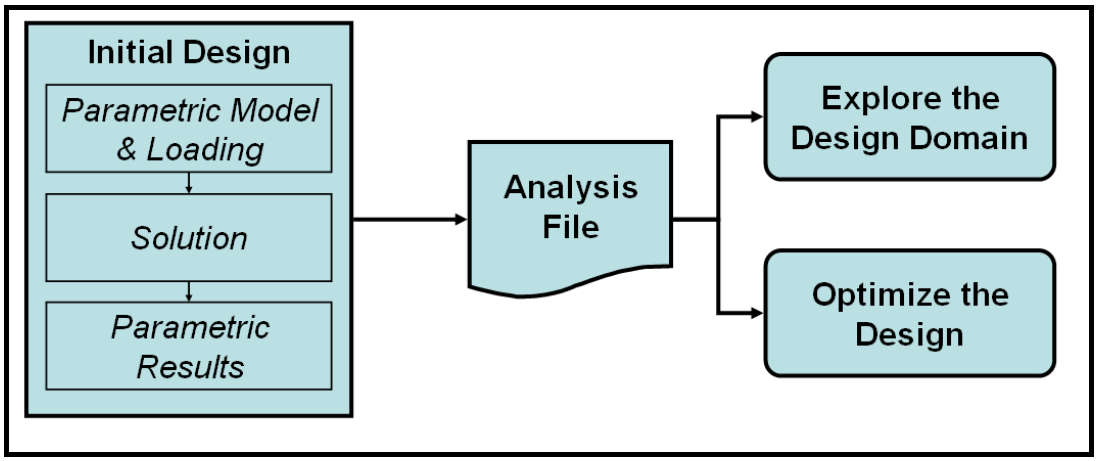

Figure 3.5 ANSYS optimization procedure [29].

In ANSYS, optimization begins with building a parametric model of the initial design and creating an analysis file. The basic requirement is that quantities to be used as DVs, SVs, and objective function must be parameters. For example, if the objective function is the weight of the wing then the volume of the wing must be available as a parameter as well as all the design constraints.

The procedure to build and analyze a parametric model is the same as for a normal ANSYS analysis except that parameters are used wherever appropriate. The following steps are recommended in order to build and analyze an initial design [28, 29].

Step 1 - Define Parameters

In this step the standard Name=Value format is used to define parameters. For parameters to be used as DVs, the values specified are used for the initial design only.

Steps 2, 3 - Modeling, Meshing & Loading Using Parameters

Appropriate parameters are used in this step to construct the geometrical model, mesh and apply the loads and boundary conditions.

Step 4 - Parameterize the Results

The results from the initial analysis, such as the maximum stress/deflection, volume of the geometry are retrieved at this step and stored as parameters. These parameters are then used as state variables and objective function.

Step 5 - Create the Analysis file

In this step the analysis file is created. The analysis file contains ANSYS commands for the complete parametric analysis including geometric modeling, meshing, loading, solution and post processing. The optimizer uses it to loop through multiple designs.

Upon the creation of the analysis file the next step is to enter the optimization module, specify analysis file and declare the optimization variables. ANSYS allows the user to specify a single objective function. Maximum 60 design variables and 100 state variables can be used in the model.

After these steps, the design is optimized using one of the optimization methods available in ANSYS. In the next section, ANSYS Optimization methods are presented.

3.3.2 ANSYS Optimization Methods

Two optimization methods are available in ANSYS; The Subproblem Approximation Method and the First Order Method [28, 29].

The Subproblem Approximation Method

The Subproblem Approximation Method is an advanced zero-order method. It requires only the values of the dependent variables, and not their derivatives. In the Subproblem Approximation Method, approximations are used for objective function and state variables and the constrained optimization problem turned into an unconstrained optimization problem by adding penalty functions to objective function.

Approximations for Objective Function and State Variables

In Subproblem Approximation Method, the relationship between the objective function and the DVs are established by curve fitting. The objective function is calculated for several sets of DVs and a least square fit is performed between the data points. The resulting curve (or surface) is called an approximation. Each optimization loop generates a new data point, and the objective function approximation is updated. This approximation to the objective function is minimized in the optimization process.

State variables are handled in the same manner. An approximation is generated for each state variable and updated at the end of each loop.

A linear, quadratic or quadratic plus cross terms fit can be used for the curve fitting approximation.

Conversion of a Constrained Problem to an Unconstrained Problem

The ANSYS converts the constrained optimization problem to an unconstrained optimization problem because minimization techniques for the latter are more efficient. The conversion is done by adding penalties to the objective function approximation to account for the imposed constraints.

The search for a minimum of the unconstrained objective function approximation is carried out by applying a Sequential Unconstrained Minimization Technique (SUMT) at each iteration.

Convergence Checking

At the end of each loop, a check for convergence is made. The problem is said to have converged if the current, previous, or best design is feasible and *any* of the following conditions are satisfied

- The change in objective function from the best feasible design to the current design is less than the objective function tolerance.
- The change in objective function between the last two designs is less than the objective function tolerance.

- The changes in all design variables from the current design to the best feasible design are less then their respective tolerances.
- The changes in all design variables between the last two designs are less than their respective tolerances.

The First Order Method

In the First Order Method the constrained optimization problem is turned into an unconstrained one by adding penalty functions like in the Subproblem Approximation Method. However in this method no approximation is made and the actual finite element representation is minimized.

The First Order Method uses gradients of the dependent variables with respect to the design variables. Each iteration may involve several analyses (loops through the analysis file) to determine the proper search direction. Various steepest descent and conjugate direction searches are employed during each iteration. For each iteration, gradient calculations are performed in order to determine a search direction, and a line search strategy is adopted to minimize the unconstrained problem.

Convergence Checking

First order iterations continue until convergence is achieved. The problem is said to have converged if, when comparing the current iteration design set to the previous and best sets, one of the following conditions is satisfied:

- The change in objective function from the best design to the current design is less than the objective function tolerance.
- The change in objective function from the previous design to the current design is less than the objective function tolerance.

It is also a requirement that the final iteration uses a steepest descent search, otherwise additional iterations are performed.

3.3.3 Exploring the Design Domain

Using the optimization tools of ANSYS, different designs can be tested in order to measure and understand the design domain of the problem. The following tools are available [28, 29]:

Single Loop Run

This tool performs one loop and produces one FEA solution at a time. Single Loop Run provides a quick look at the design with a set of design variables.

Random Design Generation

Multiple loops are performed, with random design variable values at each loop. This tool is useful for studying the overall design space, and for establishing feasible design sets for subsequent optimization analysis.

Sweep Generation

Starting from a reference design set, this tool generates several sequences of design sets. Specifically, it varies one design variable at a time over its full range using uniform design variable increments. This tool makes global variational evaluations of the objective function and of the state variables possible.

Factorial Evaluation

This is a statistical tool that is used to generate design sets at all extreme combinations of design variable values. The primary aim is to compute main and interaction effects for the objective function and the state variables.

Gradient Evaluation

At a user-specified reference design set, this tool calculates the gradients of the objective function and the state variables with respect to the design variables. Local design sensitivities can be investigated using this tool.

3.4 MODELING DETAILS FOR THE WING

In the finite element model of the wing,

- shell-type elements (SHELL93) are used for spar/rib webs
- layered shell-type elements (SHELL99) are used for skin panels
- beam-type elements (BEAM189) are used for spar/rib caps.

A two-sided L-shaped cross section (which looks like a T-shaped section all together) is used for spar caps and a one-sided L-shaped cross-section for rib caps. In general, caps are connected to skin panels, spars and ribs with rivets. Cap flanges and webs for such connections should have enough lengths to insert rivets. Since the distance between the upper and lower skins for the wing geometry is too narrow, upper spar/rib cap webs almost touch lower spar/rib cap webs when adequate distance to use rivets for connections is considered. So, in the finite element model, thickness of the spar cap web is included into thickness of the spar web as seen in Figure 3.6.

The flanges of the spar caps are modeled with rectangular cross section beam elements. Likewise, thickness of the rib cap web is included into thickness of the rib web and flanges are modeled with beam elements of a rectangular cross section.

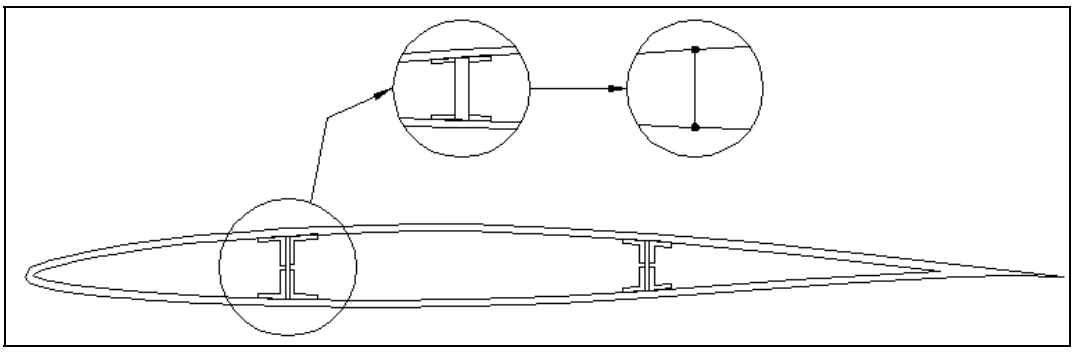

Figure 3.6 Modeling technique for spars and spar caps.

By default, nodes of a shell element are located at the midsurface of the element and nodes of a beam element are located at the centroid of the element. Offset elements are used in the model of skin panels so that the upper side of the element coincides with the wing geometry. Since SHELL93 does not have node offset option, layered shell-type elements (SHELL99) are used for both aluminum and composite skins. Beam elements that are used to model spar caps and rib caps are also offset so that they obey the wing geometry. Offset skin panel, spar cap and rib cap elements are shown in Figure 3.7 and Figure 3.8. The rectangular cross-sections for the beams with proper offset distances are created using common sections provided by ANSYS.

Using non-offset elements results in higher wing moment of inertia values which leads to unconservative results. Besides, it causes wrong moment calculations. For very thin shell elements, the difference between the results obtained from offset and non-offset elements is negligible. But, in preliminary studies it has been seen that the difference cannot be neglected for the wing considered in present study.

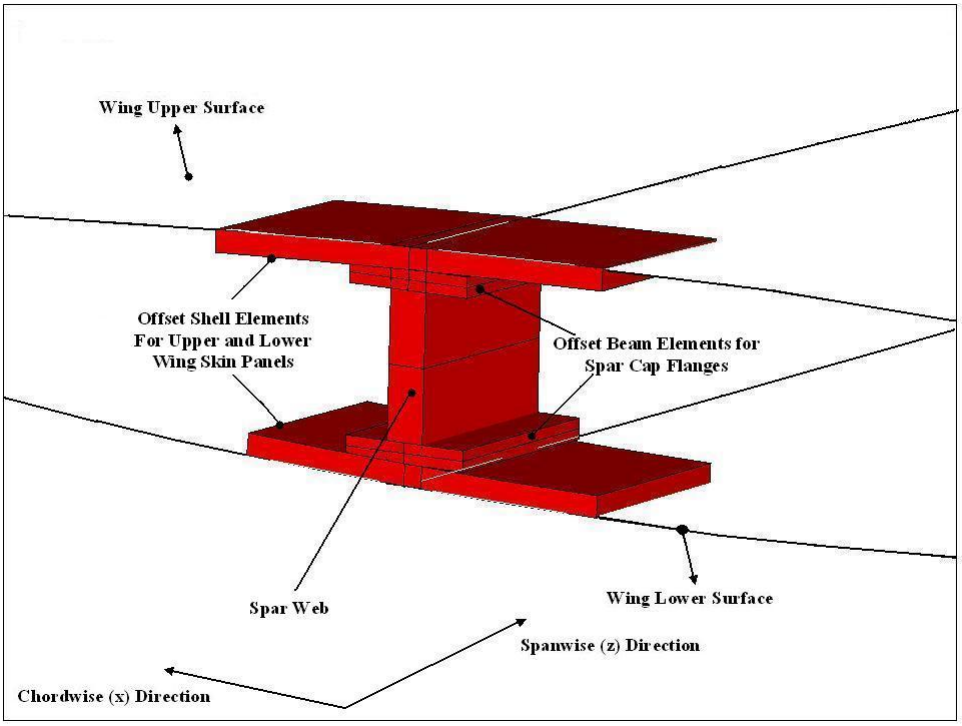

Figure 3.7 Offset skin panel and spar cap elements.

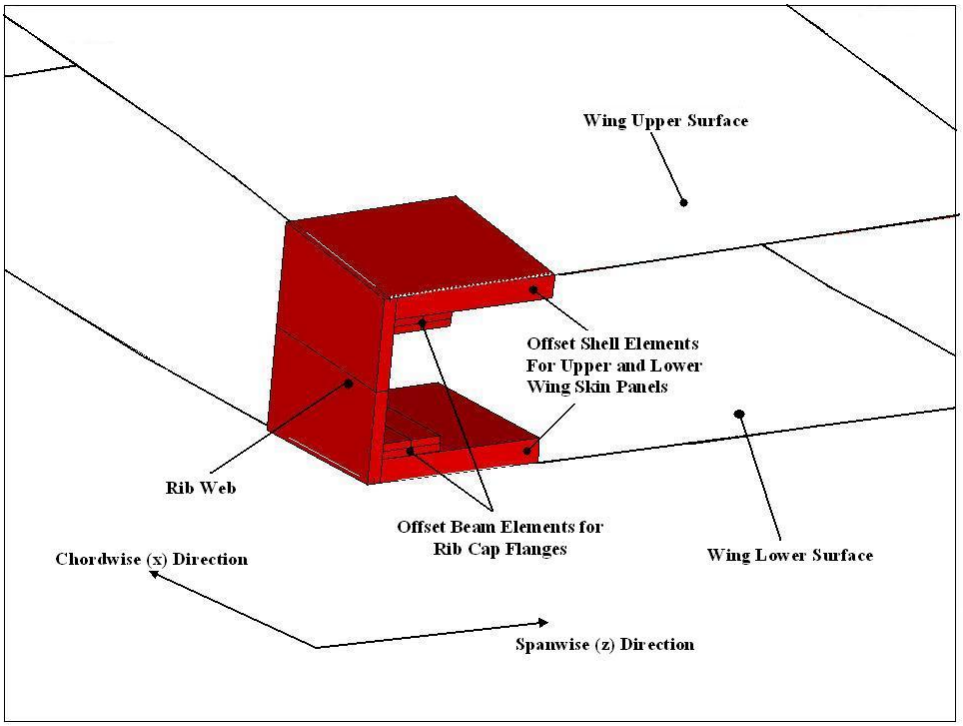

Figure 3.8 Offset skin panel and rib cap elements.

3.5 BOUNDARY CONDITIONS AND LOADING TYPES

After the Tomahawk cruise missile is launched from a platform, its wings, tail fins and engine air intake is deployed, allowing the missile to cruise towards its target. Doors in the missile's flanks open to let the wings swing out, then close again to streamline the slots through which the wings protrude [30].

Rotation of the wing over a pivot can be achieved by a mechanism which is connected to spars. So, this unfolding behavior causes the root of the spars to be the most critical part of the wing structure. Wing pivot and slot door is shown in Figure 3.9.

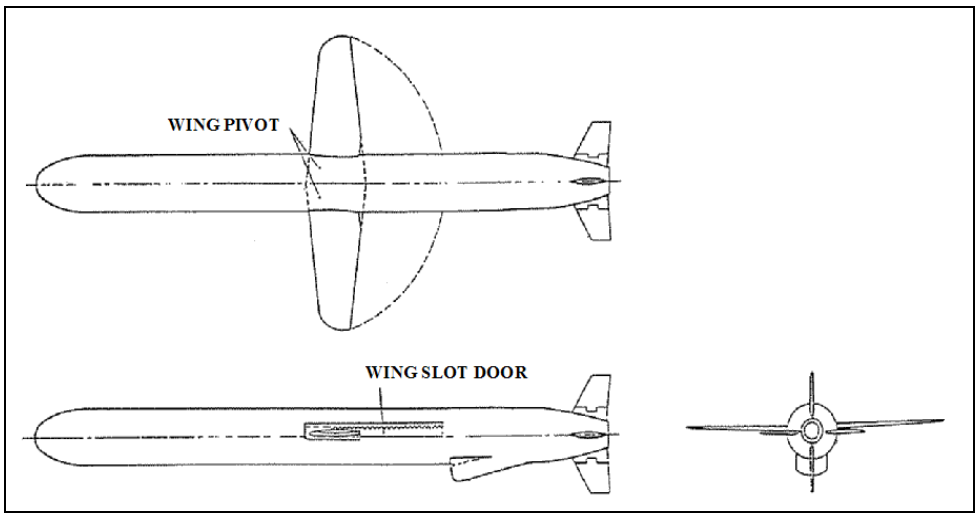

Figure 3.9 Wing pivot and slot door of Tomahawk cruise missile [25].

In the finite element model, displacement degrees of freedom in all directions (u_x, u_y, u_z) are constrained at the root of the spars and displacement degree of freedom in y direction (u_y) is constrained at the root of skin panels as shown in Figure 3.10.

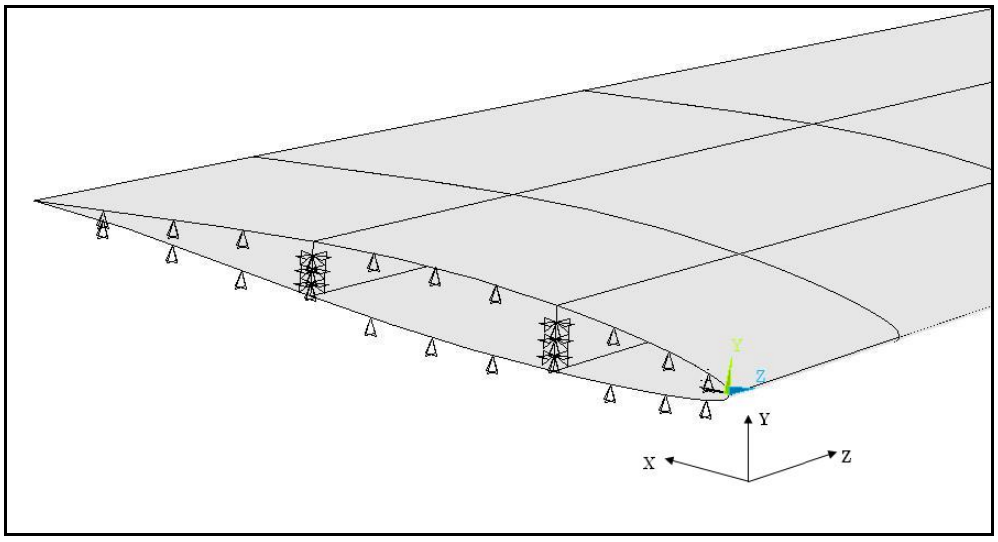

Figure 3.10 Boundary conditions for the wing.

Four load cases are created to account for all critical flight conditions (PHAA, PLAA, NHAA and NLAA) mentioned in Chapter 2. For each flight condition, pressure tables for upper surface, lower surface and tip rib are created separately. Pressures are applied on the wing surfaces using these tables. The pressure values at the nodes of the wing surfaces are automatically calculated by linear interpolation using the pressure tables. Besides the surface pressures obtained from FASTRAN, atmospheric pressure (1 atm) is applied on the inner surfaces of the wing.

3.6 OPTIMIZATION VARIABLES FOR THE ALUMINUM WING

To decrease the number of design variables, thicknesses of the skins, spars, ribs and spar/rib cap flanges and widths of the spar/rib cap flanges are defined as a function of the spanwise location. The functions provide the tapering of the thickness and width values from root to tip. For the thicknesses and width of the spar/rib cap flanges, linear functions are used. For the thicknesses of skins, spars and ribs, parabolic functions are used. A parabolic function is defined with three constants. The three constants can be the thickness/width value at the root and tip sections and the slope at the tip section. In defining the parabolic functions the slope of the thickness function is taken zero at the tip. Thus, a parabolic function with minimum cross-section area is used, and in addition number of design variables is decreased. For a root thickness of 5 mm and a thickness ratio (root thickness/tip thickness) of 10, graphs of the linear and parabolic thickness functions are given in Figure 3.11.

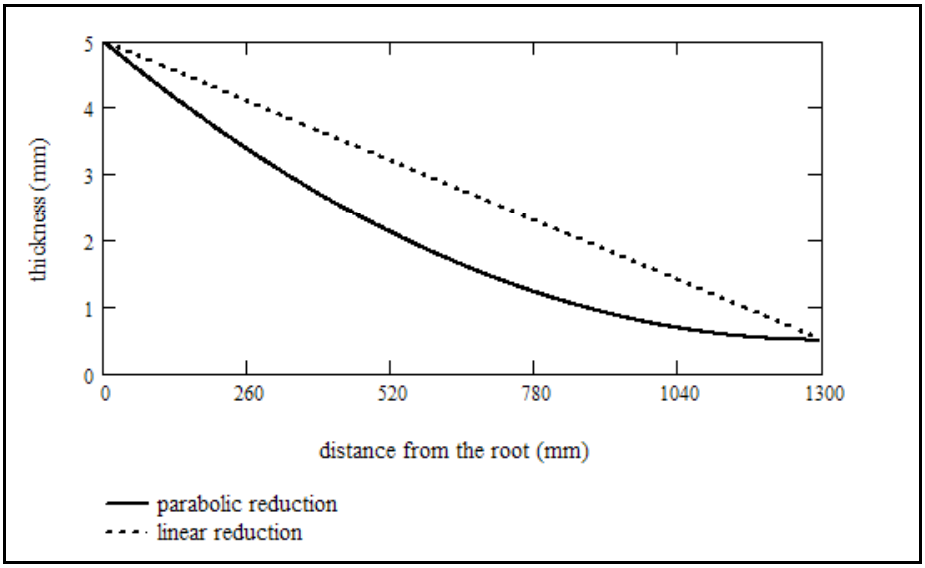

Figure 3.11 Graphs of the linear and parabolic thickness functions.

When a parabolic thickness function is used instead of a linear thickness function, percent mass reduction versus thickness ratio is given in Figure 3.12. For a thickness ratio of 10, 27% mass reduction is obtained. In addition, as thickness ratio gets closer to 100 nearly 33% mass reduction is obtained and becomes constant after that value.

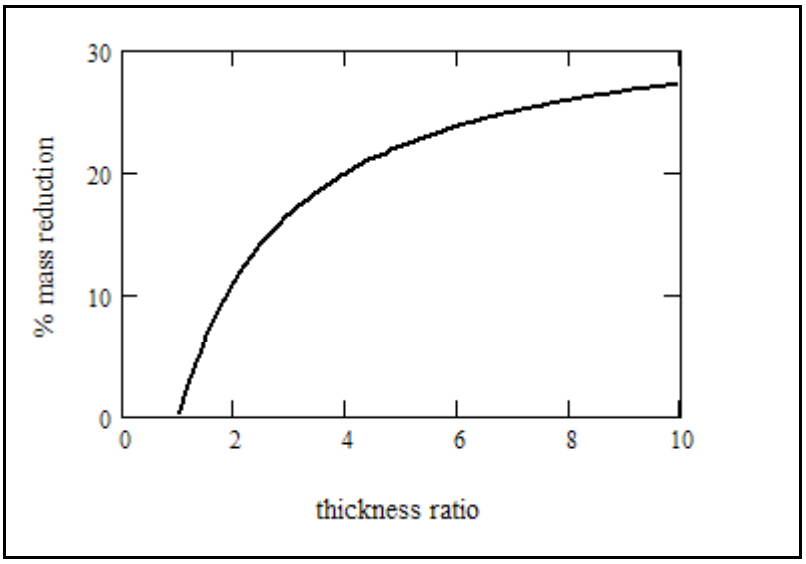

Figure 3.12 Percent mass reduction versus thickness ratio graph.

To be able to define different thickness/width values at each node as a function of spanwise location, a subprogram is written in the ANSYS input files. This subprogram determines the spanwise locations of the nodes for each element from the root, then calculates the thickness/width values using the location values. Each shell element has a thickness which decreases linearly in the spanwise direction while each beam element has a constant thickness and width values which are given the average of their nodal values calculated by the subprogram. An exaggerated view of the parabolically reduced thickness of the upper skin panels is shown in Figure 3.13.

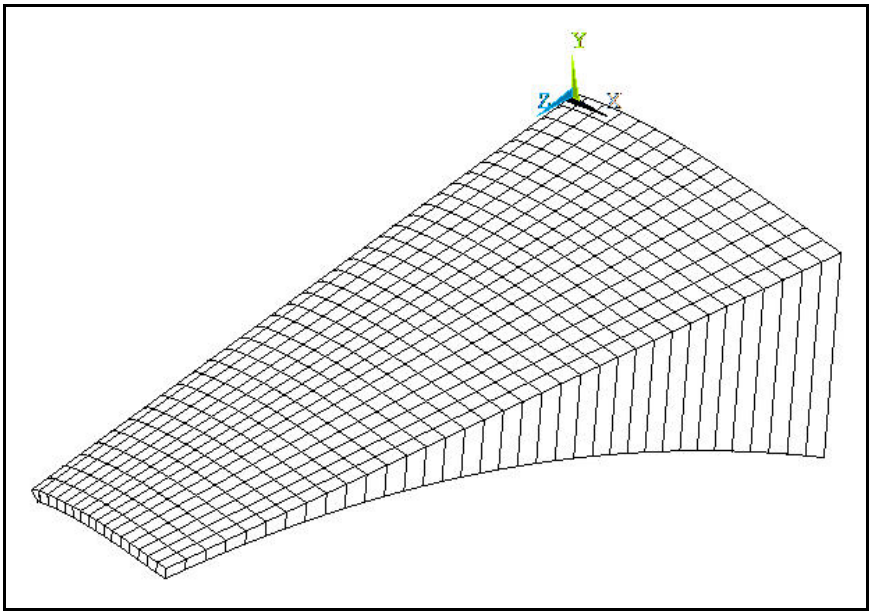

Figure 3.13 The exaggerated view for parabolically reducing thickness of the upper skin panels.

To aid reduction of the number of variables, ribs locations are defined with only one variable. Toward that end, the distance between two adjacent ribs is increased linearly from root to tip since the loading at the root side is more severe. A subprogram is written in ANSYS to find the locations of the ribs by using the number of ribs (n) and the slope of the distance ratio function (m). The distance ratio function is defined as

$$x=m(i-1)+1, \quad i = 1, 2, ..., n$$

where, i is the rib number from root to tip. This function determines the ratio of the distance between the i^{th} rib and the $(i-1)^{th}$ rib to the distance between the first rib and the root. In this definition, "0^{th} rib" corresponds to the root. As a result the distance ratios between two adjacent ribs are taken as 1: m+1: 2m+1…m(n-1)+1 from root to tip. For example, if the slope is zero, then the distances between the ribs are equal; if the slope is one, then the distance ratios are taken as 1, 2, 3…n from root to tip. The graph of the distance ratio function for different slope values is given in Figure 3.14.

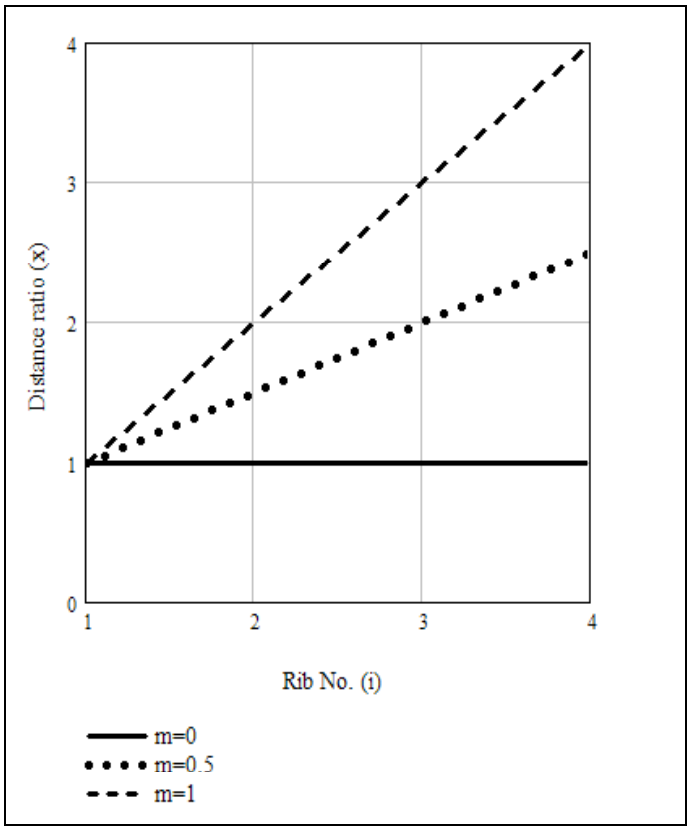

Figure 3.14 Distance ratio function for different m values.

The design variables defined in the ANSYS input file, abbreviations and the upper and lower bounds are listed in Table 3.1. As mentioned before spar/rib thicknesses include also spar/cap flange thicknesses. The locations of the spars are the distances from the leading edge given as percent of the chord length.

Table 3.1 Design variables, abbreviations and bounds for the aluminum wing.

Design Variables	Abbreviations	Min.	Max.
Number of ribs	n	1	5
Slope of the distance ratio function	m	0	1
Location of the 1st spar (% c)	c1	10	30
Location of the 2nd spar (% c)	c2	50	80
Upper skin root thickness (mm)	tr_us	2	6
Upper skin thickness ratio	t_ratio_us	2	12
Lower skin root thickness (mm)	tr_ls	2	6
Lower skin thickness ratio	t_ratio_ls	2	12
Spar web root thickness (mm)	tr_sw	4	15
Spar web thickness ratio	t_ratio_sw	2	10
Spar cap flange root thickness (mm)	tr_sc	1	5
Spar cap flange thickness ratio	t_ratio_sc	2	10
Spar cap flange root width (mm)	wr_sc	12.5	15
Spar cap flange width ratio	w_ratio_sc	1	1.7
Rib web root thickness (mm)	tr_rw	1	4
Rib web thickness ratio	t_ratio_rw	1	4
Rib cap flange root thickness (mm)	tr_rc	1	4
Rib cap flange thickness ratio	t_ratio_rc	2	8
Rib cap flange root width (mm)	wr_rc	12	15
Rib cap flange width ratio	w_ratio_rc	1	1.7

The reason for taking the ratios (root value/tip value) as design variables instead of tip values for thicknesses and widths is to provide the tapering of thicknesses and widths from root to tip for all conditions.

In ANSYS only continuous variables can be defined. So discrete variables, such as number of ribs, found after an optimization iteration are used at the following iteration by rounding them to integer numbers. For this purpose, controls for optimization looping are adjusted. This adjustment is done by adding a command (oploop, prep,

process) at the optimization module. With this command optimization loop starts from preprocessor module and design variables are processed during looping.

The analysis file is created with 20 design variables. But after some trial analyses it has been seen that spar/rib cap flange widths can be taken as constant since the minimum and maximum values are very close to each other. The spar cap flange width is taken as linearly decreasing from 12.5 mm at the root to 9 mm at tip. The rib cap flange width is taken as linearly decreasing from 12 mm at root to 9 mm at the tip.

Optimization analyses are continued with 16 design variables. Among them, four design variables determine the number of ribs and location of ribs and spars and changing the values of these design variables lead to mesh change. After examining the results of the optimization analyses, it is observed that design variables for the best design have the values which create the largest element sizes and the results are highly mesh-dependent. So, it is decided to take the design variables which lead to a mesh change as constant. The values taken for these design variables are:

Number of ribs (n): 4
Slope of the distance ratio function (m): 0.5
Location of the 1st spar (c1): 0.25c from the leading edge
Location of the 2nd spar (c2): 0.6c from the leading edge

The value of 0.5 for m means that the distance ratios are taken as 1, 1.5, 2, 2.5 from root to tip as seen in Figure 3.14. For subsequent analyses, the inner and outer meshes of the wing structure with 1636 elements and 4138 nodes are given in Figure 3.15.

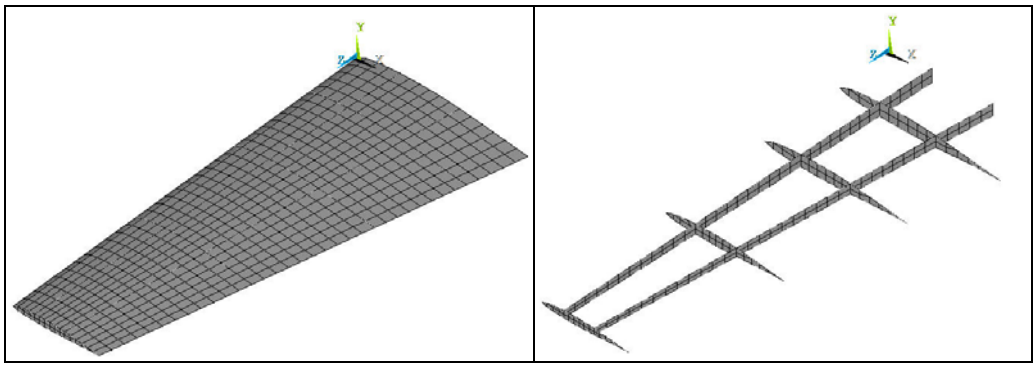

Figure 3.15 Mesh of the wing structure.

From the preliminary studies it has been seen that high strength aluminum is necessary for the cruise missile wing. So, 7075 series aluminum is used which has a yield strength of nearly 400 MPa. The material properties for the aluminum are taken as

E=70000 MPa

ν=0.3

ρ=2700 kg/m^3

After the static analysis, a buckling (eigenvalue) analysis is performed for each of the four load cases mentioned above. After these analyses, maximum von Mises stresses for shell elements and axial stresses for beam elements in each portion of the wing, buckling load factors (eigenvalues) and the volume of the wing are retrieved and parameterized. Axial stresses for beam elements are referred to as von Mises stresses, since other stress components are negligible compared to axial stresses in a beam element.

Stresses are retrieved using element tables which use the average results for top, middle or bottom of shell elements. So, top and bottom stresses for shell elements are retrieved separately, and then the maximum of the results for each portion is used. All the elements from root to first rib constitutes the first portion, including the first rib; all the elements from first rib to second rib constitutes the second portion, excluding the first rib and including the second rib and so on until the fourth portion.

The state variables (strength, buckling and size constraints) defined in the ANSYS input file, abbreviations and the upper and lower bounds are listed in Table 3.2. Objective function for the optimization analyses is the mass of the wing.

ANSYS input file for the aluminum wing is given in Appendix A.

Table 3.2 State variables, abbreviations and bounds for the aluminum wing.

State Variables	**Abbreviations**	**Min.**	**Max.**
Max. von Mises stress in each portion of the wing for PHAA (MPa)	smax1_1, smax1_2, smax1_3, smax1_4	-	400
Max. von Mises stress in each portion of the wing for PLAA (MPa)	smax2_1, smax2_2, smax2_3, smax2_4	-	400
Max. von Mises stress in each portion of the wing for NHAA (Mpa)	smax3_1, smax3_2, smax3_3, smax3_4	-	400
Max. von Mises stress in each portion of the wing for NLAA (Mpa)	smax4_1, smax4_2, smax4_3, smax4_4	-	400
Buckling load factor for PHAA	buckling1	1	-
Buckling load factor for PLAA	buckling2	1	-
Buckling load factor for NHAA	buckling3	1	-
Buckling load factor for PHAA	buckling4	1	-
Upper skin tip thickness (mm)	tt_us	0.5	-
Lower skin tip thickness (mm)	tt_ls	0.5	-
Spar web tip thickness (mm)	tt_sw	1.5	-
Spar cap flange tip thickness (mm)	tt_sc	0.5	-
Rib web tip thickness (mm)	tt_rw	1	-
Rib cap flange tip thickness (mm)	tt_rc	0.5	-

3.7 OPTIMIZATION VARIABLES FOR THE COMPOSITE WING

For the composite wing, four ribs and two spars are used as in the aluminum wing with the same locations. The spar/rib cap flange widths are also taken constant having the same values with the aluminum wing for the same reason as explained in the previous section.

Optimization of composite structures requires too many design variables to be used. But as mentioned earlier, ANSYS optimization module does not have the capability of dealing with too many design variables. So for the composite wing, four portions are separately optimized. The elements constituting these four portions are as in the aluminum wing.

In each portion, spar web and spar flange thicknesses are defined as a function of the spanwise location. The functions provide the linear reduction of the thicknesses from the beginning to the end of each portion.

Composites differ from metals having coupling behavior between in-plane and bending deformations. In other words, in-plane loads can create out-of-plane deformations in addition to in-plane deformations and vice versa. This behavior is described with the following formulae [3]:

$$\mathbf{N} = \mathbf{B}\kappa + \mathbf{A}\varepsilon^{o} \quad (3.1)$$

$$\mathbf{M} = \mathbf{B}\varepsilon^{o} + \mathbf{D}\kappa \quad (3.2)$$

where,

N: in-plane stress resultants
M: moment resultants (stress couples)
A: extensional stiffness matrix (or in-plane stiffness matrix)
B: coupling matrix
D: flexural stiffness matrix
ε^{o}**:** mid-plane strain
κ**:** curvature of the layer

Detailed formulations for the matrices given above can be found in almost every book about composites, [3] being one of them.

In this study symmetric balanced stacking sequence is used for the composite skin panels having layers with 0^o, 90^o and $\pm 45^o$ orientations. For each portion, numbers of each orientation for upper and lower skin panels are taken as design variables.

As the **B** matrix vanishes with the use of symmetric laminates, coupling between in-plane and out-of-plane responses of a laminate is eliminated. Balanced laminates are obtained by placing a -45^o ply orientation for every occurrence of a 45^o one. Vanishing of A_{16} and A_{26} terms in **A** matrix with the use of balanced laminates, shear-extension coupling is eliminated. Furthermore, balanced laminates with adjacent layers of 45^o and -45^o orientation have smaller bending-twisting coupling terms (D_{16} and D_{26}).

As the **B** matrix is eliminated from equation (3.1), in-plane behavior of a symmetric composite laminate depends on only **A** matrix. In addition, **A** matrix is affected by the number of each orientation not the stacking sequence. So, for a symmetric composite structure subjected to only in-plane loads, stacking sequence is not important.

For a wing skin panel, in-plane loads are usually dominant. So, considering only number of layers for each orientation is a good approximation for the strength calculations of wing skin panels. But on the contrary, buckling is an out-of-plane phenomenon which depends on flexural stiffness matrix and is highly affected by the stacking sequence.

Initially, number of layers for each ply orientation subject to strength constraints alone was optimized for the first two portions of the wing. Buckling analyses were then performed for different stacking sequences. It was seen that buckling was not a problem for the first portion, since the skin panels were thick enough to resist buckling. The second portion, on the other hand, buckled whatever the stacking sequence was, since the thin skin panels were sufficient for strength constraints only. So, it is understood that strength and buckling optimization must be performed simultaneously.

One of the remedies to handle such a complex problem is to create a response surface for the optimum buckling load as a function of number of 0^o, 90^o and $\pm 45^o$ stacks and in-

plane loads and use genetic algorithms for stacking sequence optimization [16, 17]. In these studies analytical buckling formulations are used.

For simply-supported plates subjected to in-plane normal loads N_x&N_y, analytical formulation is available only for specially orthotropic composites (B_{ij}=0, D_{16}, D_{26}=0) which have only 0^o and 90^o layers. For a simply-supported plate subjected to shear loads N_{xy}, analytical formulation is available only for specially orthotropic and infinite strip (a>>b) [31, 32]. Comparison of buckling loads of a simply-supported plate calculated using the formulations given in [22] for isotropic plates, [31] and [32] for composite plates and the finite element method is given in Appendix B. For the plates violating the assumptions of analytical formulations, buckling load factors obtained by analytical formulations differ from the numerical solutions as seen in Appendix B.

Genetic algorithms are effective in producing global optimum solutions when only a few variables are involved, and analyses are not so expensive [33]. So, use of genetic algorithm may not be effective for the stacking sequence optimization for the wing considered in this study.

In the current study, stacking sequence is not dealt with and a stacking sequence of $[(90^o)_{n90}/(0^o)_{n0}/(\pm45^o)_{n45}]_s$ is used for every skin panels, where n90, n0 and n45 are half the number of 90^o, 0^o, $\pm45^o$ layers, respectively. In 0^o layers, fibers are in the chordwise direction. In 90^o layers, fibers are in the spanwise direction. Layer thickness is taken as 0.125 mm. With the assumption of perfectly bonded layers, it is possible to take $(90^o)_{n90}$ layers as one layer with a thickness of 0.125x(n90) and $(0^o)_{n0}$ layers as one layer with a thickness of 0.125x(n0).

The design variables defined in the ANSYS input file, abbreviations and the upper and lower bounds for the first portion are listed in Table 3.3. As in the aluminum wing, spar/rib web thicknesses include also spar/rib cap web thicknesses. For the other portions, thicknesses of spar web and spar cap flanges at the beginning of each portion are taken the same as the values of the thicknesses at the end of the previous portions. So, these portions have two design variables less than the first portion.

Number of layers for each orientation found in an optimization iteration are used at the following iteration by rounding it to an integer number as explained in the previous section.

In order to use '0' as a lower bound for number of layers for each orientation, design variables are used with adding '1' to them since design variables cannot take the value '0'.

Table 3.3 Design variables, abbreviations and bounds for Portion-1 of the composite wing.

Design Variables	**Abbr.**	**Min.**	**Max.**
Half the number of 90^o layers at the upper skin	n90_us1	0	24
Half the number of 0^o layers at the upper skin	n0_us1	0	24
Half the number of $\pm 45^o$ layers at the upper skin	n45_us1	0	12
Half the number of 90^o layers at the lower skin	n90_ls1	0	24
Half the number of 0^o layers at the lower skin	n0_ls1	0	24
Half the number of $\pm 45^o$ layers at the lower skin	n45_ls1	0	12
Spar web root thickness (mm)	tr_sw1	2	15
Spar web thickness ratio	t_ratio_sw1	1	10
Spar cap flange root thickness (mm)	tr_sc1	1	5
Spar cap flange thickness ratio	t_ratio_sc1	1	10
Rib web thickness (mm)	t_rw1	1	4
Rib cap flange thickness (mm)	t_rc1	1	4

After the static analysis, a buckling (eigenvalue) analysis is performed for each of the four load cases as in the aluminum wing. After these analyses, the volume of the portion optimized, maximum von Mises stresses for shell elements and axial stresses for beam elements for the aluminum parts and buckling load factors (eigenvalues) are retrieved and parameterized.

Stresses of the portion optimized are retrieved using element tables which use the average results for top, middle or bottom of shell elements. So, top and bottom stresses are retrieved separately, and then the maximum of the results for each portion is used.

There are various types of failure criteria for composite layers: The most frequently used ones are the maximum stress, maximum strain, Tsai-Hill, Hoffman and Tsai-Wu criteria. While the application of maximum stress and maximum strain criteria is straightforward, these criteria fail to represent interactions of different stress components in failure mechanisms. Quadratic failure criteria similar to the von Mises criterion such as Tsai-Hill, Hoffman and Tsai-Wu can account for this interaction [3]. Tsai-Wu criterion is one-of the most commonly used among others.

The failure criteria mentioned above are all referred to as first-ply failure criteria since only the most critical ply is considered. Failure of only one layer does not always mean failure of the whole structure. So, in some applications degraded laminate failure (or referred to as progressive failure) analysis is performed in which each layer of a laminate is assumed to be degraded and, thus, to carry loads with a reduced performance.

In ANSYS, three different failure criteria for composites are available: maximum stress, maximum strain and Tsai-Wu. For Tsai-Wu failure criteria there are two different formulations used by different researchers. ANSYS offers both of them and distinguishes them with the names Tsai-Wu and inverse Tsai-Wu. The criterion referred to as Tsai-Wu in ANSYS is the 3-D version of the failure criterion reported in Tsai and Hahn [34] and Gürdal *et al.* [3]. The criterion referred to as inverse Tsai-Wu in ANSYS is the 3-D version of the failure criterion reported in of Tsai [35] and Barbero [36].

In this study, maximum stress, maximum strain and inverse Tsai-Wu failure criteria are used. For the inverse Tsai-Wu failure criterion, -1 is used for the coupling coefficient (C_{xy}) which is the default value in ANSYS and the recommended value in Barbero [36]. C_{xy} is twice the value of F^*_{xy} used by Tsai and Hahn and the value of f_{12} given in Barbero. The reason for selecting the inverse Tsai-Wu instead of Tsai-Wu failure criterion is explained later.

Failure criteria values are calculated in integration points or nodes of elements in ANSYS. So, a subprogram is written in the ANSYS input file in order to use element stresses and strains for the failure criteria value calculations for the portion optimized.

The state variables (strength, buckling and size constraints) defined in the ANSYS input file, abbreviations and the upper and lower bounds for the first portion are listed in Table 3.4. The state variables for the other portions are the same except for the abbreviations for the size constraints. Objective function for the optimization analyses is the mass of the wing.

Table 3.4 State variables, abbreviations and bounds for Portion-1 of the composite wing.

State Variables	**Abbreviations**	**Min.**	**Max.**
Max. von Mises stress for aluminum elements for PHAA, NHAA, PLAA, NLAA (MPa)	smax_alu1 smax_alu2 smax_alu3 smax_alu4	-	400
Max. stress/strain/Tsai-Wu failure criterion values for composite elements for PHAA, NHAA, PLAA, NLAA	fcs1, fce1, fctwi1 fcs2, fce2, fctwi2 fcs3, fce3, fctwi3 fcs4, fce4, fctwi4	-	1
Buckling load factor for PHAA, NHAA, PLAA, NLAA	buckling1 buckling2 buckling3 buckling4	1	-
Upper skin thickness (mm)	t_us1	0.5	6
Lower skin thickness (mm)	t_ls1	0.5	6
Spar web tip thickness (mm)	tt_sw1	1.5	-
Spar cap flange tip thickness (mm)	tt_sc1	0.5	-

For the aluminum parts, 7075 series aluminum is used with the same material properties given in the previous section. In order to choose the composite material, four different composite types are compared first. Mechanical properties used for these composites with a fiber volume fraction of 0.6 are given in Table 3.5.

Table 3.5 Mechanical properties of the unidirectional fiber reinforced epoxy composites [37].

Property	**E-glass**	**High strength graphite**	**High modulus graphite**	**Ultrahigh modulus graphite**
ρ (kg/m^3)	2100	1580	1640	1700
E_1 (GPa)	45	145	220	290
E_2 (GPa)	12	10	6.9	6.2
G_{12} (GPa)	5.5	4.8	4.8	4.8
ν_{12} (GPa)	0.28	0.25	0.25	0.25
S_{1t} (MPa)	1020	1240	760	620
S_{1c} (MPa)	620	1240	690	620
S_{2t} (MPa)	40	41	28	21
S_{2c} (MPa)	140	170	170	170
S_{12} (MPa)	70	80	70	60
ε_{1t} (%)	2.3	0.9	0.3	0.2
ε_{1c} (%)	1.4	0.9	0.3	0.2
ε_{2t} (%)	0.4	0.4	0.4	0.3
ε_{2c} (%)	1.1	1.6	2.8	2.8
ε_{12} (%)	1.6	1.6	1.6	0.64

S: strength

ε: failure strain

1: longitudinal (fiber) direction

2: transverse (perpendicular to fiber) direction

t: tension

c: compression

The geometry and stacking properties used in comparing the four composite materials are given in Table 3.6. The thicknesses of the portions are 5.5, 5, 4, 3 mm from root to tip for both upper and lower skin panels.

Table 3.6 The geometric properties of the wing used in the comparison analyses.

	Portion-1	**Portion-2**	**Portion-3**	**Portion-4**
n90_us	10	10	8	6
n0_us	4	2	2	2
n45_us	4	4	3	2
n90_ls	10	10	8	6
n0_ls	4	2	2	2
n45_ls	4	4	3	2
tr_sw (mm)	12	-	-	-
t_ratio_sw	6	1	1	1
tr_sc (mm)	3	-	-	-
t_ratio_sc	6	1	1	1
t_rw (mm)	1	1	1	1
t_rc (mm)	0.93	0.82	0.68	0.5

The strength and buckling results for the four flight conditions are given in Table 3.7. ‘fcs1’, ‘fce1’, ‘fctw1’, ‘fctwi1’ are the abbreviations for maximum stress, maximum strain, Tsai-Wu and inverse Tsai-Wu failure criteria values respectively for the first load case (PHAA flight condition).

Table 3.7 Results of the analyses for Portion-1 for different epoxy composites.

Failure properties	E-glass	High strength graphite	High modulus graphite	Ultrahigh modulus graphite
smax_alu1 (MPa)	479.05	325.68	279.55	248.60
smax_alu2 (MPa)	137.62	91.13	77.74	68.84
smax_alu3 (MPa)	441.47	317.17	274.72	245.77
smax_alu4 (MPa)	127.47	91.12	78.18	69.66
fcs1	1.97	0.97	1.18	1.43
fce1	1.81	1.12	1.23	1.53
fctw1	2.63	1.13	1.54	2.22
fctwi1	2.04	1.10	1.27	1.52
fcs2	0.55	0.26	0.31	0.38
fce2	0.50	0.30	0.32	0.40
fctw2	0.50	0.23	0.20	0.20
fctwi2	0.50	0.23	0.33	0.40
fcs3	2.25	1.10	1.25	1.54
fce3	2.05	1.26	1.32	1.65
fctw3	3.15	1.33	1.70	2.47
fctwi3	2.31	1.23	1.34	1.60
fcs4	0.55	0.27	0.30	0.37
fce4	0.50	0.31	0.32	0.39
fctw4	0.50	0.23	0.21	0.22
fctwi4	0.57	0.30	0.32	0.38
buckling1	1.28	2.41	3.18	3.92
buckling2	5.07	9.40	12.19	14.93
buckling3	1.25	2.35	3.09	3.80
buckling4	5.38	9.98	13.04	16.04
mass (kg)	2.89	2.30	2.37	2.44

With the use of e-glass/epoxy, skin panels become very critical (high failure criteria values) for PHAA and PLAA conditions when strength is considered, and also von Mises stresses for the aluminum parts are greater than the yield stress of 7075. It is understood from the results that root thickness must be very thick if e-glass/epoxy is used for the skin panels.

With the use of graphite/epoxy, von Mises stresses for the aluminum parts become lower than the yield stress of 7075. Furthermore, as the modulus of the graphite/epoxy increases, von Mises stresses for the aluminum parts decrease and buckling load factors increase. But, mass and failure criteria values for composite skin panels increase. So, high strength graphite is used for skin panels, since the strength for skin panels are more critical than the aluminum parts.

Tsai-Wu failure criteria values are much greater than the other criteria values for PHAA and NHAA conditions as seen in Table 3.7. So, different failure criteria values are also compared for a split disk test conducted in accordance with ASTM D 2290-00 [38] which is presented in Appendix C. It is observed that, Tsai-Wu failure criterion gives conservative results compared to other three failure criteria, namely maximum stress, maximum strain and inverse Tsai-Wu.

CHAPTER 4

RESULTS AND DISCUSSION

4.1 INTRODUCTION

In ANSYS, convergence of an optimization analysis usually does not indicate an optimum design, especially when there is large number of design variables. So, it is necessary to continue (restart) optimization with different tolerance values or with a different set of designs to determine whether the design is indeed optimum.

For the subproblem method, initially N+2 design sets must exist to form the approximations (N=number of DVs). Otherwise, random design sets are generated until the required number is obtained. By supplying known good designs the quality of the approximations can be improved.

For the optimization of two wing configurations, initial designs are created with sweep and random tool, and then several restarts are performed using subproblem method and N+2 best designs of the previous run. After some restarts, only one best design is selected for the next optimization run. By this way, the optimizer is forced to follow a different path by creating some random design sets.

After performing some optimization executions, certain design variables are eliminated for subsequent optimizations. Then analyses are performed using the first order method. Finally local sensitivity analyses using the gradient tool are performed to obtain a better design.

In this chapter, the procedures followed when performing optimization analyses and the results are presented for both the aluminum and composite wing.

4.2 RESULTS FOR THE ALUMINUM WING

Although the ANSYS input file is created with 20 design variables given in Table 3.1, 8 variables are decided to be taken constant as explained in the previous chapter. Furthermore, from the global sensitivity analyses performed with the sweep tool in ANSYS, it is seen that the effect of the rib web and rib flange thicknesses on the strength and buckling results are negligible. So, for the subsequent optimization analyses, 4 design variables representing rib web/cap flange thicknesses and ratios are eliminated and taken constant as:

Rib web root thickness (tr_rw): 1 mm
Rib web thickness ratio (t_ratio_rw): 1
Rib cap flange root thickness (tr_rc): 1 mm
Rib cap flange thickness ratio (t_ratio_rc): 2

After every static analysis, von Mises stresses for each element; and after every buckling (eigenvalue) analyses, buckling load factors are retrieved. To see the effect of the number of state variables for stresses and buckling load factors, three input files are created with different number of state variables. In addition to the four size constraints for the tip thicknesses for upper skin, bottom skin, spar web and spar cap flange, the following constraints are added:

In the first input file (OPT1), two state variables are used: maximum von Mises stress and minimum buckling load factor of the four load cases.

In the second input file (OPT2), eight state variables are used: maximum von Mises stress and minimum buckling load factor for each of the four load cases.

In the third input file (OPT3), twenty state variables are used: maximum von Mises stress for each of the four portions and four load cases and minimum buckling load factor for each of the four load cases.

A design with 8.55 kg weight found from the previous trial optimization analyses is used as the initial design. Optimization analyses with 16 executions are performed using subproblem method for the three input files.

Weight change with the number of executions for three optimization analyses with different number of state variables is given in Table 4.1. ANSYS refers to each iteration as a set. Number of sets (iterations) in each execution is counted from the very beginning.

Table 4.1 Weight change with the number of executions for the aluminum wing.

OPT1 (6 state variables)								
No. of Execution	1	2	3-6	7	8	9	10-12	13-16
No. of Set	69	250	313	544	558	598	664	814
Mass (kg)	**8.593**	**8.540**	**8.532**	**8.513**	**8.502**	**8.487**	**8.254**	**8.234**
OPT2 (12 state variables)								
No. of Execution	1	2	3	4	5	6	7	8	9-16
No. of Set	27	30	73	93	161	183	199	220	255
Mass (kg)	**8.540**	**8.516**	**8.361**	**8.283**	**8.222**	**8.215**	**8.215**	**8.141**	**8.025**
OPT3 (24 state variables)								
No. of Execution	1	2-3	4	5-7	8	9-16		
No. of Set	21	59	138	167	251	291		
Mass (kg)	**8.564**	**8.254**	**8.125**	**7.945**	**7.944**	**7.942**		

For the optimization analysis with six state variables, the best design is obtained in the 13^{th} execution with 814 sets; for the optimization analysis with twelve state variables, the best design is obtained in the 9^{th} execution with 255 sets; for the optimization analysis with twenty-four state variables, the best design is obtained in the 9^{th} execution with 291 sets.

As the number of state variables is increased from six to twelve, a great enhancement is achieved in optimization time and weight minimization, and a further enhancement is obtained with the use of twenty-four state variables.

The location or load case for the maximum stress and the load case for the maximum buckling load factor may change in each loop. So, choosing only one maximum for the stress and one minimum for the buckling load factor may result in poor quality

approximations for the state variables. On the other hand, choosing so many state variables may result in a local minimum. Using twenty-four state variables seems to work well for subsequent optimization analyses.

It is also observed that only one execution is not enough for the wing optimization. By using restarts with the best designs of previous executions, much better designs are obtained.

The initial design and best design optimization variables for three analyses are given in Table 4.2. Percent mass reduction with respect to initial design is also given in Table 4.2. The meaning for each abbreviation is given in the previous chapter in Table 3.1 and Table 3.2.

To obtain a better design, optimization analyses are continued by taking the best design given in Table 4.2 as the initial design using the subproblem method with smaller objective function tolerance. Then the first order method and again the subproblem method are used with the best designs of previous analyses. After all, local sensitivity analyses are performed with the gradient tool.

The best design optimization variables and percent mass reduction for subsequent optimization analyses with different methods are given in Table 4.3. Percent mass reduction is calculated with respect to initial design given in Table 4.2.

Table 4.2 Best design optimization variables for three analyses with different number of state variables for the aluminum wing.

		Initial Design	Best Design		
			OPT1	OPT2	OPT3
		SET 1	SET 814	SET 255	SET 291
DVs	tr_us	4.79	4.46	4.07	4.07
	t_ratio_us	5.07	4.12	3.24	3.29
	tr_ls	4.32	3.81	3.19	2.98
	t_ratio_ls	7.32	6.35	5.45	5.09
	tr_sw	7.91	10.49	12.16	13.30
	t_ratio_sw	5.12	5.73	7.85	8.71
	tr_sc	3.94	2.81	3.70	3.47
	t_ratio_sc	6.68	5.63	7.41	6.86
SVs	smax1_1	394.70	398.92	399.78	394.28
	smax1_2	167.51			190.76
	smax1_3	155.83			171.26
	smax1_4	118.43			119.63
	smax2_1	108.84		113.52	112.41
	smax2_2	47.19			58.98
	smax2_3	50.95			63.27
	smax2_4	90.12			90.07
	smax3_1	403.77		395.51	394.88
	smax3_2	176.54			193.32
	smax3_3	167.52			174.90
	smax3_4	245.50			248.13
	smax4_1	101.47		326.55	104.67
	smax4_2	54.60			78.70
	smax4_3	116.88			183.94
	smax4_4	300.94			332.56
	buckling1	0.99	0.99	1.01	1.00
	buckling2	2.16		1.52	1.41
	buckling3	0.99		1.00	0.99
	buckling4	0.99		1.02	1.01
	tt_us	0.94	1.08	1.25	1.24
	tt_ls	0.59	0.60	0.59	0.59
	tt_sw	1.55	1.83	1.55	1.53
	tt_sc	0.59	0.50	0.50	0.51
OBJ	mass (kg)	**8.547**	**8.234**	**8.025**	**7.942**
% mass reduction		-	3.66	6.11	7.08

Table 4.3 Best design optimization variables for subsequent optimization analyses for the aluminum wing.

		Sub-problem	First order	Sub-problem	Gradient
DVs	**tr_us**	4.06	4.00	4.05	4.05
	t_ratio_us	3.24	2.97	3.17	3.17
	tr_ls	2.88	2.68	2.82	2.82
	t_ratio_ls	4.81	4.27	4.69	4.69
	tr_sw	13.60	14.97	14.49	14.16
	t_ratio_sw	9.05	9.44	9.57	9.44
	tr_sc	3.33	2.70	2.71	2.69
	t_ratio_sc	6.58	5.05	4.96	5.37
SVs	**smax1_1**	395.68	381.35	376.16	379.60
	smax1_2	194.41	201.94	197.53	198.39
	smax1_3	173.78	178.94	176.65	177.28
	smax1_4	119.35	116.43	119.55	119.91
	smax2_1	113.03	112.36	111.00	111.96
	smax2_2	60.40	63.33	61.52	61.67
	smax2_3	63.81	64.51	64.55	64.67
	smax2_4	88.32	83.09	87.47	87.52
	smax3_1	398.19	402.81	400.26	403.94
	smax3_2	194.16	196.43	195.40	195.99
	smax3_3	175.27	175.24	176.18	176.63
	smax3_4	242.01	226.19	239.50	239.61
	smax4_1	106.04	108.40	106.89	107.71
	smax4_2	82.38	90.25	84.76	84.83
	smax4_3	187.91	194.78	191.13	191.11
	smax4_4	324.85	306.02	323.15	323.29
	buckling1	1.00	1.03	1.00	1.00
	buckling2	1.38	1.32	1.34	1.34
	buckling3	1.00	1.02	1.00	0.99
	buckling4	1.02	1.05	1.01	1.01
	tt_us	1.25	1.35	1.28	1.28
	tt_ls	0.60	0.63	0.60	0.60
	tt_sw	1.50	1.59	1.52	1.50
	tt_sc	0.51	0.53	0.55	0.50
OBJ	**mass (kg)**	**7.899**	**7.879**	**7.864**	**7.826**
% mass reduction		7.58	7.82	7.99	8.44

After nine executions with subproblem method (OPT3 results given in Table 4.1 and Table 4.2), little changes are obtained with the subsequent executions with the subproblem and first order methods as seen from Table 4.3. However, by only slightly changing the design variables with the gradient tool, more reduction in weight is obtained compared to other methods after performing several restarts with subproblem method.

First order method is so slow and found as inefficient for the optimization of the wing. One iteration takes approximately 35 minutes for the first order method and 2 minutes for the subproblem method using a personal computer with 3 GHz Intel-Pentium processor and 2 GB of RAM.

After gradient analyses, slight changes are obtained for the values of four design variables representing the root thickness and ratio of the spar web (tr_sw, t_ratio_sw), and the root thickness and ratio of the spar cap flange (tr_sc, t_ratio_sc) leading to the lower bound values for the tip thicknesses of spar web and spar cap flanges (tt_sw, tt_sc).

The PHAA (smax1_i) and PLAA (smax3_i) flight conditions are more critical than the NHAA (smax2_i) and NLAA (smax4_i) flight conditions for strength. It is an expected result since the load factors are higher for the PHAA and PLAA conditions as explained in Chapter 2.

It can be seen from Table 4.3 that buckling is more critical rather than strength for the aluminum wing. Because, buckling load factors for PHAA, PLAA and NLAA flight conditions (buckling1, buckling3, buckling4) take the lower bound value “1”, whereas maximum von Mises stresses (smax3_1) are below the upper bound value “400 MPa” except the first portion for the PLAA flight condition.

The upper skin thickness (4.05 mm) is thicker than the lower skin thickness (2.82 mm) as it is expected. The aerodynamic loads on the wing during PHAA and PLAA flight conditions bend it upwards, as a result the upper side of the wing is loaded in compression and buckling becomes a problem at these regions. In addition, the aerodynamic loads on the wing during NHAA and NLAA flight conditions bend it

downwards, as a result the lower side of the wing is loaded in compression and buckling becomes a problem at these regions. But since positive load factor is greater than the negative load factor in magnitude, upper skin panels are more critical than the lower skin panels.

Root thickness for the spar web is found to be very close to the upper bound value. This is an expected result because of the boundary conditions which are selected considering the mechanism for unfolding wings. This choice of boundary condition makes the root of the spars to be the most critical part of the wing structure as explained in Section 5 of Chapter 3.

The von Mises stress distribution for top of the shell elements are given in Figure 4.1 and for bottom of the shell elements are given in Figure 4.2. The axial stress distribution for beam elements is given in Figure 4.3. Stress distributions given are the results of the PLAA flight condition. The skin panels carry also bending load especially at the root as understood from the difference in results between top and bottom of shell elements.

U_y distributions for the most critical panels obtained from the buckling analyses for each flight condition are given in Figure 4.4. Upper skin panels at the second and third portions are the most critical parts for PHAA and PLAA flight conditions, lower skin panels at the third portion are the most critical parts for NHAA flight condition and lower skin panels at the fourth portion are the most critical parts for NLAA flight condition when considering buckling.

Hence, the best design weight for the wing is found as ***15.652 kg*** (7.826x2). Weight for the wing is 1.3% of the total weight of the cruise missile. For different aircrafts this ratio changes between 7.5-12% [1]. But using the weight estimation formulae for light utility aircraft given in [1], the estimated weight is found as 19.241 kg for the cruise missile wing which is 1.6% of the total weight of the cruise missile. The estimated weight is greater than the best design weight found by ANSYS as expected. This is because, weight found for the cruise missile will increase when connection elements are included and fatigue and thermal loads are taken into consideration. Another factor that reduces the weight of the wing is the absence of control surfaces.

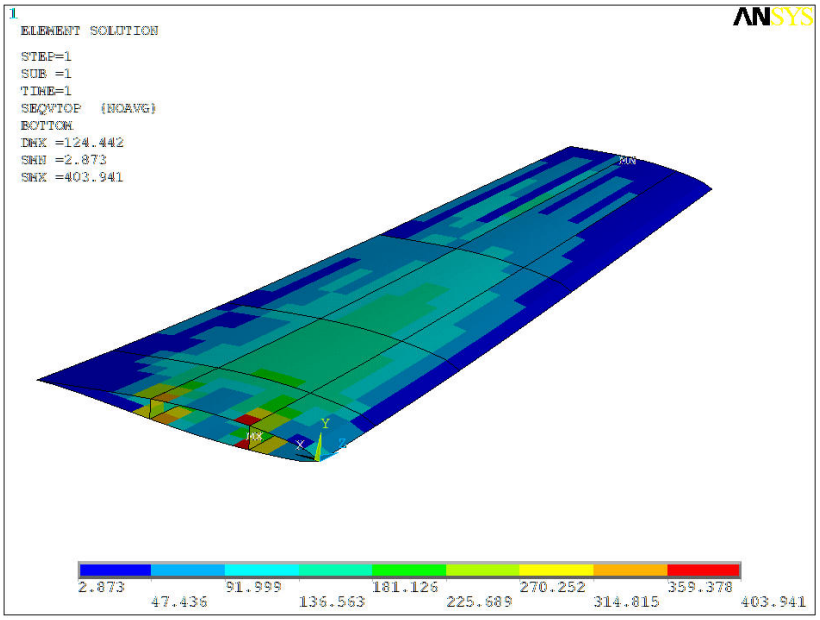

Figure 4.1 The von Mises stress (MPa) distribution for top of the shell elements for PLAA flight condition for the aluminum wing.

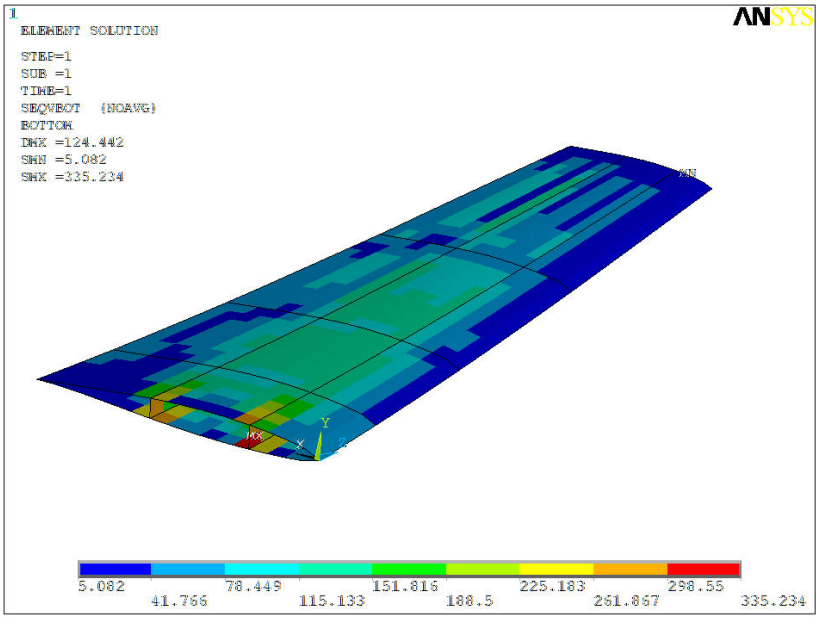

Figure 4.2 The von Mises stress (MPa) distribution for bottom of the shell elements for PLAA flight condition for the aluminum wing.

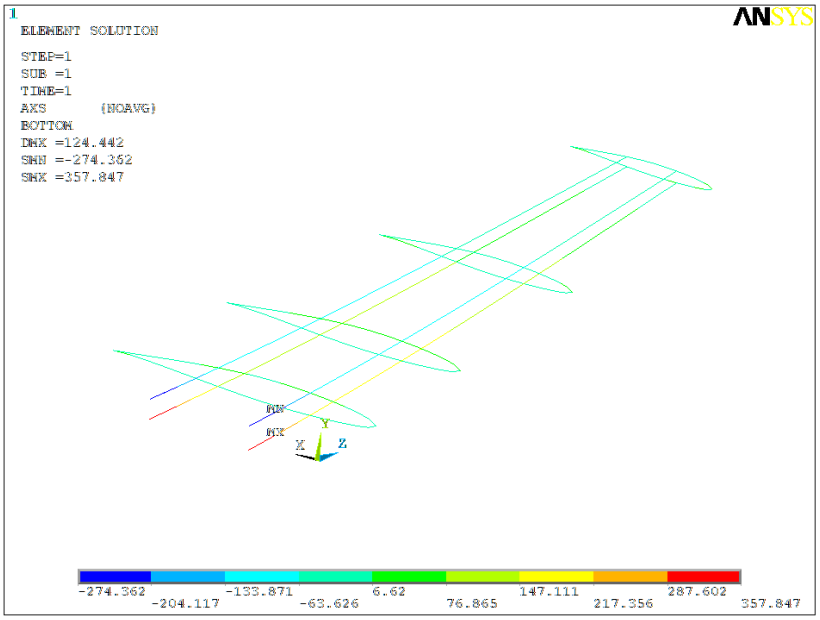

Figure 4.3 The axial stress (MPa) distribution for beam elements for PLAA flight condition for the aluminum wing.

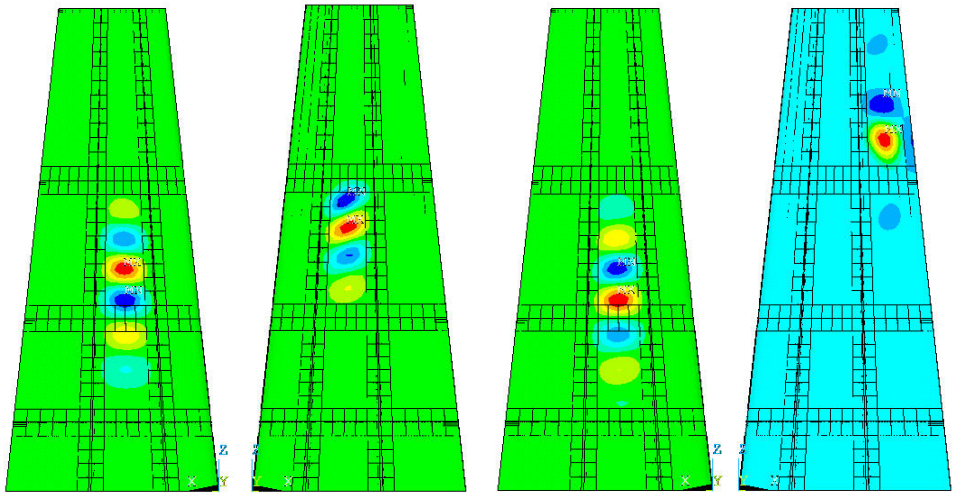

PHAA (upper skin) | NHAA (lower skin) | PLAA (upper skin) | NLAA (lower skin)

Figure 4.4 U_y distributions obtained from the buckling analyses for each flight condition for the aluminum wing.

4.3 RESULTS FOR THE COMPOSITE WING

For the composite wing, four portions are separately optimized. The optimization analyses are started for the first portion which includes all the elements from root to first rib, including the first rib. When this portion is optimized the values of the design variables for the other portions are taken as constant. These values are chosen after some preliminary analyses in order to provide the other portions not to buckle and also not have an unrealistic geometry. Because, buckling load factor is given only for the most critical part of the wing structure after a buckling analysis. So, it is important to provide the buckling of the portion to be optimized instead of others in order to have a good approximation for the buckling. The selected design variable values for other portions and the values of initial design for the first portion are given in Table 3.6.

After the first portion is optimized, optimization analyses are started for the second portion which includes all the elements from first rib to second rib, excluding the first rib and including the second rib. When this portion is optimized, the values of the design variables for the first portion are taken as constant which has the values of best design of the first portion. The values of the design variables for the third and fourth portions and the values of initial design for the second portion are the same with the values used in the first portion optimization as given in Table 3.6. Optimization analyses have the same procedure for the third and fourth portions.

From the global sensitivity analyses performed with the sweep tool in ANSYS, it is seen that the effect of the rib web and rib flange thicknesses on the strength and buckling results are negligible as in the aluminum wing. So, for the subsequent optimization analyses, two design variables representing rib web and rib cap flange thicknesses (t_rw, t_rc) are eliminated for each portion and taken constant as given in Table 3.6.

It must be also noted that the upper bound for the root thickness of the spar web (tr_sw) is taken as 10 mm in the first analyses but it is seen that infeasible designs are created by the optimizer. So, root thickness of the spar web is increased to 15 mm for the subsequent analyses.

4.3.1 Optimization of the First Portion without Buckling Constraints

Initially, as it is mentioned in Chapter 3, optimization analyses are performed without buckling constraints. After creating initial designs with sweep and random tools, several restarts are performed using subproblem method then finished with the gradient tool. The best design optimization variables for the first portion without buckling constraints are given in Table 4.4. The meaning for each abbreviation is given in the previous chapter in Table 3.3 and Table 3.4.

Table 4.4 Best design optimization variables for Portion-1 of the composite wing without buckling constraints.

DVs	**n90_us1**	7	**SVs**	**smax_alu1**	401.04
	n45_us1	2		**smax_alu2**	107.90
	n0_us1	0		**smax_alu3**	379.57
	n90_ls1	5		**smax_alu4**	109.68
	n45_ls1	9		**fcs1**	0.85
	n0_ls1	0		**fce1**	0.98
	tr_sw1	14.97		**fctwi1**	1.00
	t_ratio_sw1	1.63		**fcs2**	0.40
	tr_sc1	4.94		**fce2**	0.43
	t_ratio_sc1	6.82		**fctwi2**	0.42
				fcs3	0.95
				fce3	1.01
				fctwi3	0.99
				fcs4	0.33
				fce4	0.37
				fctwi4	0.36
				t_us1	2.75
				t_ls1	5.75
				tt_sw1	9.19
				tt_sc1	0.72
			OBJ	**mass (kg)**	**2.058**

Without buckling constraints, upper skin thickness (2.75 mm) is found as nearly half of the bottom skin thickness (5.75 mm). In PHAA and PLAA flight conditions which is more critical than the NHAA and NLAA flight conditions, upper skin panels are loaded in compression and lower skin panels are loaded in tension. This is the reason of thicker lower skin panels since the tensile strength is much smaller than the compressive strength in transverse direction for high strength carbon/epoxy material (Table 3.5).

It is also observed that numbers of 0^o ply orientations for both upper and lower skin panels are found as zero after optimization analysis for the first portion. The stacking sequences of the best design are $(90_7/(\pm45)_2)_s$ for the upper skin panels and $(90_5/(\pm45)_9)_s$ for the lower skin panels. This is an indication of much greater stiffness requirement in spanwise direction than the requirement in chordwise direction as expected. Because, 0^o ply orientations increase the stiffness in chordwise direction.

Root thickness for the spar web is found to be very close to the upper bound as in the aluminum wing. This is an expected result because of the boundary conditions as explained in the previous section.

After performing the optimization analyses for the first portion, buckling analyses are performed and minimum buckling load factor is obtained as 0.92 for the PLAA flight condition at the upper skin panels of the first portion. U_y displacement distributions obtained from the buckling analyses for each flight condition is given in Figure 4.5. Lower skin panels at the second portion is more critical than the first portion for NHAA and NLAA flight conditions as seen in Figure 4.5.

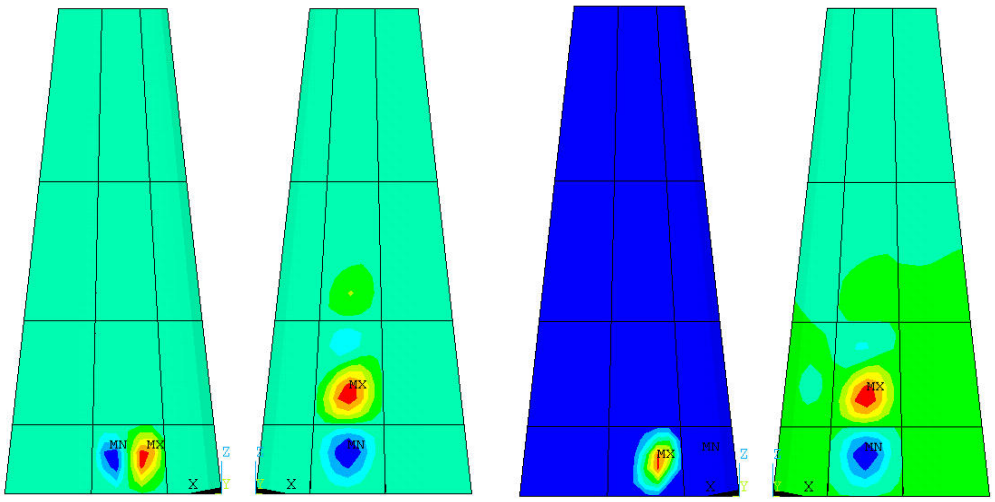

Figure 4.5 U_y displacement distributions obtained from the buckling analyses for each flight condition for composite wing (optimization results for Portion-1 without buckling constraints).

In order to have a buckling load factor greater than one, analyses are repeated for different stacking sequences of the upper skin panels for the first portion and at the first trial a feasible design is obtained. The buckling load factors with different stacking sequences are given in Table 4.5. The maximum stress values and failure criteria values for the stacking sequences given in Table 4.5 are very close to each other.

Table 4.5 Buckling load factors for different stacking sequences of the upper skin panels for Portion-1 of the composite wing without buckling constraints.

	$(90_7/(\pm45)_2)_s$	$(90_4/\pm45/90_2/\pm45/90)_s$	$(90_2/\pm45/90_4/\pm45/90)_s$
buckling1	0.99	1.05	1.08
buckling2	9.36	9.35	9.35
buckling3	0.92	1.01	1.06
buckling4	9.82	9.82	9.82

Buckling load factors for the NHAA and NLAA flight conditions (buckling2, buckling4) are nearly the same for different stacking sequences given in Table 4.5, since buckling occurs at the lower skin panels for these flight conditions and the stacking sequence of the lower skin panels is not changed. Furthermore, buckling load factors are very large for NHAA and NLAA flight conditions. Because, lower skin panels are very thick to have sufficient strength for tensile loading in PHAA and PLAA flight conditions.

Using a stacking sequence of $(90_2/\pm45/90_4/\pm45/90)_s$ for the upper skin panels of the first portion instead of $(90_7/(\pm45)_2)_s$, 9% increase in the buckling load factor for the PHAA flight condition (buckling1) and 15% increase in the buckling load factor for the PLAA flight condition (buckling3) is obtained. Differences in buckling load factors are caused by the differences in flexural stiffness matrix (**D**) for different stacking sequences.

4.3.2 Optimization of the Second Portion without Buckling Constraints

Using the best design optimization variables for the first portion given in Table 4.4, optimization analyses are then performed for the second portion without buckling constraints. The best design optimization variables found for the second portion are given in Table 4.6.

End thicknesses for spar web and spar cap flanges take the lower bound values after optimization analyses and the thicknesses for both upper and lower skin panels are found as 1.5 mm as seen in Table 4.6. The stacking sequence of the best design is $(90/0_3/\pm45)_s$ for the upper skin panels and $(90_2/(\pm45)_2)_s$ for the lower skin panels of the second portion.

Table 4.6 Best design optimization variables for Portion-2 of the composite wing without buckling constraints.

DVs	**n90_us2**	1		**smax_alu1**	372.55
	n45_us2	1		**smax_alu2**	101.82
	n0_us2	3		**smax_alu3**	361.12
	n90_ls2	2		**smax_alu4**	97.14
	n45_ls2	2	**SVs**	**fcs1**	0.75
	n0_ls2	0		**fce1**	0.71
	t_ratio_sw2	6.19		**fctwi1**	0.73
	t_ratio_sc2	1.45		**fcs2**	0.42
				fce2	0.50
				fctwi2	0.50
				fcs3	0.89
				fce3	0.94
				fctwi3	0.99
				fcs4	0.90
				fce4	0.91
				fctwi4	0.89
				t_us2	1.50
				t_ls2	1.50
				tt_sw2	1.49
				tt_sc2	0.50
			OBJ	**mass (kg)**	**1.044**

After performing the optimization analyses for the second portion, buckling analyses are performed and buckling load factors are obtained as 0.252, 0.620, 0.248, 0.482 for the PHAA, NHAA, PLAA and NLAA flight conditions respectively. The minimum buckling load factor is obtained for the PLAA flight condition at the upper skin panels of the second portion. So, analyses are repeated for different stacking sequences of the upper skin panels of the second portion for the PLAA flight condition. The buckling load factors with different stacking sequences are given in Table 4.7.

Table 4.7 Buckling load factors for different stacking sequences of the upper skin panels for Portion-2 of the composite wing without buckling constraints.

	buckling3
$\mathbf{(0_3/\pm45/90)_s}$	0.143
$\mathbf{(0/\pm45/0/90/0)_s}$	0.201
$\mathbf{(0/90/\pm45/0_2)_s}$	0.242
$\mathbf{(90/0_3/\pm45)_s}$	0.248
$\mathbf{(\pm45/90/0_3)_s}$	0.260
$\mathbf{(90/0/\pm45/0_2)_s}$	0.264
$\mathbf{(90/\pm45/0_3)_s}$	0.276

The buckling load factor changes between 0.143 and 0.276 as seen in Table 4.7. The upper skin panels of the second portion buckle whatever the stacking sequence is, since very thin skin panels are sufficient for strength constraints. It is also observed that if the 90^o layers are on the outside and the 0^o layers are in the interior, maximum buckling load factor is obtained; minimum buckling load factor is obtained in the opposite case.

The optimization analyses without buckling constraints are stopped at this point and, it is understood that strength and buckling optimization must be performed simultaneously. Then the optimization analyses are performed with the addition of buckling constraints for each portion.

4.3.3 Optimization of the First Portion

Initially, optimization analyses are performed for the first portion. After creating initial designs with sweep and random tools, several restarts are performed using subproblem method. After a while, it is observed that the stresses and failure criteria values are much smaller than the allowable values and the buckling load factors are much greater than one for the NHAA and NLAA flight conditions. It is also observed that, root thickness of the spar web takes the upper bound value “15 mm”, numbers of 0^o ply orientations for both upper and lower skin panels take the lower bound value “0” and the thickness of the spar cap flanges at the end of the first portion takes the lower bound value “0.5 mm”. So for the subsequent analyses, two load cases are eliminated (NHAA and NLAA flight

conditions) and four design variables (n0_us1, n0_bs1, t_ratio_sc1, tr_sw1) are taken as constant. By this way, weight minimization is obtained in a shorter time. Then optimization analyses are finished with the gradient tool. The best design variables for the first portion are given in Table 4.8.

Table 4.8 Best design optimization variables for Portion-1 of the composite wing.

DVs	**n90_us1**	8	**SVs**	**smax_alu1**	374.03
	n45_us1	2		**smax_alu2**	100.10
	n0_us1	0		**smax_alu3**	355.58
	n90_ls1	6		**smax_alu4**	101.96
	n45_ls1	9		**fcs1**	0.85
	n0_ls1	0		**fce1**	0.91
	tr_sw1	15		**fctwi1**	0.92
	t_ratio_sw1	1.82		**fcs2**	0.38
	tr_sc1	4.81		**fce2**	0.42
	t_ratio_sc1	9.62		**fctwi2**	0.41
				fcs3	0.94
				fce3	1.01
				fctwi3	0.99
				fcs4	0.32
				fce4	0.36
				fctwi4	0.35
				buckling1	1.19
				buckling2	9.62
				buckling3	1.11
				buckling4	10.17
				t_us1	3
				t_ls1	6
				tt_sw1	8.25
				tt_sc1	0.5
			OBJ	**mass (kg)**	**2.115**

The stacking sequences of the best design for the first portion are $(90_8/(\pm45)_2)_s$ for the upper skin panels and $(90_6/(\pm45)_9)_s$ for the lower skin panels. When compared with the results without buckling constraints (Table 4.4), an increase of 0.25 mm in both the upper and lower skin thicknesses is obtained with the addition of buckling constraints.

In addition, half the number of ±45^o and 0^o ply orientations are the same for both of the cases, and numbers of 90^o ply orientations obtained with buckling constraints are one more than the numbers of 90^o ply orientations obtained without buckling constraints.

Mass of the best design for the first portion is found as 2.115 kg which is very close to the mass found without buckling constraints (2.058 kg) as expected. Because, thicknesses are very thick to have sufficient strength for the loading in PHAA and PLAA flight conditions.

4.3.4 Optimization of the Second Portion

After the optimization of the first portion is completed, optimization analyses are started for the second portion. Since the thickness of the spar cap flanges is found to be the lower bound value "0.5 mm" at the end of the first portion, thickness of the spar cap flanges at the second portion is taken as constant (t_ratio_sc2=1). In addition, after a while it is observed that, the thickness of the spar web at the end of the second portion takes the lower bound value "1.5 mm". So, the subsequent optimization analyses are continued with six design variables (half the number of 0^o, 90^o and (45/-45)^o ply orientations).

Optimization analyses with two different initial designs for the second portion lead to two different best designs with a mass of 1.64 kg. Then subsequent analyses are performed using these two designs as initial designs. After performing several restarts using subproblem method, an optimum design with a mass of 1.57 kg is obtained which is 50% higher than the mass obtained without buckling constraints (1.044 kg). Local sensitivity analyses are also performed for the best design by decreasing the each number of ply orientations by "1", but for six of the analyses infeasible designs are obtained. The best design variables for the second portion are given in Table 4.9.

The stacking sequences of the best design for the second portion are $(90/0/(\pm45)_6)_s$ for the upper skin panels and $(90_4/(\pm45)_2)_s$ for the lower skin panels. When compared with the results without buckling constraints (Table 4.6), thicknesses are increased from 1.5 mm to 3.5 mm for the upper skin panels and from 1.5 mm to 2 mm for the lower skin panels.

The upper skin thickness for the second portion (3.5 mm) is found as greater than the upper skin thickness for the first portion (3 mm). A reduction in skin panels from root to tip can be obtained by adding a rib in between the first and second ribs.

It is seen from Table 4.9, that strength constraints are smaller than the upper bound values and buckling load factors are very close to lower bound value of one. So, buckling constraints have primary importance on the thicknesses of the skin panels for the second portion.

Table 4.9 Best design optimization variables for Portion-2 of the composite wing.

DVs	**n90_us2**	1	**SVs**	**smax_alu1**	226.69
	n45_us2	6		**smax_alu2**	58.60
	n0_us2	1		**smax_alu3**	259.59
	n90_ls2	4		**smax_alu4**	58.06
	n45_ls2	2		**fcs1**	0.48
	n0_ls2	0		**fce1**	0.71
	t_ratio_sw2	5.5		**fctwi1**	0.80
	t_ratio_sc2	1		**fcs2**	0.33
				fce2	0.36
				fctwi2	0.35
				fcs3	0.49
				fce3	0.73
				fctwi3	0.81
				fcs4	0.55
				fce4	0.60
				fctwi4	0.58
				buckling1	1.00
				buckling2	1.07
				buckling3	0.99
				buckling4	1.21
				t_us2	3.5
				t_ls2	2
				tt_sw2	1.5
				tt_sc2	0.5
			OBJ	**mass (kg)**	**1.570**

4.3.5 Optimization of the Third and Fourth Portions

With the completion of optimization analyses for the second portion, optimization analyses for the third portion then for the forth portion are performed. Since the thickness of the spar cap flanges is found to be the lower bound value "0.5" at the end of the first portion and the thickness of the spar web at the end of the second portion is found to be the lower bound value "1.5", thicknesses of the spar cap flanges and spar webs at the third and fourth portions are taken as constant. The best design variables for the third portion are given in Table 4.10.

Table 4.10 Best design optimization variables for Portion-3 of the composite wing.

DVs	**n90_us3**	1	**SVs**	**smax_alu1**	223.55
	n45_us3	4		**smax_alu2**	55.77
	n0_us3	2		**smax_alu3**	247.78
	n90_ls3	2		**smax_alu4**	57.24
	n45_ls3	1		**fcs1**	0.73
	n0_ls3	2		**fce1**	0.81
	t_ratio_sw2	1		**fctwi1**	0.79
	t_ratio_sc2	1		**fcs2**	0.22
				fce2	0.25
				fctwi2	0.24
				fcs3	0.74
				fce3	0.80
				fctwi3	0.79
				fcs4	0.69
				fce4	0.70
				fctwi4	0.68
				buckling1	1.03
				buckling2	1.16
				buckling3	1.02
				buckling4	1.34
				t_us3	2.75
				t_ls3	1.5
				tt_sw3	1.5
				tt_sc3	0.5
			OBJ	**mass (kg)**	**1.251**

The stacking sequences of the best design for the third portion are $(90/0_2/(\pm45)_4)_s$ for the upper skin panels and $(90_2/0_2/\pm45)_s$ for the lower skin panels. The thickness is found as 2.75 mm for the upper skin panels and as 1.5 mm for the lower skin panels.

Using different methods, objective function tolerances and limits for the design variables, three optimum designs are obtained for the fourth portion with the same mass:

- The stacking sequence of the first alternative design is $(90/0_3/\pm45)_s$ for the upper skin panels and $(90/0/\pm45)_s$ for the lower skin panels.

- The stacking sequence of the second alternative design is $(90/0/(\pm45)_2)_s$ for the upper skin panels and $(0_2/\pm45)_s$ for the lower skin panels.

- The stacking sequence of the third alternative design is $(90/\pm45/0_3)_s$ for the upper skin panels and $((\pm45)_2)_s$ for the lower skin panels.

The buckling coefficients are nearly the same, but strength values differ for these optimum designs. Maximum von Mises stresses are nearly the same for the second and third alternative designs, but failure criteria values are smaller for the third one. First alternative design has the smallest values for the maximum von Mises stresses, but failure criteria values are larger than the third one. Although maximum von Mises stresses are so small compared to yield stress of aluminum, failure criteria values are close to one for the NLAA flight condition in the first alternative design. So, the third alternative design is chosen for the fourth portion of the composite wing.

The best design variables for the fourth portion are given in Table 4.11 for the first alternative and in Table 4.12 for the second alternative.

Subsequent analyses are performed using these three designs as initial designs. But a better design cannot be obtained by this way. It is also observed that when there is more than one best designs with the same objective function value, ANSYS lists the best design with the smallest set number. However, in order to use the best design for a subsequent analysis, ANSYS selects the best design with the largest set number.

It must be also noted that, no better results can be obtained with the first-order method for any portions of the composite wing and this method is found so slow and inefficient as in the aluminum wing.

Table 4.11 Best design optimization variables for Portion-4 of the composite wing (1st alternative).

DVs	**n90_us4**	1	**SVs**	**smax_alu1**	144.78
	n45_us4	1		**smax_alu2**	41.30
	n0_us4	3		**smax_alu3**	141.76
	n90_ls4	1		**smax_alu4**	90.78
	n45_ls4	1		**fcs1**	0.45
	n0_ls4	1		**fce1**	0.49
	t_ratio_sw2	1		**fctwi1**	0.48
	t_ratio_sc2	1		**fcs2**	0.26
				fce2	0.27
				fctwi2	0.26
				fcs3	0.66
				fce3	0.66
				fctwi3	0.65
				fcs4	0.87
				fce4	0.88
				fctwi4	0.86
				buckling1	1.01
				buckling2	1.01
				buckling3	1.00
				buckling4	1.15
				t_us4	1.5
				t_ls4	1
				tt_sw4	1.5
				tt_sc4	0.5
			OBJ	**mass (kg)**	**0.780**

Table 4.12 Best design optimization variables for Portion-4 of the composite wing (3rd alternative, chosen one).

DVs	**n90_us4**	1	**SVs**	**smax_alu1**	213.65
	n45_us4	1		**smax_alu2**	60.75
	n0_us4	3		**smax_alu3**	199.50
	n90_ls4	0		**smax_alu4**	82.99
	n45_ls4	2		**fcs1**	0.43
	n0_ls4	0		**fce1**	0.42
	t_ratio_sw2	1		**fctwi1**	0.55
	t_ratio_sc2	1		**fcs2**	0.19
				fce2	0.15
				fctwi2	0.23
				fcs3	0.42
				fce3	0.45
				fctwi3	0.49
				fcs4	0.56
				fce4	0.45
				fctwi4	0.61
				buckling1	1.01
				buckling2	1.01
				buckling3	1.00
				buckling4	1.15
				t_us4	1.5
				t_ls4	1
				tt_sw4	1.5
				tt_sc4	0.5
			OBJ	**mass (kg)**	**0.780**

It is seen from Table 4.10 and Table 4.12, that strength constraints are smaller than the upper bound values and buckling load factors are very close to lower bound value of one. So, buckling constraints have also primary importance on the thicknesses of the skin panels for the third and fourth portions as for the second portion.

With the completion of optimization analyses for the fourth portion, optimum design is obtained for the whole composite wing with a total mass of ***11.432 kg*** (5.716x2). With the use of carbon/epoxy instead of aluminum for the skin panels, a mass reduction of 27% is obtained.

4.3.6 Final Checks and Adjustments for the Best Design of the Composite Wing

For the composite wing, when a portion is optimized the values of the design variables for the other portions are taken as constant. Although the values of the design variables for the portions at the root side have the best design values, the values of the design variables for the portions at the tip side of the wing are taken different from the best designs of each portion. So, after the completion of optimization analyses for the four portions, strength constraints are recalculated for the first, second and third portions.

Comparison of the values of the strength constraints found after the optimization of a portion with the values for the best design is given in Table 4.13. The constraint values under the column of "before" in Table 4.13 is the values obtained after the optimization analyses for that portion which are given before in Table 4.8, Table 4.9 and Table 4.10. The constraint values under the column of "after" is the values obtained for that portion for the best design of the wing. In addition, P-1, P-2 and P-3 represents Portion-1, Portion-2 and Portion-3 respectively.

Table 4.13 Comparison of the values of the strength constraints found after the optimization of a portion with the values for the best design for Portions 1-3 of the composite wing.

	P-1 before	**P-1 after**	**P-2 before**	**P-2 after**	**P-3 before**	**P-3 after**
smax_alu1	374.03	379.30	226.69	227.89	223.55	229.32
smax_alu2	100.10	101.21	58.60	59.24	55.77	56.77
smax_alu3	355.58	360.65	259.59	252.06	247.78	233.74
smax_alu4	101.96	102.74	58.06	94.53	57.24	102.76
fcs1	0.85	0.83	0.48	0.48	0.73	0.77
fce1	0.91	0.91	0.71	0.70	0.81	0.84
fctwi1	0.92	0.92	0.80	0.79	0.79	0.82
fcs2	0.38	0.38	0.33	0.33	0.22	0.21
fce2	0.42	0.42	0.36	0.36	0.25	0.24
fctwi2	0.41	0.41	0.35	0.35	0.24	0.24
fcs3	0.94	0.92	0.49	0.49	0.74	0.78
fce3	1.01	0.99	0.73	0.72	0.80	0.85
fctwi3	0.99	0.97	0.81	0.80	0.79	0.83
fcs4	0.32	0.32	0.55	0.58	0.69	0.69
fce4	0.36	0.36	0.60	0.63	0.70	0.70
fctwi4	0.35	0.35	0.58	0.61	0.68	0.68

As seen from Table 4.13, there are negligible changes for the values of the strength constraints except the maximum von Mises stresses for the aluminum parts of the second and third portions for the NLAA flight condition (smax_alu4). When the stresses are examined, it is seen that the location of the maximum stress is changed from spar web to rib web. Although these stresses are still much below the yield stress of the aluminum, for a similar study it is recommended to include the rib at the root side and exclude the rib at the tip side for the portion optimized.

U_y distributions for the most critical panels obtained from the buckling analyses for each flight condition are given in Figure 4.6. Upper skin panels at the first and second portions are the most critical parts for PHAA and PLAA flight conditions, lower skin panels at the second portion are the most critical parts for NHAA and NLAA flight conditions when considering buckling.

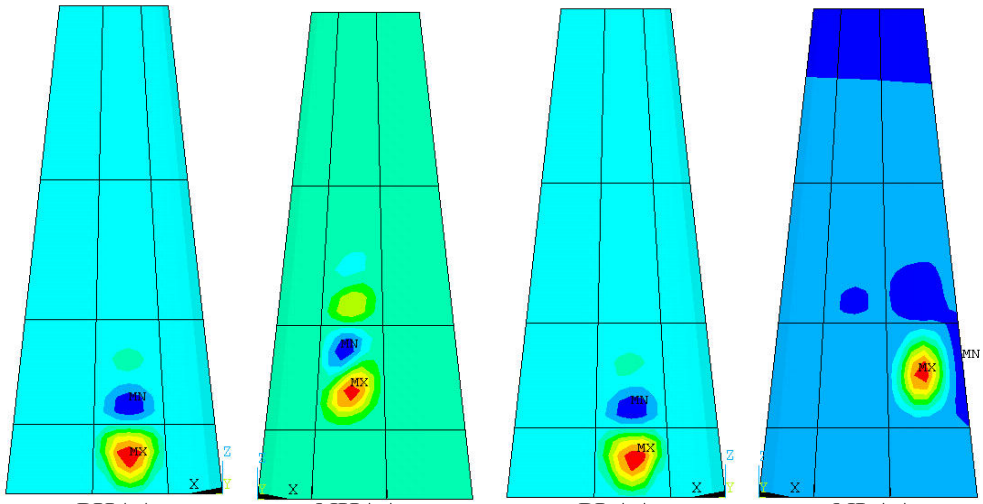

Figure 4.6 U_y displacement distributions obtained from the buckling analyses for each flight condition for the composite wing.

Laminates with more than four contiguous layers of the same fiber orientation are generally assumed to be not practical because of thermal stresses created during the curing process, which can lead to matrix cracking [3]. So, different stacking sequences for the most critical panels with not more than four contiguous layers, stress and buckling analyses are repeated for the four load cases.

The values of the strength and buckling constraints for different stacking sequences of the upper skin panels for the first portion is given in Table 4.14 and for different stacking sequences of the lower skin panels for the second portion is given in Table 4.15.

Stacking sequences used in Table 4.14 are as follows:

First Stacking Sequence	(SS_1):	$(90_3/\pm45/90_3/\pm45/90_2)_s$
Second Stacking Sequence	(SS_2):	$(90_4/\pm45/90_4/\pm45)_s$
Third Stacking Sequence	(SS_3):	$(90_4/\pm45/90_2/\pm45/90_2)_s$
Fourth Stacking Sequence	(SS_4):	$(90_2/\pm45/90_4/\pm45/90_2)_s$

Stacking sequences used in Table 4.15 are as follows:

First Stacking Sequence	(SS_1):	$(\pm45/90_2/\pm45/90_2)_s$
Second Stacking Sequence	(SS_2):	$(90_3/\pm45/90/\pm45)_s$
Third Stacking Sequence	(SS_3):	$(90_2/\pm45/90_2/\pm45)_s$

For the upper skin panels of the first portion, fourth stacking sequence "$(90_2/\pm45/90_4/\pm45/90_2)_s$" gives the best results compared to other stacking sequences as seen in Table 4.14. For the lower skin panels for the second portion, first stacking sequence "$(\pm45/90_2/\pm45/90_2)_s$" gives the best results compared to other stacking sequences as seen in Table 4.15. But it is also seen that, there is not much difference in the values of the strength and buckling constraints for different stacking sequences.

Table 4.14 The values of the strength and buckling constraints for different stacking sequences of the upper skin panels for Portion-1 of the composite wing.

	SS_1	SS_2	SS_3	SS_4
smax_alu1	379.02	379.14	379.09	378.93
smax_alu2	101.08	101.13	101.11	101.05
smax_alu3	360.44	360.54	360.50	360.38
smax_alu4	102.61	102.66	102.64	102.58
fcs1	0.83	0.83	0.83	0.83
fce1	0.88	0.88	0.88	0.88
fctwi1	0.88	0.88	0.88	0.87
fcs2	0.37	0.38	0.37	0.37
fce2	0.41	0.41	0.41	0.41
fctwi2	0.40	0.40	0.40	0.40
fcs3	0.92	0.92	0.92	0.92
fce3	0.98	0.99	0.98	0.98
fctwi3	0.96	0.96	0.96	0.96
fcs4	0.32	0.32	0.32	0.32
fce4	0.36	0.36	0.36	0.36
fctwi4	0.35	0.35	0.35	0.35
buckling1	1.08	1.06	1.07	1.10
buckling2	1.01	1.01	1.01	1.01
buckling3	1.07	1.05	1.06	1.08
buckling4	1.15	1.15	1.15	1.15

Table 4.15 The values of the strength and buckling constraints for different stacking sequences of the lower skin panels for Portion-2 of the composite wing.

	SS_1	SS_2	SS_3
smax_alu1	227.50	227.67	227.43
smax_alu2	58.29	59.03	58.81
smax_alu3	252.69	252.07	252.15
smax_alu4	57.55	81.79	67.62
fcs1	0.48	0.48	0.48
fce1	0.70	0.70	0.70
fctwi1	0.79	0.79	0.79
fcs2	0.23	0.28	0.26
fce2	0.26	0.32	0.30
fctwi2	0.26	0.32	0.30
fcs3	0.49	0.49	0.49
fce3	0.72	0.72	0.72
fctwi3	0.80	0.80	0.80
fcs4	0.30	0.53	0.48
fce4	0.35	0.57	0.52
fctwi4	0.34	0.56	0.51
buckling1	1.01	1.01	1.01
buckling2	1.09	1.03	1.05
buckling3	1.00	1.00	1.00
buckling4	1.24	1.19	1.20

CHAPTER 5

CONCLUSION

Weight minimization of a cruise missile wing subjected to strength and buckling constraints has been achieved by use of ANSYS Finite Element program for two configurations having different materials for the skin panels; 7075 aluminum and high-strength carbon/epoxy. All the other structural members (spars, spar caps, ribs and rib caps) were 7075 aluminum for both of the wing configurations.

In order to perform a structural analysis, it is important to determine the most critical loads on the structure. The maneuvers of a flight vehicle usually create the most critical loads for a wing structure. So before the optimization analyses have started, a V-n diagram was constructed based on the CFD analyses performed in FASTRAN program.

The load factors for the cruise missile wing were found as +2.8 and -0.8. The negative load factor was found a little small compared to other types of airplanes. In FAR 23 [24], it is mentioned that negative load factor may not be less than 0.4 times the positive load factor for the normal and utility airplanes and not less than 0.5 times the positive load factor for the acrobatic airplanes. But since a cruise missile need not make an upside down flight, a negative load factor smaller than one in magnitude is acceptable. Nevertheless using a higher velocity for the NHAA flight condition would increase the absolute value of the negative load factor.

The pressure distributions for the flight conditions at the corner points of the V-n diagram were then transferred to ANSYS to create the four load cases of the optimization analyses. Since the fluid and the structural meshes do not match at the wing surface, transfer of the pressure data creates some errors. As the element size of the structural model decreases, errors also decrease. But, since too many analyses have to be performed for optimization and small element size will increase optimization time,

a compromise was made between the transfer error and optimization time for the element size.

The design variables which determines the number of ribs and location of ribs and spars were taken as constant since changing the values of these design variables caused the mesh to change and the results were highly mesh-dependent. However, it is possible to include these design variables using a finer mesh in the finite element model and performing the analyses using more powerful computers.

In ANSYS, as the number of design variables increases the efficiency of the optimization decreases. So, a great effort was made to minimize the number of design variables when creating the ANSYS input files for the two wing configurations. In addition, a further decrease in design and state variables was made during the optimization analyses to provide a better result in a shorter time. A study was also done to see the effect of number of state variables for strength and buckling constraints. For the aluminum wing and for each portion of the composite wing, sixteen strength constraints, four buckling constraints and four size constraints were used.

For the composite skin panels, maximum stress, maximum strain and inverse Tsai-Wu failure criteria were used. For Tsai-Wu failure criteria there are two different formulations used by different researchers. ANSYS offers both of them and distinguishes them with the names Tsai-Wu and inverse Tsai-Wu. Different failure criteria values were compared for a split disk test and it was observed that, Tsai-Wu failure criterion gives conservative results compared to other three failure criteria.

In the optimization analyses, better designs were obtained performing subsequent executions (restart) with the best designs of previous execution with the subproblem method. For the best design obtained after several restarts, local sensitivity analyses using the gradient tool were performed to obtain a better design. First order method was so slow and found as inefficient for the optimization of both aluminum and composite wing.

After the optimization analyses, total mass of the wing was found as 15.652 kg for the aluminum wing and 11.432 kg for the composite wing. So, a mass reduction of 27% was obtained with the use of carbon/epoxy instead of aluminum for the skin panels.

Optimization analyses were successfully performed for the aerodynamic loads for four different flight conditions. Since the weight of the cruise missile wing was so small, gravity loads were not included. For a future study, other types of loadings such as thermal loads can be taken into consideration.

Structural optimization may easily involve more than 10 design variables, which is about the number that can be handled by ANSYS efficiently. A code written specifically for structural optimization purposes, GENESIS being one of them, may be preferable in a future study.

REFERENCES

[1] Niu M.C.Y., "*Airframe Structural Design"*, 2nd Edition, Hong Kong Conmilit Press Ltd., Hong Kong ,2002, pp 247.

[2] Bruhn E.F., "*Analysis and Design of Flight Vehicle Structures"*, 2nd Edition, Jacobs Publishing, Inc., Indianapolis, IN, 1973.

[3] Gürdal Z., Haftka R.T., Hajela P., "*Design and Optimization of Laminated Composite Materials"*, John Wiley & Sons, Inc, New York, 1999.

[4] Venkataraman S., Haftka R.T., "Optimization of Composite Panels – A Review", Proceedings of the 14th Annual Technical Conference of the American Society of Composites, Dayton, OH, Sep. 27-29, 1999

[5] "Buckling of Thin Walled Circular Cylinders", NASA SP-8007, NASA Space Vehicle Design Criteria (Structures), September 1965.

[6] Venkataraman S., Haftka R.T., "Structural Optimization: What Has Moores's Law Done for Us", AIAA-2002-1342, 43rd AIAA/ASME/ASCE /AHS/ASC Structures, Structural Dynamics and Materials Conference, Denver, CO, Apr. 22-25, 2002.

[7] Khot N.S., Venkayya V.B., Johnson C.D., Tischler V.A., "Optimization of Fiber Reinforced Composite Structures", International Journal of Solids and Structures, 1973. Vol.9, pp 1225-1236.

[8] Khot N.S., Venkayya V.B., Berke L., "Optimum Design of Composite Structures with Stress and Displacement Constraints", AIAA Journal, Vol.14 No.2, February 1976, pp 131-132.

[9] Haftka R., Starnes J.H., " Applications of Quadratic Extended penalty Function for Structural Optimization", AIAA Journal, Vol.14 No.2, February 1976, pp 718-724.

[10] Haftka R., Starnes J.H., "Preliminary Design of Composite Wings for Buckling, Strength and Displacement Constraints", AIAA Journal, Vol.16 No.8, August 1979, pp 564-570.

[11] Liu I.W., Lin C.C., “A Refined Optimality Criterion Technique Applied to Aircraft Wing Structural Design”, Computers & Structures, Vol.33 No.2, 1989, pp 427-434.

[12] Liu I.W., Lin C.C., “Optimum Design of Wing Structures by a Refined Optimality Criterion”, Computers & Structures, Vol.17, 1991, pp 51-65.

[13] Nagendra G.K., Fleury C., “Sensitivity and Optimization of Composite Structures in MSC/NASTRAN”, Finite Elements in Analysis and Design Vol.5, 1989, pp 223-235.

[14] Yurkovich R., “ The Use of Taguchi Techniques with the ASTROS Code for Optimum Wing Structural Design”, AIAA-94-1484

[15] Röhl P.J., Mavris D.N., Schrage D.P., “ HSCT Wing Design Through Multilevel Decomposition” AIAA 95-3944, 1st Aircraft Engineering, Technology and Operations Congress, Los Angeles, CA, Sept. 19-21, 1995.

[16] Liu B., Haftka R.T., Akgün M.A., “Composite Wing Structural Optimization Using Genetic Algorithms and Response Surfaces” AIAA 98-4854, 7th AIAA/USAF/NASA/ISSMO Symposium on Multidisciplinary Analysis and Optimization, St Louis, MO, Sept. 2-4, 1998.

[17] Liu B., Haftka R.T., Akgün M.A., “Two-Level Composite Wing Structural Optimization Using Response Surfaces” Structural and Multidisciplinary Optimization, Vol.20, 2000, pp 87-96.

[18] Liu B., Haftka R.T.,” Composite Wing Structural Design Optimization with Continuity Constraints” AIAA 2001-1205, 42nd AIAA/ASME/ASCE/ AHS/ASC Structures, Structural Dynamics and Materials Conference, Seattle, WA, Apr. 16-19, 2001.

[19] Liu B., Haftka R.T., Akgün M.A., Todoroki A., “Permutation Genetic Algorithm for Stacking Sequence Design of Composite Laminates”, Computational Methods in Applied Mechanical Engineering, Vol. 186, 2000, pp 357-372

[20] Kapania K.R., Chun S., “Preliminary Design of a Structural Wing-Box under a Twist Constraint”, AIAA 2003-2004, 44th AIAA/ASME/ASCE/ AHS/ASC Structures, Structural Dynamics and Materials Conference, Norfolk, VA, Apr. 7-10, 2003.

[21] Engelstad S.P., Barker D.K., Ellsworth C.S., Proctor L., “Optimization Strategies for the F/A-22 Horizontal Stabilizer”, AIAA 2003-1456, 44th AIAA/ASME/ASCE/AHS/ASC Structures, Structural Dynamics and Materials Conference, Norfolk, VA, Apr. 7-10, 2003.

[22] Peery D.J., Azar J.J., *"Aircraft Structures"*, McGraw- Hill, Inc.,1982

[23] Raymer D.P., "*Aircraft Design: A Conceptual Approach"*, AIAA Education Series, 2nd Edition,1992

[24] FAR23 Chapter 1- Federal Aviation Administration, Department of Transportation, Part 23- Airworthiness Standards: Normal, Utility

[25] Rooney E.C., Craig R.E., "Development of techniques and correlation of results to accurately establish the lift/drag characteristics of an air breathing missile from analytical predictions, sub-scale and full scale wind tunnel tests and flight tests", AGARD Flight Mechanics Panel, 16.1-16.18, Paris, France, 1977.

[26] Reddy J.N., "*Mechanics of Laminated Composite Plates and Shells: Theory and Analysis",* Boca Raton, CRC Press, 2nd edition, 2004

[27] Cook R.D., Malkus D.S., Plesha M.E., Concepts and Applications of Finite Element Analysis, 3rd Edition, John Wiley & Sons, New York, 1989.

[28] ANSYS Online Help Documentation, ANSYS Inc.

[29] Design Optimization Training Manual for Release 5.6, Volume 1; Mar.2000, ANSYS Inc.

[30] Macknight N., "*Tomahawk Cruise Missile",* Motorbooks International Mil-Tech Series, 1995

[31] Whitney J.M., "*Structural Analysis of Laminated Anisotropic Plates",* Lancaster: Tecnomic Publishing Company, 1987

[32] Lekhnitskii S.G., "*Anisotropic Plates",* Translated from the second Russion edition by Tsai S.W and Cheron T., Gordon and Breach Science Publishers Inc, 1968

[33] Juan P.L., Ghosh D.K., Rastogi N., "A New Approach in Stacking Sequence Optimization of Composite Laminates Using GENESIS Structural Analysis and Optimization Software", AIAA 2002-5451, 9th AIAA/ISSMO Symposium on Multidisciplinary Analysis and Optimization, Atlanta, Georgia, 4-6 Sept. 2002

[34] Tsai S.W. and Hahn H.T., "*Introduction to Composite Materials"*, Section 7.2, Technomic Publishing Company, 1980

[35] Tsai S.W., "*Composites Design"*, Third Edition, Section 11.6, Think Composites, Dayton, Ohio, 1987

[36] Barbero E. J., "*Introduction to Composite Materials Design"*, Taylor & Francis Inc., 1998

[37] Mallick P.K., "*Composites Engineering Handbook"*, Marcel Dekker Inc., 1997

[38] ASTM D 2290-00, "Standard Test Method for Apparent Hoop Tensile Strength of Plastic or Reinforced Plastic Pipe by Split Disk Method", 2000

APPENDIX A

ANSYS INPUT FILE FOR THE ALUMINUM WING

```
!Items prefaced by an exclamation point (!) are comments.
!dimensions are in mm's

!INPUT VARIABLES
wr_sc=12.5              !root width of the spar cap flange
w_ratio_sc=12.5/9       !root width/tip width for the spar cap flange
wr_rc=12                !root width of the rib cap flange
w_ratio_rc=12/9         !root width/tip width for the rib cap flange
n=4                     !number of ribs except root rib
m=0.5                   !space between two ribs (if 0: equal space, if 1: 1, 2…n)
c1=25                   !% c placement of spar1
c2=60                   !% c placement of spar2
tr_rw=1                 !root thickness of the rib web
t_ratio_rw=1            !root thickness/tip thickness for the rib web
tr_rc=1                 !root thickness of the rib cap flange
t_ratio_rc=2            !root thickness/tip thickness for the rib cap flange

!DESIGN VARIABLES
tr_us=4.7898            !root thickness of the upper skin
t_ratio_us=5.0699       !root thickness/tip thickness for the upper skin
tr_ls=4.3175            !root thickness of the lower skin
t_ratio_ls=7.3244       !root thickness/tip thickness for the lower skin
tr_sw=7.9125            !root thickness of the spar web
t_ratio_sw=5.1151       !root thickness/tip thickness for the spar web
tr_sc=3.9442            !root thickness of the spar cap flange
t_ratio_sc=6.6761       !root thickness/tip thickness for the spar cap flange

/PREP7
!resuming the tables of pressure distributions for different flight conditions and array of
!airfoil data
PARRES,CHANGE,'pressure_and_airfoil_data_NS-opt'

!During optimization, converts some real numbers to integers:
!n=nint(n)

tt_us=tr_us/t_ratio_us          !tip thickness of the upper skin
tt_ls=tr_ls/t_ratio_ls          !tip thickness of the lower skin
tt_sw=tr_sw/t_ratio_sw          !tip thickness of the spar web
tt_sc=tr_sc/t_ratio_sc          !tip thickness of the upper spar cap flange
wt_sc=wr_sc/w_ratio_sc          !tip width of the upper spar cap flange
tt_rw=tr_rw/t_ratio_rw          !tip thickness of the rib web
```

```
tt_rc=tr_rc/t_ratio_rc                !tip thickness of the rib cap flange
wt_rc=wr_rc/w_ratio_rc                !tip width of the rib cap flange

ro=2.7e-9                             !density of aluminum (ton/mm3)
cr=575                                !chord of the root rib
ct=288                                !chord of the tip rib
bh=1300                               !half span
*afun,deg
a1=6.342                              !leading edge sweep
a2=atan((cr-ct-bh*tan(a1))/bh)        !trailing edge sweep

!calculating Σx(i) (for i:1…n) for finding the z locations of the ribs (x(i)=m(i-1)+1)
!It makes the ratios of distances between two ribs as 1:m+1:2m+1…m(n-1)+1 from root
!to tip.
x=0
xt=0
*do,i,1,n
xt=xt+m*(i-1)+1
*enddo
!L.E. radius = 0.455 percent c
!slope of mean line at LE = 0.084

!CREATING THE RIBS AND DIVIDING THEM INTO 3
*do,i,0,n
*if,i,eq,0,then
   x=0
*else
   x=x+m*(i-1)+1                      !it calculates Σx(i) (for i:1…i)
*endif
z=1300*(x/xt)
d1=z*tan(a1)
d2=z*tan(a2)
c=cr-d1-d2

!creating the keypoints of the ribs using the "airfoil" array
*do,j,1,50
k,j+i*6,airfoil(j,1)*c/100+d1,airfoil(j,2)*c/100,z
*enddo

!creating spline at the upper part of the rib with 26 keypoint
FLST,3,26,3
*do,j,0,26
FITEM,3,1+j+i*6
*enddo
BSPLIN, ,P51X

!creating spline at the lower part of the rib with 26 keypoint
FLST,3,26,3
FITEM,3,1+i*6
*do,j,0,23
FITEM,3,27+j+i*6
```

```
*enddo
FITEM,3,26+i*6
BSPLIN, ,P51X
!creating L.E. radius with fillet
LFILLT,1+i*8 ,2+i*8 ,0.455*c/100, ,

!dividing the fillet at y=0
wpro,,90
LSBW,3+i*8

!adding two lines at the upper and lower parts of the rib
LCOMB,1+i*8 ,4+i*8 ,0
LCOMB,2+i*8 ,5+i*8 ,0

!creating the rib areas
AL,1+i*8 ,2+i*8

!deleting the unused keypoints
ALLSEL,BELOW,AREA
KSEL,INVE
KDELE,ALL
ALLSEL,ALL

!arranging the numbers
NUMCMP,ALL

!dividing the rib into 3 areas
KWPAVE,2+i*6
wpro,,,90
wpoff,,,C*c1/100
ASBW,1+i*3
wpoff,,,C*(c2-c1)/100
ASBW,2+i*3
NUMCMP,ALL
WPCSYS,-1,0
*enddo

!reversing the lower trailing edge, upper leading&mid edge lines of the ribs
*do,i,0,n
lreverse,2+8*i,0
lreverse,4+8*i,0
lreverse,7+8*i,0
*enddo

!on a rib; # of KP:6, # of L:8, # of A:3

!creating the lines in z direction
*do,i,0,n*6-1
l,1+i,7+i
*enddo
```

```
ln=(n+1)*8                    !total line numbers on the ribs
an=(n+1)*3                    !max area number on the ribs

!CREATING THE SKIN AND SPAR AREAS
*do,i,0,n-1
!creating 2*(n-1) spars
al,3+i*8,11+i*8,ln+3+i*6,ln+4+i*6
al,6+i*8,14+i*8,ln+5+i*6,ln+6+i*6

!creating 3*(n-1) upper skins
askin,4+i*8,12+i*8
askin,7+i*8,15+i*8
askin,1+i*8,9+i*8

!creating 3*(n-1) lower skins
askin,5+i*8,13+i*8
askin,8+i*8,16+i*8
askin,2+i*8,10+i*8
*enddo

!deleting the root areas
ADELE,1,3

!CREATING COMPONENTS
ASEL,S, , ,4,an,1,1
CM,RIBS,AREA

ASEL,S, , ,an-2,an,1,1
CM,TIP_RIB,AREA

ASEL,S, , ,an+1,an+1+n*8,8,
ASEL,A, , ,an+2,an+2+n*8,8,
CM,SPARS,AREA

ASEL,S, , ,an+3,an+5,1,
*do,i,0,n-1
ASEL,A, , ,an+3+i*8,an+5+i*8,1,
*enddo
CM,UPPER_SKINS,AREA

ASEL,S, , ,an+6,an+8,1,
*do,i,0,n-1
ASEL,A, , ,an+6+i*8,an+8+i*8,1,
*enddo
CM,LOWER_SKINS,AREA

ASEL,S, , ,an+3,an+8,1,
*do,i,0,n-1
ASEL,A, , ,an+3+i*8,an+8+i*8,1,
*enddo
CM,SKINS,AREA
```

```
lsel,s,,,ln+6,ln+6+(n-1)*6,6
*do,i,0,2
lsel,a,,,ln+3+i,ln+3+i+(n-1)*6,6
*enddo
CM,SPAR_CAPS,LINE

lsel,s,,,ln+3,ln+3+(n-1)*6,6
lsel,a,,,ln+5,ln+5+(n-1)*6,6
CM,UPPER_SPAR_CAPS,LINE

lsel,s,,,ln+4,ln+4+(n-1)*6,6
lsel,a,,,ln+6,ln+6+(n-1)*6,6
CM,LOWER_SPAR_CAPS,LINE

LSEL,S, , ,9,15,3
*do,i,1,n
LSEL,A, , ,1+i*8,7+i*8,3
LSEL,A, , ,2+i*8,8+i*8,3
*enddo
CM,RIB_CAPS,LINE

LSEL,S, , ,9,15,3
*do,i,2,n
LSEL,A, , ,1+i*8,7+i*8,3
*enddo
CM,UPPER_RIB_CAPS,LINE

LSEL,S, , ,10,16,3
*do,i,2,n
LSEL,A, , ,2+i*8,8+i*8,3
*enddo
CM,LOWER_RIB_CAPS,LINE

ALLSEL,ALL

!DEFINING THE ELEMENT TYPES
ET,1,SHELL93          !for spar&rib webs

ET,2,BEAM189

ET,3,SHELL99
KEYOPT,3,2,1          !tapered layer
KEYOPT,3,8,1          !storage of all layers data
KEYOPT,3,11,2         !nodes @ top face (for the skins)

!DEFINING THE MATERIAL PROPERTIES OF THE ALUMINUM
MP,EX,1,70000
MP,PRXY,1,0.33

!MESHING
es1=40                !element size
```

```
ESIZE,es1,0
MSHKEY,1                !MAPPED MESH
type,3
AMESH, UPPER_SKINS
AMESH, LOWER_SKINS

es2=30                  !element size
ESIZE,es2,0
type,1
AMESH,SPARS
MSHKEY,0                !QUAD MESH
AMESH,RIBS

!defining the beam section orientations and properties for the spar cap flanges with the
!appropriate keypoints
!LATT, MAT, REAL, TYPE, --, KB, KE, SECNUM
lsel,s,,,ln+3,ln+3+(n-1)*6,6
LATT,1,,2, ,4,,1
lsel,s,,,ln+4,ln+4+(n-1)*6,6
LATT,1,,2, ,3,,2
lsel,s,,,ln+5,ln+5+(n-1)*6,6
LATT,1,,2, ,6,,1
lsel,s,,,ln+6,ln+6+(n-1)*6,6
LATT,1,,2, ,5,,2

!defining the beam section orientations for the rib cap flanges with the appropriate
!keypoints
*do,i,1,n
lsel,s,,,1+i*8
LATT,1,,2, , ,6+i*6,3
lsel,s,,,4+i*8
LATT,1,,2, , ,4+i*6,3
lsel,s,,,7+i*8
LATT,1,,2, ,4+i*6,6+i*6,3
lsel,s,,,2+i*8
LATT,1,,2, , ,5+i*6,4
lsel,s,,,5+i*8
LATT,1,,2, , ,3+i*6,4
lsel,s,,,8+i*8
LATT,1,,2, ,3+i*6,5+i*6,4
*enddo

ALLSEL

LMESH,SPAR_CAPS
LMESH,RIB_CAPS


!CREATING COMPONENTS FOR ELEMENTS
CMSEL,S,UPPER_SKINS
ESLA,S
```

```
CM,UPPER_SKINS_ELEMENTS,ELEM

CMSEL,S,LOWER_SKINS
ESLA,S
CM,LOWER_SKINS_ELEMENTS,ELEM

CMSEL,S,SPARS
ESLA,S
CM,SPARS_ELEMENTS,ELEM

CMSEL,S,SPAR_CAPS
ESLL,S
CM,SPAR_CAPS_ELEMENTS,ELEM

CMSEL,S,UPPER_SPAR_CAPS
ESLL,S
CM,UPPER_SPAR_CAPS_ELEMENTS,ELEM

CMSEL,S,LOWER_SPAR_CAPS
ESLL,S
CM,LOWER_SPAR_CAPS_ELEMENTS,ELEM

CMSEL,S,RIBS
ESLA,S
CM,RIBS_ELEMENTS,ELEM
CMSEL,S,RIB_CAPS
ESLL,S
CM,RIB_CAPS_ELEMENTS,ELEM

CMSEL,S,UPPER_RIB_CAPS
ESLL,S
CM,UPPER_RIB_CAPS_ELEMENTS,ELEM

CMSEL,S,LOWER_RIB_CAPS
ESLL,S
CM,LOWER_RIB_CAPS_ELEMENTS,ELEM

!/ESHAPE,1.0


!DEFINING THE REAL CONSTANT SETS AND SECTION PROPERTIES FOR
!SKINS, SPAR WEBS, SPAR CAP FLANGES, RIB WEBS AND RIB CAP
!FLANGES

rn=0                                    !number of real constants
sn=0                                    !number of common sections

!PARABOLICALLY REDUCING THICKNESS FOR UPPER SKINS AND
!LINEARLY REDUCING WEB-FLANGE THICKNESS&WIDTH FOR UPPER
!SPAR CAP FLANGES
*do,i,1,n                               !number of lines along half span
```

```
lsel,s,,,ln+1+(i-1)*6,
en=(distkp(1+(i-1)*6,7+(i-1)*6))/es1                !number of elements on a line
*if,en,gt,nint(en),then
   en=nint(en)+1
*else
   en=nint(en)
*endif
dz=(kz(7+(i-1)*6)-kz(1+(i-1)*6))/en                 !element length in z direction
*do,j,1,en
z1=kz(1+(i-1)*6)+dz*(j-1)
z2=kz(1+(i-1)*6)+dz*j

!only the following two commands differ from the linearly reducing thickness definition
tz1=tr_us-(tr_us-tt_us)*2/bh*z1+(tr_us-tt_us)/bh**2*z1**2
tz2=tr_us-(tr_us-tt_us)*2/bh*z2+(tr_us-tt_us)/bh**2*z2**2

!for Shell99
r, rn+j,1,0
rmore
rmore,1,0,tz1,tz1,tz2,tz2

!for Shell63 or Shell93
!r,rn+j,tz1,tz1,tz2,tz2

!Dimensions for the T-beam section
tzs1=tr_sc-(tr_sc-tt_sc)*z1/bh
tzs2=tr_sc-(tr_sc-tt_sc)*z2/bh
tzs=(tzs1+tzs2)/2

Lzs1=wr_sc-(wr_sc-wt_sc)*z1/bh
Lzs2=wr_sc-(wr_sc-wt_sc)*z2/bh
Lzs=(Lzs1+Lzs2)/2

!Defining the T-beam section properties for the upper spar cap flanges
SECTYPE,sn+j,BEAM,RECT,
SECOFFSET,USER,0,-(tz1+tz2+tzs)/2
SECDATA,2*Lzs,tzs

CMSEL,S,UPPER_SKINS_ELEMENTS
NSEL,S,LOC,Z,z2
ESLN,R
EMODIF,ALL,REAL,rn+j,

CMSEL,S,UPPER_SPAR_CAPS_ELEMENTS
NSEL,S,LOC,Z,z2
ESLN,R
EMODIF,ALL,SEC,sn+j,
*enddo
sn=sn+en
rn=rn+en
*enddo
```

```
!PARABOLICALLY REDUCING THICKNESS FOR LOWER SKINS AND
!LINEARLY REDUCING WEB-FLANGE THICKNESS&WIDTH FOR LOWER
!SPAR CAP FLANGES
*do,i,1,n                                   !number of lines along half span
lsel,s,,,ln+1+(i-1)*6,
en=(distkp(1+(i-1)*6,7+(i-1)*6))/es1        !number of elements on a line
*if,en,gt,nint(en),then
   en=nint(en)+1
*else
   en=nint(en)
*endif
dz=(kz(7+(i-1)*6)-kz(1+(i-1)*6))/en         !element length in z direction
*do,j,1,en
z1=kz(1+(i-1)*6)+dz*(j-1)
z2=kz(1+(i-1)*6)+dz*j

tz1=tr_ls-(tr_ls-tt_ls)*2/bh*z1+(tr_ls-tt_ls)/bh**2*z1**2
tz2=tr_ls-(tr_ls-tt_ls)*2/bh*z2+(tr_ls-tt_ls)/bh**2*z2**2

r, rn+j,1,0
rmore
rmore,1,0,tz1,tz1,tz2,tz2

!Dimensions for the T-beam section
tzs1=tr_sc-(tr_sc-tt_sc)*z1/bh
tzs2=tr_sc-(tr_sc-tt_sc)*z2/bh
tzs=(tzs1+tzs2)/2

Lzs1=wr_sc-(wr_sc-wt_sc)*z1/bh
Lzs2=wr_sc-(wr_sc-wt_sc)*z2/bh
Lzs=(Lzs1+Lzs2)/2

!Defining the T-beam section properties for the lower spar cap flanges
SECTYPE,sn+j,BEAM, RECT,
SECOFFSET,USER,0,-(tz1+tz2+tzs)/2
SECDATA,2*Lzs,tzs

CMSEL,S,LOWER_SKINS_ELEMENTS
NSEL,S,LOC,Z,z2
ESLN,R
EMODIF,ALL,REAL,rn+j,

CMSEL,S,LOWER_SPAR_CAPS_ELEMENTS
NSEL,S,LOC,Z,z2
ESLN,R
EMODIF,ALL,SEC,sn+j,
*enddo
sn=sn+en
rn=rn+en
*enddo
```

```
!PARABOLICALLY REDUCING THICKNESS FOR SPAR WEBS
*do,i,1,n                                   !number of lines along half span
lsel,s,,,ln+1+(i-1)*6,
en=(distkp(1+(i-1)*6,7+(i-1)*6))/es1        !number of elements on a line
*if,en,gt,nint(en),then
   en=nint(en)+1
*else
   en=nint(en)
*endif
dz=(kz(7+(i-1)*6)-kz(1+(i-1)*6))/en         !element length in z direction
*do,j,1,en
z1=kz(1+(i-1)*6)+dz*(j-1)
z2=kz(1+(i-1)*6)+dz*j

tz1=tr_sw-(tr_sw-tt_sw)*2/bh*z1+(tr_sw-tt_sw)/bh**2*z1**2
tz2=tr_sw-(tr_sw-tt_sw)*2/bh*z2+(tr_sw-tt_sw)/bh**2*z2**2

r,rn+j,tz1,tz1,tz2,tz2

CMSEL,S,SPARS_ELEMENTS
NSEL,S,LOC,Z,z2
ESLN,R
EMODIF,ALL,REAL,rn+j,
*enddo
rn=rn+en
*enddo

!PARABOLICALLY REDUCING THICKNESS FOR RIB WEBS AND LINEARLY
!REDUCING WEB-FLANGE THICKNESS&WIDTH FOR LOWER&UPPER RIB
!CAPS
*do,i,1,n                                   !number of lines along half span

z=kz(7+(i-1)*6)                             !rib location in z direction
tz=tr_rw-(tr_rw-tt_rw)*2/bh*z+(tr_rw-tt_rw)/bh**2*z**2

r,rn+i,tz

!upper&lower skin thicknesses for beam offset
tzu=tr_us-(tr_us-tt_us)*2/bh*z+(tr_us-tt_us)/bh**2*z**2
tzb=tr_ls-(tr_ls-tt_ls)*2/bh*z+(tr_ls-tt_ls)/bh**2*z**2

!Dimensions for the L-beam section
tzr=tr_rc-(tr_rc-tt_rc)*z/bh
Lzr=wr_rc-(wr_rc-wt_rc)*z/bh

!Defining the L-beam section properties for the upper rib cap flanges
SECTYPE,sn+i,BEAM, RECT,
SECOFFSET,USER,-(tz+Lzr)/2,-tzu-tzr/2
SECDATA,Lzr,tzr
```

```
!Defining the L-beam section properties for the lower rib cap flanges
SECTYPE,sn+n+i,BEAM,RECT,
SECOFFSET,USER,-(tz+Lzr)/2,-tzb-tzr/2
SECDATA,Lzr,tzr

CMSEL,S,RIBS_ELEMENTS
NSEL,S,LOC,Z,z
ESLN,R
EMODIF,ALL,REAL,rn+i,

CMSEL,S,UPPER_RIB_CAPS_ELEMENTS
NSEL,S,LOC,Z,z
ESLN,R
EMODIF,ALL, SEC,sn+i

CMSEL,S,LOWER_RIB_CAPS_ELEMENTS
NSEL,S,LOC,Z,z
ESLN,R
EMODIF,ALL, SEC,sn+n+i

*enddo
rn=rn+n
sn=sn+2*n


!APPLYING THE BOUNDARY CONDITIONS AND THE LOADS
/SOLU
ANTYPE,STATIC              !Static analysis
PSTRES,ON                  !Calculate pre-stress effects

LSEL,S,LOC,Z,0,
DL,ALL,,UY
CMSEL,S,SPARS
ALLSEL,BELOW,AREA
LSEL,R,LOC,Z,0
DL,ALL,,UX
DL,ALL,,UZ


!LOAD CASE 1 (PHAA)
CMSEL,S,UPPER_SKINS
SFA,ALL,1,PRES, 0.1
SFA,ALL,2,PRES, %XZP_UST_M07_AOA7%
CMSEL,S,LOWER_SKINS
SFA,ALL,1,PRES, 0.1
SFA,ALL,2,PRES, %XZP_ALT_M07_AOA7%
CMSEL,S, TIP_RIB
SFA,ALL,1,PRES, 0.1
SFA,ALL,2,PRES, %XYP_TIP_M07_AOA7%
ALLSEL,ALL
LSWRITE,1
```

```
!LOAD CASE 2 (NHAA)
CMSEL,S,UPPER_SKINS
SFA,ALL,1,PRES, 0.1
SFA,ALL,2,PRES, %XZP_UST_M07_AOA_4%
CMSEL,S,LOWER_SKINS
SFA,ALL,1,PRES, 0.1
SFA,ALL,2,PRES, %XZP_ALT_M07_ AOA_4%
CMSEL,S, TIP_RIB
SFA,ALL,1,PRES, 0.1
SFA,ALL,2,PRES, %XYP_TIP_M07_ AOA_4%
ALLSEL,ALL
LSWRITE,2

!LOAD CASE 3 (PLAA)
CMSEL,S,UPPER_SKINS
SFA,ALL,1,PRES, 0.1
SFA,ALL,2,PRES, %XZP_UST_M095_AOA4_2%
CMSEL,S,LOWER_SKINS
SFA,ALL,1,PRES, 0.1
SFA,ALL,2,PRES, %XZP_ALT_M095_AOA4_2%
CMSEL,S, TIP_RIB
SFA,ALL,1,PRES, 0.1
SFA,ALL,2,PRES, %XYP_TIP_M095_AOA4_2%
ALLSEL,ALL
LSWRITE,3

!LOAD CASE 4 (NLAA)
CMSEL,S,UPPER_SKINS
SFA,ALL,1,PRES, 0.1
SFA,ALL,2,PRES, %XZP_UST_M095_AOA_1_3%
CMSEL,S,LOWER_SKINS
SFA,ALL,1,PRES, 0.1
SFA,ALL,2,PRES, %XZP_ALT_M095_AOA_1_3%
CMSEL,S, TIP_RIB
SFA,ALL,1,PRES, 0.1
SFA,ALL,2,PRES, %XYP_TIP_M095_AOA_1_3%
ALLSEL,ALL
LSWRITE,4
!LSSOLVE,1,4,1

!SOLVING, RETRIEVING AND PARAMETRIZING THE MAX. VON MISES
!STRESS, MINIMUM BUCKLING LOAD FACTORS (EIGENVALUES) AND THE
!VOLUME OF THE WING

!LOAD CASE 1 (PHAA)
LSSOLVE,1

/POST1

ETABLE,VOLU,VOLU
SSUM
```

```
*GET,V,SSUM,,ITEM,VOLU
mass=v*ro*1000                          !kg

port=0
ASEL,S, , ,4+port*3,6+port*3,1,1        !(port+1)th portion of the ribs
ASEL,A, , ,an+1+port*8,an+2+port*8      !(port+1)th portion of the spars
ASEL,A, , ,an+3+port*8,an+8+port*8,1,   !(port+1)th portion of the skins
(composite areas)
ESLA,S
shell,top
ETABLE,seqvtop,S,EQV
ESORT,ETAB,seqvtop
*GET, seqvtop,SORT,,MAX
shell,bot
ETABLE,seqvbot,S,EQV
ESORT,ETAB,seqvbot
*GET, seqvbot,SORT,,MAX
ASEL,S, , ,4+port*3,6+port*3,1,1        !(port+1)th portion of the ribs
ASEL,A, , ,an+1+port*8,an+2+port*8      !(port+1)th portion of the spars
ALLSEL,BELOW,AREA
ESLL,S                          !selecting elements associated with the lines
ETABLE,AXS,LS,1
ESORT,ETAB,AXS,0,1, ,           !sort elements on absolute value descending
order
*GET,axs,SORT,,MAX
smax1_1=max(seqvtop, seqvbot, abs(axs))

port=1
ASEL,S, , ,4+port*3,6+port*3,1,1        !(port+1)th portion of the ribs
ASEL,A, , ,an+1+port*8,an+2+port*8      !(port+1)th portion of the spars
ASEL,A, , ,an+3+port*8,an+8+port*8,1    !(port+1)th portion of the skins
                                        !(composite areas)
ESLA,S
shell,top
ETABLE,seqvtop,S,EQV
ESORT,ETAB,seqvtop
*GET, seqvtop,SORT,,MAX
shell,bot
ETABLE,seqvbot,S,EQV
ESORT,ETAB,seqvbot
*GET, seqvbot,SORT,,MAX
ASEL,S, , ,4+port*3,6+port*3,1,1        !(port+1)th portion of the ribs
ASEL,A, , ,an+1+port*8,an+2+port*8      !(port+1)th portion of the spars
ALLSEL,BELOW,AREA
ESLL,S                          !selecting elements associated with the lines
ETABLE,AXS,LS,1
ESORT,ETAB,AXS,0,1, ,           !sort elements on absolute value descending
order
*GET,axs,SORT,,MAX
smax1_2=max(seqvtop, seqvbot, abs(axs))
```

```
port=2
ASEL,S, , ,4+port*3,6+port*3,1,1                !(port+1)th portion of the ribs
ASEL,A, , ,an+1+port*8,an+2+port*8              !(port+1)th portion of the spars
ASEL,A, , ,an+3+port*8,an+8+port*8,1,           !(port+1)th portion of the skins
(composite areas)
ESLA,S
shell,top
ETABLE,seqvtop,S,EQV
ESORT,ETAB,seqvtop
*GET, seqvtop,SORT,,MAX
shell,bot
ETABLE,seqvbot,S,EQV
ESORT,ETAB,seqvbot
*GET, seqvbot,SORT,,MAX
ASEL,S, , ,4+port*3,6+port*3,1,1                !(port+1)th portion of the ribs
ASEL,A, , ,an+1+port*8,an+2+port*8              !(port+1)th portion of the spars
ALLSEL,BELOW,AREA
ESLL,S                                  !selecting elements associated with the lines
ETABLE,AXS,LS,1
ESORT,ETAB,AXS,0,1, ,                   !sort elements on absolute value descending
order
*GET,axs,SORT,,MAX
smax1_3=max(seqvtop, seqvbot, abs(axs))

port=3
ASEL,S, , ,4+port*3,6+port*3,1,1                !(port+1)th portion of the ribs
ASEL,A, , ,an+1+port*8,an+2+port*8              !(port+1)th portion of the spars
ASEL,A, , ,an+3+port*8,an+8+port*8,1,           !(port+1)th portion of the skins
(composite areas)
ESLA,S
shell,top
ETABLE,seqvtop,S,EQV
ESORT,ETAB,seqvtop
*GET, seqvtop,SORT,,MAX
shell,bot
ETABLE,seqvbot,S,EQV
ESORT,ETAB,seqvbot
*GET, seqvbot,SORT,,MAX
ASEL,S, , ,4+port*3,6+port*3,1,1                !(port+1)th portion of the ribs
ASEL,A, , ,an+1+port*8,an+2+port*8              !(port+1)th portion of the spars
ALLSEL,BELOW,AREA
ESLL,S                                  !selecting elements associated with the lines
ETABLE,AXS,LS,1
ESORT,ETAB,AXS,0,1, ,                   !sort elements on absolute value descending
order
*GET,axs,SORT,,MAX
smax1_4=max(seqvtop, seqvbot, abs(axs))

ALLSEL
/SOLU
ANTYPE,BUCKLE                           !Buckling analysis
```

```
BUCOPT,LANB,1                    !Use Block Lanczos solution method, extract 1
mode
MXPAND,1                         !Expand 1 mode shape
SOLVE
/POST1
*GET,buckling1,MODE,1,FREQ

!LOAD CASE 2 (NHAA)
…

!LOAD CASE 3 (PLAA)
…

!LOAD CASE 4 (NLAA)
…


!DEFINING THE DESIGN VARIABLES, STATE VARIABLES AND THE
!OBJECTIVE
/OPT

opvar, tr_us,dv,2,6
opvar, t_ratio_us,dv,2,12
opvar, tr_ls,dv,2,6
opvar, t_ratio_ls,dv,2,12
opvar, tr_sw,dv,4,15
opvar, t_ratio_sw,dv,2,10
opvar, tr_sc,dv,1,5
opvar, t_ratio_sc,dv,2,10

opvar,smax1_1,sv,,400
opvar,smax1_2,sv,,400
opvar,smax1_3,sv,,400
opvar,smax1_4,sv,,400
opvar,smax2_1,sv,,400
opvar,smax2_2,sv,,400
opvar,smax2_3,sv,,400
opvar,smax2_4,sv,,400
opvar,smax3_1,sv,,400
opvar,smax3_2,sv,,400
opvar,smax3_3,sv,,400
opvar,smax3_4,sv,,400
opvar,smax4_1,sv,,400
opvar,smax4_2,sv,,400
opvar,smax4_3,sv,,400
opvar,smax4_4,sv,,400
opvar, buckling1,sv,1
opvar, buckling2,sv,1
opvar, buckling3,sv,1
opvar, buckling4,sv,1
opvar, tt_us,sv,0.5
```

```
opvar, tt_ls,sv,0.5
opvar, tt_sw,sv,1.5
opvar, tt_sc,sv,0.5

opvar,mass,obj,,,

!oploop,prep,process          !starts fom the /PREP7 and DV's are processed
                              !(for discrete variables)
!OPKEEP,ON                    !creates *.bdb and *.brst for the best design

optype,sweep
opsweep,,10
opexe
OPSAVE,' KANAT_alu-1'

OPSEL,10
optype,random
oprand,50,50
opexe
OPSAVE,' KANAT_alu-2'

OPSEL,10
optype,subp
OPSUBP,100,100
opexe
OPSAVE,'KANAT_alu-3'

opvar,mass,obj,,,0.001
OPSEL,10
optype,subp
OPSUBP,100,100
opexe
OPSAVE,'KANAT_alu-4'

OPSEL,10
optype,subp
OPSUBP,100,100
opexe
OPSAVE,'KANAT_alu-5'

OPSEL,1
optype,subp
OPSUBP,100,100
opexe
OPSAVE,'KANAT_alu-6'

…
```

APPENDIX B

COMPARISON OF ANALYTICAL AND NUMERICAL SOLUTIONS FOR BUCKLING LOAD OF A SIMPLY-SUPPORTED PLATE

Material properties for the aluminum:

E=70000 MPa ν=0.3

Material properties for the e-glass/epoxy:

E_{11}=39000 MPa E_{22}=8600 MPa G_{12}=3800 MPa ν_{12}=0.28

N_x, N_y: normal loads per unit length in x and y directions, N/mm

N_{xy}: shear load per unit length, N/mm

$u_{x,}$ $u_{y,}$ $u_{z,}$: displacement degrees of freedom in x, y, and z directions, mm

1. SIMPLY-SUPPORTED PLATE SUBJECTED TO NORMAL LOADS N_x&N_y

Dimensions of the plate:

a=250 mm dimension of the plate which is subjected to normal load N_y

b=100 mm dimension of the plate which is subjected to normal load N_x

t=1 mm thickness

Test Case 1 (N_x): Aluminum plate

Test Case 2 (N_x): E-glass/epoxy plate, $(0/90)_s$
(Specially orthotropic plate, B_{ij}=0, D_{16}, D_{26}=0)

Test Case 3 (N_x): E-glass/epoxy plate, $(\pm45)_s$
(Symmetric plate, B_{ij}=0, D_{16}, D_{26}#0)

Test Case 4 (N_x): E-glass/epoxy plate, $(0/90)_2$
(B_{ij}#0, D_{16}, D_{26}=0)

Test Case 5 (N_x&N_y): E-glass/epoxy plate, $(0/90)_s$

(Specially orthotropic plate, $B_{ij}=0$, D_{16}, $D_{26}=0$)

Boundary conditions and loading types for Test Cases 1-4

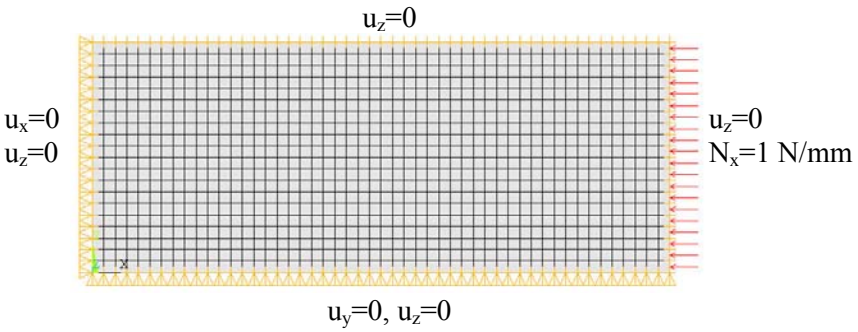

Boundary conditions and loading types for Test Case 5

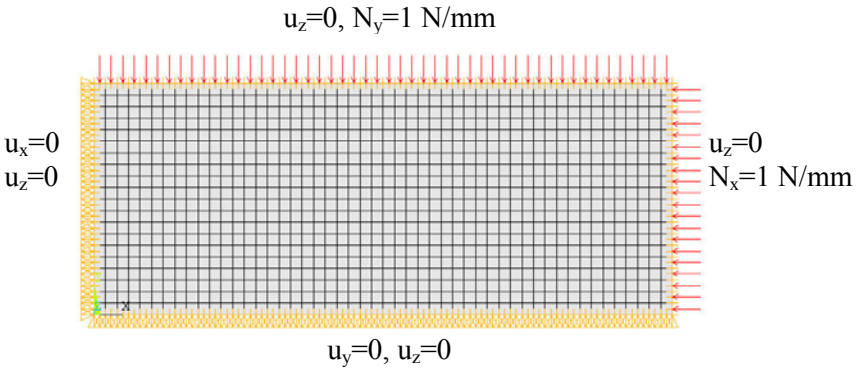

Buckling load factors

	Analy1[1]	**Analy2**[2]	**ANSYS (element size=10 mm)**	**ANSYS (element size=5 mm)**	**ANSYS (element size=1 mm)**
Test Case 1	26.712	26.712	26.530	26.665	26.710
Test Case 2	5.160	-	5.128	5.135	5.135
Test Case 3	8.157	-	6.964	6.982	6.981
Test Case 4	5.905	-	5.545	5.553	5.553
Test Case 5	1.188	-	1.183	1.184	1.184

1: Analytical formula for specially orthotropic and simply-supported plate subjected to normal loads N_x&N_y [31]:

$$\lambda_n^{(m,n)} = \pi^2 \frac{D_{11}\left(\frac{m}{a}\right)^4 + 2\left(D_{12} + 2D_{66}\right)\left(\frac{m}{a}\right)^2\left(\frac{n}{b}\right)^2 + D_{22}\left(\frac{n}{b}\right)^4}{\left(\frac{m}{a}\right)^2 N_X + \left(\frac{n}{b}\right)^2 N_y}$$

where m and n are the number of half waves (bubbles) in the buckled plate in the x and y directions, respectively. The pair (m,n) that yields the smallest value of $\lambda_n^{(m,n)}$ varies with the loading case, total number of plies, material and the plate aspect ratio (a/b). $\lambda_n^{(m,n)}$ is the buckling load factor due to normal loads N_x and N_y.

2: Analytical formula for isotropic flat plates in compression [22]:

$$\lambda_n^{(m)} = \frac{\pi^2 E}{12(1-\nu^2)}\left(\frac{bm}{a} + \frac{a}{bm}\right)^2\left(\frac{t^3}{b^2}\right)\frac{1}{N_X}$$

where b is the side that the load is applied.

u_z displacement distributions

Test Case 1

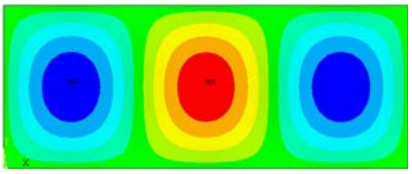

Test Case 2

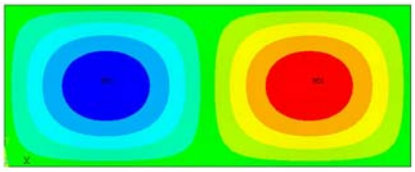

Test Case 3

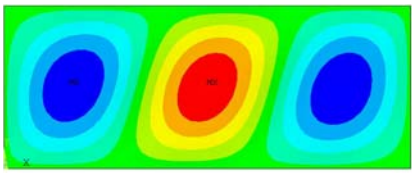

Test Case 4

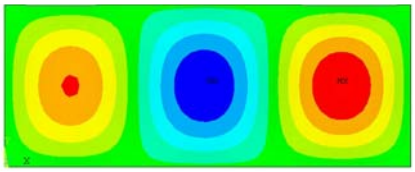

Test Case 5

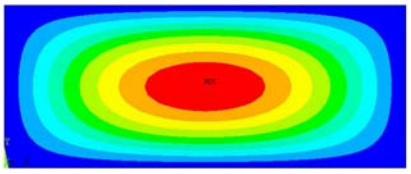

2. SIMPLY-SUPPORTED PLATE SUBJECTED TO SHEAR LOADS N_{xy}

Dimensions of the plate:

b=100 mm t=1 mm for different "a" values

Boundary conditions and loading types for Test Cases 6-7

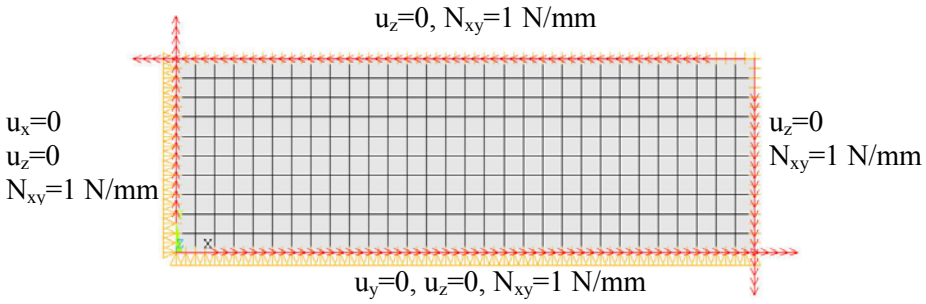

Test Case 6: Isotropic plate (E=10000 MPa, ν=0.3)

Using analytical formula for elastic shear buckling of flat plates [22]:

$$\lambda_s = K.E.\left(\frac{t^3}{b^2}\right)\frac{1}{N_{xy}}$$

λ_s=K K is a function of a/b and given for ν=0.3 in Figure 11.44 of [22].

Using analytical formula for specially orthotropic and infinite strip (a>>b) simply-supported plate subjected to shear loads N_{xy} [31]:

$$\Gamma = \frac{\sqrt{D_{11}D_{22}}}{D_{12}+2D_{66}}$$

$$\lambda_s = \frac{4\beta_1(D_{11}D_{22}^3)^{1/4}}{b^2 N_{xy}} \qquad \text{for } 1 \le \Gamma \le \infty$$

$$\lambda_s = \frac{4\beta_1\sqrt{D_{22}(D_{12}+2D_{66})}}{b^2 N_{xy}} \qquad \text{for } 0 \le \Gamma \le 1$$

Values of β_1 are given in Table 5.6 of [31] for different values of Γ:

Γ	**β_1**
0	11.71
0.2	11.8
0.5	12.2
1	13.17
2	10.8
3	9.95
5	9.25
10	8.7
20	8.4
40	8.25
∞	8.125

λ_s=4.824 for all "a" values

Buckling load factors

a/b	ANSYS (element size=10 mm)
1	8.934
1.5	6.478
2	5.754
3	5.174
4	5.018
6	4.893
8	4.854
10	4.838
12	4.827

The graph of "K" found from ANSYS with respect to a/b

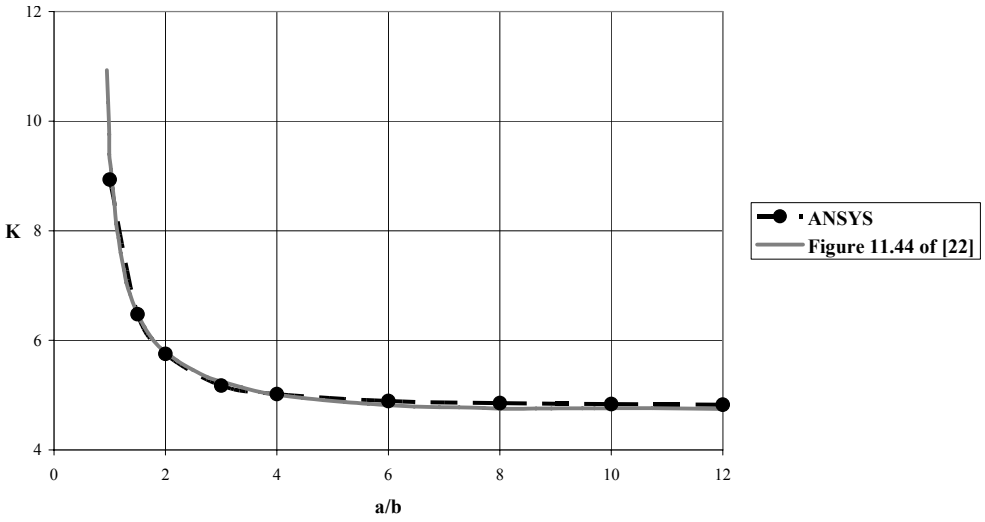

u_z displacement distribution for Test Case 6 (a/b=6)

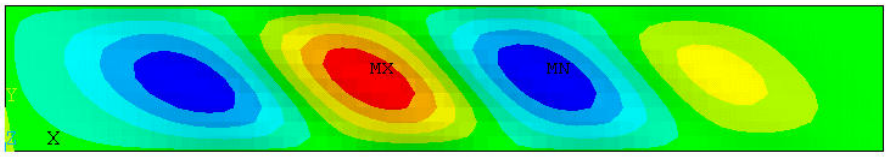

Test Case 7: E-glass/epoxy plate, $(0/90)_s$

(Specially orthotropic plate, $B_{ij}=0$, D_{16}, $D_{26}=0$)

Using analytical formula for specially orthotropic and infinite strip (a>>b) simply-supported plate subjected to shear loads Nxy [31] which is given above:

λ_s=5.843 for all "a" values

Buckling load factors

a/b	ANSYS (element size=10 mm)
1	14.369
2	7.068
3	6.431
4	6.125
5	5.999
6	5.963
8	5.891
10	5.866
12	5.846

u_z displacement distribution for Test Case 7 (a/b=6)

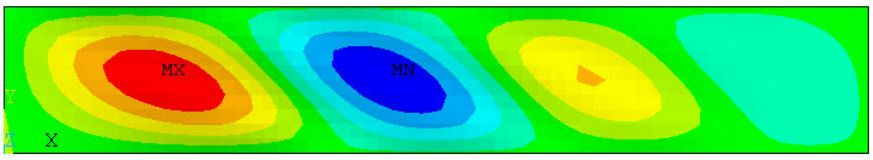

As seen from the buckling load factors for different a/b values for Test Cases 6-7, buckling load factor found with the analytical formula for specially orthotropic and infinite strip gets incompatible with the values found with numerical solutions as a/b gets smaller. In addition, the difference between numerical and analytical solutions increases too much especially for a/b smaller than four.

3. SIMPLY-SUPPORTED PLATE SUBJECTED TO COMBINATION OF NORMAL AND SHEAR LOADS

Dimensions of the plate:

a=1200 mm b=100 mm t=1 mm

Test Case 8: E-glass/epoxy plate, $(0/90)_s$

(Specially orthotropic plate, $B_{ij}=0$, D_{16}, $D_{26}=0$)

Using analytical formulae in [31]:

$\lambda_n=1.042$

$\lambda_s=5.843$ (from Test Case 7)

For combination [32]

$$\lambda_c^{(m,n)} = \frac{1}{\frac{1}{\lambda_n^{(m,n)}} + \frac{1}{\lambda_s^{\,2}}}$$

λ_c=1.011 (analytical)

Boundary conditions and loading types for Test Case 8

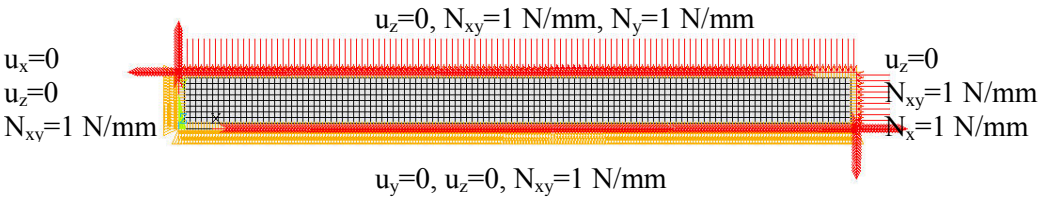

λ_c=1.009 (ANSYS (element size=10 mm))

APPENDIX C

COMPARISON OF DIFFERENT FAILURE CRITERIA FOR COMPOSITES

Finite element analysis is performed for a split disk test and then different failure criteria values are compared. A static analysis is performed for the maximum load in the test. The tests are conducted in BARIŞ Elektrik Endüstrisi A.Ş. in accordance with ASTM D 2290-00 [38]. The test specimen is loaded through the split disk test fixture which applies tensile stress to the test ring.

Material: E-glass/epoxy
Stacking sequence: $(\pm 45^{o})_3$
Material properties: given in Table 3.5
Tensile test machine: Instron 4200

Split disk test fixture

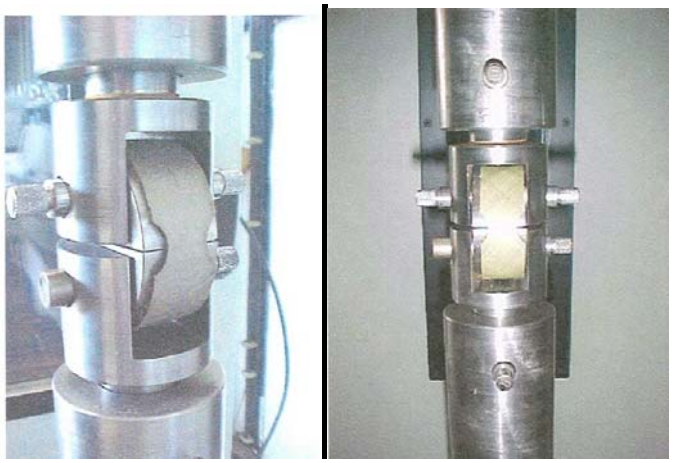

Assumptions in the finite element model:

- Only the ruptured region (notch) is modeled in ANSYS as a flat plate with Shell99 elements.
- Bending moment created during the tensile test is ignored since the text fixture is designed to minimize the effect of this moment [38].
- In order to prevent the boundary condition effects, loading and boundary conditions are defined far from the interested region (notch).
- Half of the maximum load is applied as a pressure distribution to the one side of the model and the nodes of the other side is constrained in all directions. Then a static analysis is performed.

Mesh, boundary conditions and the loading type

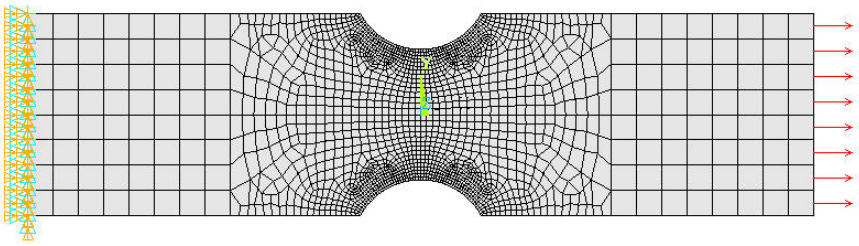

Stress Distributions (MPa) for all layers obtained after the analysis

layer1 layer2 layer3 layer4 layer5 layer6

In longitudinal (fiber) direction

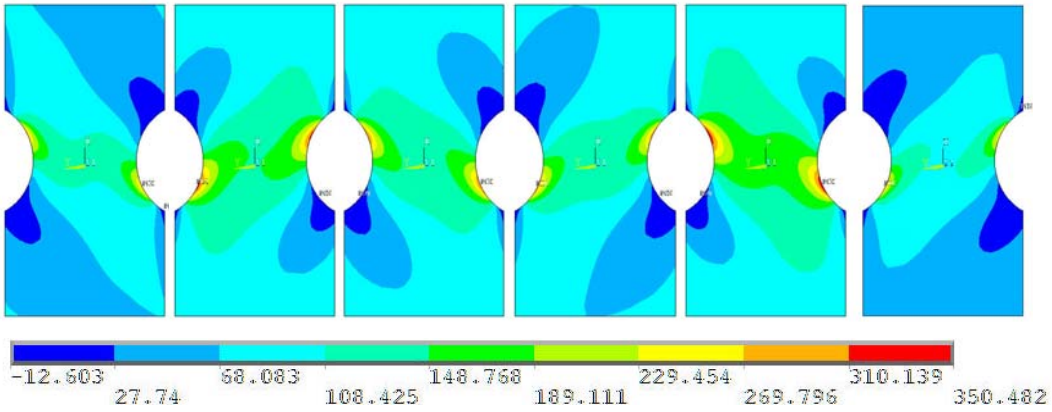

In transverse (perpendicular to fiber) direction

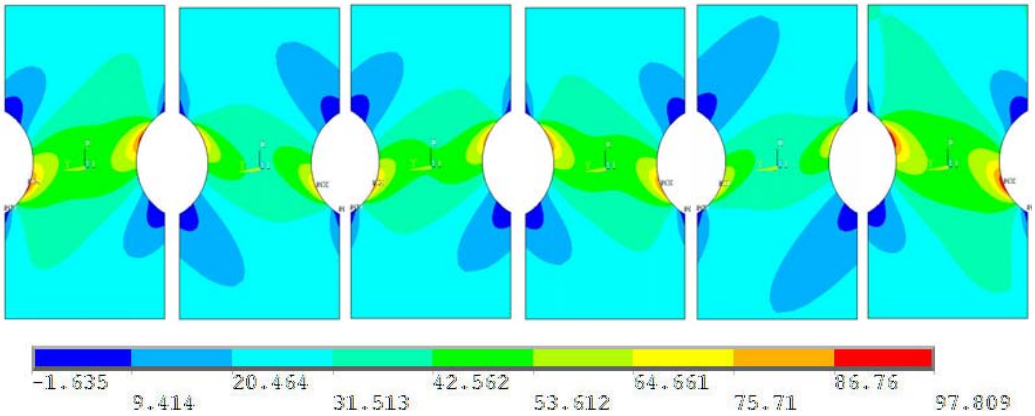

Shear

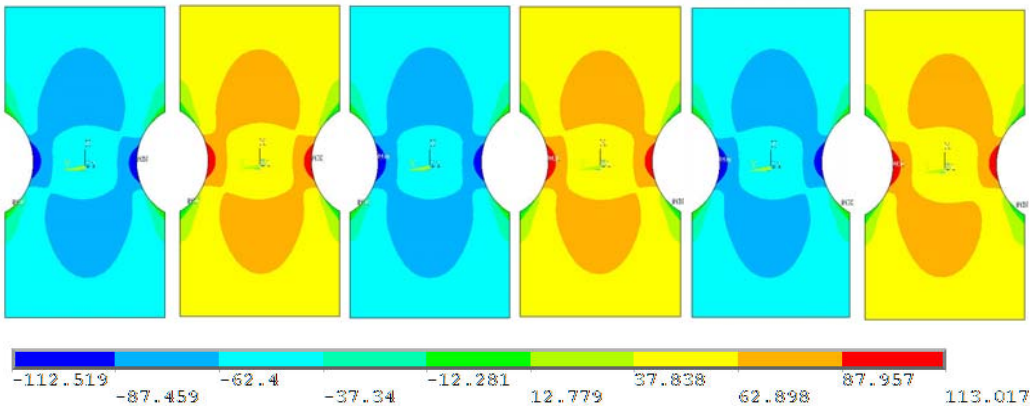

Maximum failure criteria value distribution obtained after the analysis

Maximum Strain

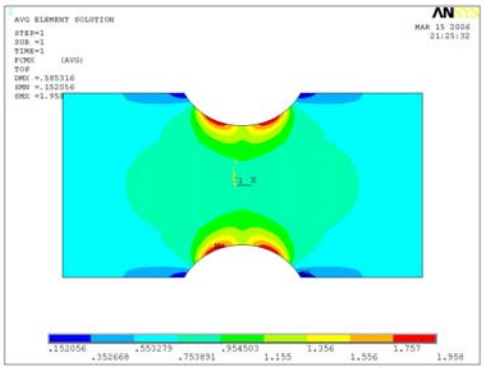

Maximum Stress

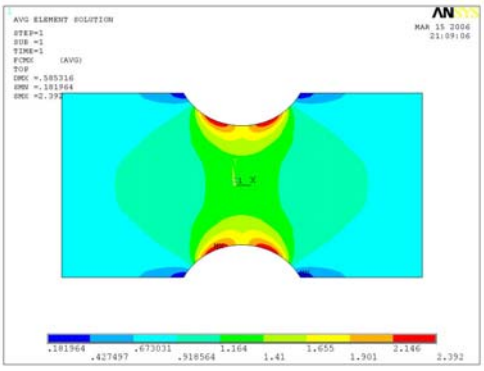

Tsai-Wu (C_{xy}=-1)

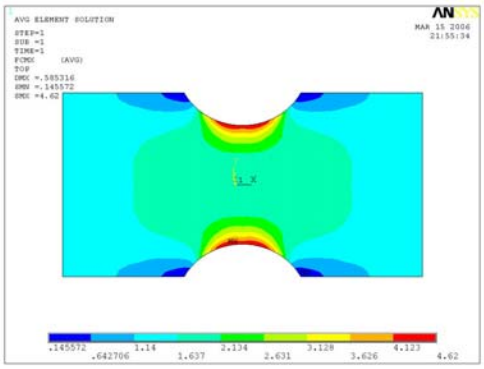

Tsai-Wu (C_{xy}=-0.5)

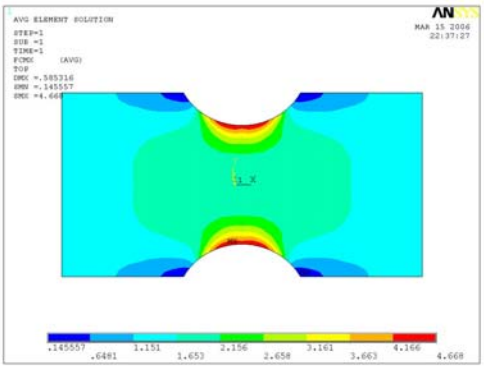

Inverse Tsai-Wu (C_{xy}=-1)

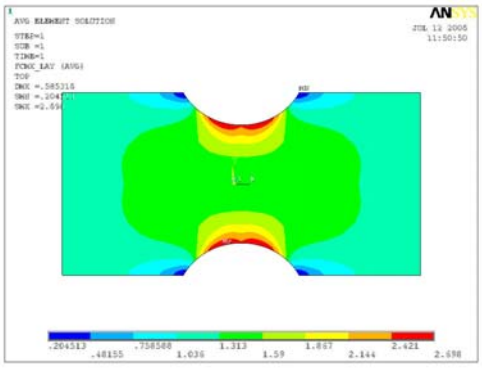

Inverse Tsai-Wu (C_{xy}=-0.5)

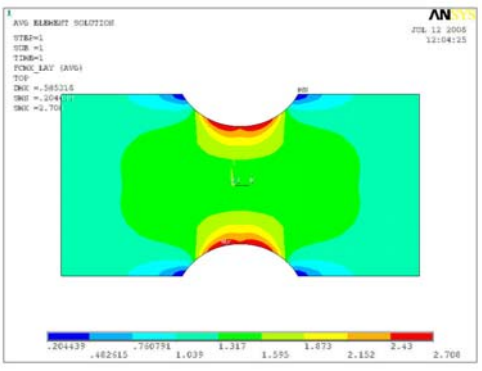

C_{xy}: coupling coeffficient for Tsai-Wu & inverse Tsai-Wu failure criteria

From the stress distribution graphs given above, it is seen that the stresses in transverse direction and shear stresses are greater than their strength values in the ruptured region although the stresses in fiber direction are smaller than the strength values in fiber direction. As seen from the figure of ruptured test specimens after the tensile test, there is not any failure in the fiber direction and the failure occurs in the transverse direction for each layer. So, the results of the finite element analysis agree qualitatively with the test results.

Ruptured test specimens after the tensile test

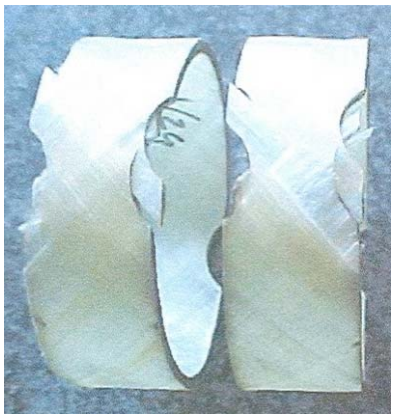

Failure of a composite structure is assumed when the failure criterion value is greater than one. So, after the analysis it is expected to obtain maximum failure criterion values to be nearly one for the ruptured regions. Figures of the maximum failure criterion value distribution for different failure criteria and coupling coefficients are given above. From these figures, it is seen that such a result is obtained for maximum strain, maximum stress and inverse Tsai-Wu failure criterion. But for Tsai-Wu failure criterion, very high failure criterion values are obtained. So, it can be said Tsai-Wu failure criterion gives conservative results compared to other three failure criteria, namely maximum stress, maximum strain and inverse Tsai-Wu.